PH.D. THESIS

Synchronization and Parameter Estimation in Wireless Communications

by Yimin Jiang
Advisor: John S. Baras

CSHCN Ph.D. 2000-2
(ISR Ph.D. 2000-6)

The Center for Satellite and Hybrid Communication Networks is a NASA-sponsored Commercial Space Center also supported by the Department of Defense (DOD), industry, the State of Maryland, the University of Maryland and the Institute for Systems Research. This document is a technical report in the CSHCN series originating at the University of Maryland.

Web site http://www.isr.umd.edu/CSHCN/

SYNCHRONIZATION AND CHANNEL PARAMETER ESTIMATION IN WIRELESS COMMUNICATIONS

by

Yimin Jiang

Dissertation submitted to the Faculty of the Graduate School of the
University of Maryland, College Park in partial fulfillment
of the requirements for the degree of
Doctor of Philosophy
2000

Advisory Committee:

Professor John S. Baras, Chairman/Advisor
Professor Carlos A. Berenstein
Professor Jerome A. Gansman
Professor Prakash Narayan
Professor Haralabos Papadopoulos

ABSTRACT

Title of Dissertation: SYNCHRONIZATION AND CHANNEL PARAMETER ESTIMATION IN WIRELESS COMMUNICATIONS

Yimin Jiang, Doctor of Philosophy, 2000

Dissertation directed by: Professor John S. Baras
Department of Electrical and Computer Engineering

This dissertation is devoted to the design and analysis of synchronization and channel parameter estimation schemes in wireless communications. Intrigued by the observation that the information is conveyed through wireless channels by uniformly spaced pulses that are some kind of "distorted" *convolution* of data symbols and a shaping pulse, we try to set up a frame work to study synchronization and channel parameter estimation problems in the frequency domain.

The dissertation consists of four major parts. Many issues in digital communications and signal processing involve the analysis of the inverse of Toeplitz matrices. In the first part, the convergence of the inverse of Toeplitz matrices and its application are presented. Under the condition that the z-transform of

the sequence with which the Toeplitz matrices are associated has no zero on the unit circle, we show that the inverse converges to a circular matrix in the weak sense. Furthermore, for the *finite boundary quadratic form*, a sufficient condition under which the convergence can be strengthened into the strong sense and an upper bound of the approximation residue error are derived. It is well known that a circular matrix can be eigendecomposed by the discrete Fourier transform (DFT) which provides the desired frequency domain approach.

In practical systems, synchronization parameters such as timing and carrier phase offsets, and channel response in fading channels are acquired with the help of a training sequence (TS) that is known to the receiver, which is called the data-aided (DA) estimation. In the second part, the performance limit that is the Cramer-Rao lower Bound (CRB) for the DA joint carrier phase and timing offsets estimation with an arbitrary TS is derived using the properties of Toeplitz matrices. Unlike the CRB derived in the literature, the bound derived in this dissertation reveals the close relation between a TS and its resultant performance limit, therefore it provides a quantitative approach to design TS for the acquisition of synchronization parameters.

Following the estimation theorem, we derive a maximum likelihood (ML) slow frequency-selective fading channel estimator using the frequency domain approach introduced by the properties of Toeplitz matrices in the third part. In the fourth part, a carrier frequency offset estimator and a joint carrier phase and timing offset estimators with moderate complexities are proposed. Their systolic VLSI implementations are also presented. The performance of the proposed estimators approaches their corresponding performance limits.

DEDICATION

To my wife and my parents

ACKNOWLEDGEMENTS

I am deeply grateful to my advisor Professor John S. Baras for his encouragement, guidance and financial support throughout my Ph.D. study. He provided me great freedom to choose my interested research topic while directed and critiqued me just in time. Without his inspiration, support and care the accomplishment of this dissertation would have been impossible.

I am also very grateful to my dissertation advisory committee, Professor Carlos A. Berenstein, Professor Jerome A. Gansman, Professor Prakash Narayan and Professor Haralabos Papadopoulos, for their helpful suggestions, comments, teaching and care during my graduate studies.

I would like to thank Dr. Feng-Wen Sun for his thoughtful discussion, comments and cooperation. His remarkable insight into the field helped me substantially. I would also like to thank my colleagues

at Hughes Network Systems, Farhad B. Verahrami, Wen-Chun Ting, Robert L. Richmond, A. Roger Hammons, Michael Eng and Feng Shen, for their discussion, support and care.

I would like to thank my friends Jie Song, Wei Luo, Mingyan Liu, Xiaowen Wang, Junfeng Gu, Chenxi Zhu, Lusheng Ji, Zhu Han, Sachin Goel, Raadhakrishnan Poovendran. I am thankful to Tina Vigil, Diane Hicks for their technical help.

Several agencies generously provided financial support for this work. In particular, the work was supported in part by Hughes Network Systems under the cooperative agreement HNS(01-4-33715)/MIPS (01-1-33305) and her employee educational assistance program.

Finally I would like to acknowledge the immeasurable contribution of my family, whose unconditional love, sacrifices and support over the years have enabled me to complete my education and live my dreams.

TABLE OF CONTENTS

LIST OF TABLES

LIST OF FIGURES

SYNCHRONIZATION AND CHANNEL
PARAMETER ESTIMATION IN
WIRELESS COMMUNICATIONS

Yimin Jiang

July 31, 2000

This comment page is not part of the dissertation.

Typeset by LaTeX using the `dissertation` class by Pablo A. Straub, University of Maryland.

Chapter 1

Introduction

The next generation wireless communication networks carry the dream of "anywhere, anytime" information access to anyone. The field is growing at an explosive rate, stimulated by a host of important emerging applications ranging from third-generation mobile telephony [1, 2, 3, 4], wireless personal communications [5, 6, 7, 8], to wireless tactical military communications [4] and mobile satellite communications [9]. These and other newly envisioned networks have both profound social implications and enormous commercial potential. For system planners and communication engineers, the projections of rapidly escalating demand for such wireless services present major challenges, and meeting these challenges will require sustained technical innovation on many fronts [10].

The fast increasing demand for mobile and portable communication ultimately calls for optimally utilizing the available bandwidth. This goal is only attainable by digital communication systems capable of operating close to the information theoretic limits [11]. The implementation of such systems has been made possible by the enormous progress in semiconductor technology that allows the communication engineer to economically implement "systems on silicon"

which execute [12]:

- Advanced compression algorithms to drastically reduce the bit rate required to represent a voice or video signal with high quality.
- Sophisticated algorithms in the receiver for power control, channel estimation, synchronization, equalization, and decoding.
- Complex protocol to manage traffic in networks.
- User-friendly graphical man-machine interface.

With the rapid advance of VLSI technology, communication engineers today can trade the physical performance measures *bandwidth* and *power efficiency* for signal processing *complexity*. As a consequence, the design process is characterized by a close interaction of architecture and algorithms design, as opposed to a separation between theory and implementation in the traditional way.

As communication engineers with digital communications and signal processing background, we are particular interested in physical layer techniques. The reason is that many of the main technical challenges in wireless communications stem from the physical layer, for example, the communication channels over which radio-frequency (RF), infrared, underwater acoustic, and other wireless systems must operate are all complex and highly dynamic. These channels suffer from numerous physical impairments that severely impact system performance, important examples of which include fading due to multipath propagation and interference from extra-network sources. In this work we focus on the design, analysis and efficient VLSI architecture of synchronization and channel parameter estimation schemes in wireless communications.

1.1 Synchronization and Channel Estimation: Key Problems

In some books on digital communications, synchronization and channel estimation are addressed superficially. This must give the reader the impression that these tasks are trivial and that the error performance is always close to the limiting case of perfect channel knowledge and synchronization. In fact this is not an accurate perception for the following reasons [12, 13]:

- Error performance: Synchronization and channel estimation are critical to error performance;
- Design effort: A large amount of design time is spent in solving these problems;
- Implementation: A very large portion of the receiver hardware and software is dedicated to synchronization and channel estimation.

Therefore one question comes out naturally: what are key problems in synchronization and channel estimation?

In synchronous digital transmissions the information is conveyed by uniformly spaced pulses and the received signal is completely known except for the data symbols and a group of variables referred to as *reference parameters*. Although the ultimate task of receivers is to produce an accurate replica of the transmitted symbol sequence with no regard to synchronization parameters, it is only by exploiting knowledge of the latter that the detection process can properly be performed.

For example, in a baseband pulse amplitude modulation (PAM) system the received waveform is first passed through a matched filter and then is *sampled* at the symbol rate. A circuit that is able to predict the optimum sampling epochs is called a *timing* synchronizer and is a vital part of any synchronous receiver. Coherent demodulation is used with wireless communications. This means that the baseband data signal is derived making use of a local reference with the same *frequency* and *phase* as the incoming carrier. This requires accurate frequency and phase measurements insofar as phase errors introduce crosstalk between the in-phase and quadrature channels of the receiver and degrade the detection process. Hence it is clear that measuring reference parameters is a vital function in wireless communication systems. This function is called *synchronization*.

Wireless channels are complex and highly dynamic [10, 14, 15]. Signal fading due to multipath propagation is a dominant source of impairment in wireless communication systems, often severely impacting performance, e.g., the dispersive Rayleigh-fading environment [15] causes intersymbol interference (ISI). Fading in signal strength arises primarily from multipath propagation of a transmitted signal due to reflections off physical objects, which gives rise to spatially distributed standing wave patterns of constructive and destructive interference. These standing wave patterns depend not only on the geometry of the constituent propagation paths from transmitter to receiver but on the carrier frequency of the transmitted signal as well. As a result, signal strength varies both with spatial location and with frequency. What is more important, when the receiver is in motion through the standing wave pattern, time variation in signal strength exists. The effect of fading can be substantially handled through the use of diversity techniques via appropriately designed signal processing algorithms at

both the transmitter and receivers. Practical, high-performance systems require that such diversity techniques be efficient in their use of resources such as power, bandwidth, and the hardware, and that they usually meet tight computational and delay constraints. To make full use of diversity techniques, channel estimation that estimates the impaired channel response caused by multipath fading according to some models is necessary in coherent communication, e.g., when the minimum mean square error (MMSE) combiner is applied to detect data symbols.

In this thesis we consider synchronization and channel estimation as a parameter estimation problem and approach it with the techniques of estimation theory [16, 17]. Synchronization parameters such as timing and carrier frequency and phase offset, and channel response are focused. Although digital synchronization and channel estimation methods are well presented in the literature [12, 13], there are still a lot of interesting issues that remain unsolved. For example, in practical wireless systems (including satellite communication systems), synchronization and channel estimation are conducted with the help of a *training sequence* that is known to the receiver, which is called *data-aided* (DA) estimation. How to design training sequence to expedite such parameter acquisitions is an open problem. The sequence design problem is related to the performance limits of DA estimation. In order to simplify the computation, some assumptions on the training sequence are made in the literature [12, 13].

We focus on two issues in this thesis: estimation performance limits and estimation algorithms with moderate implementation cost. Because time, phase and frequency are continuous-valued parameters, it is natural to evaluate the synchronization accuracy in terms of *bias* and *estimation variance*. The Cramer-Rao

lower bound (CRB) [16] that establishes a fundamental lower limit to the variance of any unbiased estimator usually serves as a benchmark for performance evaluation purposes. When nuisance parameters are involved in estimation, the CRB is sometimes difficult to obtain. The *modified* CRB (MCRB) [13, 18] can be used as a substitute.

It is widely recognized that maximum likelihood (ML) estimation techniques provide a systematic and simple guide to develop synchronization and channel estimation algorithms. In fact, ML methods offer two major advantages [13]:

- they easily give rise to appropriate circuit configurations;
- they provide optimum and near optimum performance under some circumstances.

We follow the ML approach in this work primarily. An inevitable problem involved in the ML method is the Toeplitz matrix. The following section addresses this issue.

1.2 Toeplitz Matrices

Toeplitz matrices are often encountered in digital communications and signal processing problems, e.g., the correlation matrix of any wide sense stationary process (WSS) is Toeplitz. Many issues in signal processing involve the analysis of the inverse of Toeplitz matrices. As an example, the solution of Yule-Walker equations involves the calculation of the inverse [19]. A lot of efforts in the signal processing field have been undertaken to develop efficient algorithms to compute the inverse of the Toeplitz matrix [20, 21]. However the field lacks the theoretic result to analyze this topic. Therefore good approximations are desired

in order to expedite the analysis of the problems involving the inverse of Toeplitz matrices.

One widely used technique is to replace the Toeplitz matrix with a circular matrix, based on the well-known fact that a Toeplitz matrix asymptotically converges to a circular matrix in the weak sense [22, 23]. This often leads to considerable simplification since the inverse of a circular matrix is still circular while the inverse of a Toeplitz matrix is in general no longer Toeplitz. Furthermore, the circular matrix can be eigendecomposed by the discrete Fourier Transform (DFT). This often yields additional insight in the frequency domain. However, most applications involve quadratic forms, thus a convergence in the strong sense is required to replace the matrix with a circular matrix. A widely used assertion is that as long as the original Toeplitz matrices are based on a sequence of finite order, the inverses of these matrices can be asymptotically replaced with a circular matrix with negligible amount of leakage at the boundary [24, 12].

1.3 Key Contributions

Intrigued by the observation that the transmitted signal in digital communications is some kind of *convolution* of data symbols and shaping pulses, we try to set up a frame work to solve synchronization and channel parameter estimation problems in the frequency domain. Based on the previous work, we provided the condition under which the inverse of Toeplitz matrices that are involved in many signal processing problems can be substituted by a circular matrix asymptotically [25]. The eigendecomposition of circular matrices is equivalent to the DFT that provides us the desired frequency domain approach. This dissertation

makes the following technical contributions [26, 27].

1.3.1 On the Inverse of Toeplitz Matrices

We show that the widely used assertion (proposed by Kobayashi in [24]) that the original Toeplitz matrix is based on a sequence of finite order then the inverse can be substituted by a circular matrix asymptotically is in general incorrect. It is demonstrated here by an example that the inverse of Toeplitz matrices may not converge even in the weak sense to a Toeplitz matrix and the boundary leakage can be significant. Furthermore, we show that under the condition that the z-transform of the sequence with which the Toeplitz matrices are associated has no zero on the unit circle, the inverse converges in the weak sense to a circular matrix. Moreover, for finite boundary problems, the convergence can be strengthened into strong convergence (in the quadratic form sense). A sufficient condition for the strong sense convergence is given and an upper bound for the approximation error is proposed. The strong sense convergence theory plays a pivotal role in this dissertation. The eigendecomposition of circular matrices introduces a series of frequency domain approaches that shed light on new analysis methods and algorithms in synchronization, channel estimation and linear prediction.

1.3.2 The Performance Limits of Synchronization

In this dissertation we derive a closed-form Cramer-Rao lower bound (CRB) for the data-aided (DA) timing (or joint with carrier phase) estimation. For the DA parameter estimation, the CRB typically varies with the training sequence (TS). This indicates that different training sequences offer fundamentally differ-

ent performance. In the literature [12, 13, 28, 29, 30, 31, 18] the widely cited closed-form CRB for timing and phase recovery was derived under the assumption that the TS is independently identically distributed (i.i.d.) and the length of TS is sufficiently long. We found that the CRB for some particular TS could be significantly lower than that with the long i.i.d. assumption. Therefore the widely cited CRB in previous works hides the fundamental link between a TS and its corresponding performance limit. A closed-form formula of the CRB for timing and phase recovery with respect to any TS with arbitrary data pattern and length is derived in this dissertation. The bound reveals the close relation between the TS and the fundamental limit on timing and phase synchronization. The eigendecomposition of the inverse of Toeplitz matrix is applied in the computation of the bound.

The similar methodology can be expanded to calculate the performance limits of synchronization in fading channel. It is mathematically intractable to deal with the fading noise that is a nuisance parameter for synchronizer. Fortunately, the *modified* CRB (MCRB) [13, 18] provides people a tool to handle such nuisance noise. In this dissertation, the MCRB for DA timing estimation is derived.

1.3.3 Training Sequence Design for Synchronization

The CRB's provide communication engineers a guideline to design training sequences. Training sequences are widely used in practical wireless systems to expedite the synchronization and channel estimation. For example, in TDMA systems, preamble is added in front of payload data in its frame structure; in CDMA systems, a *pilot* channel provides the receiver with known data patterns

to recover channel parameters. This dissertation illustrates TS design for timing recovery in a general Gaussian channel. This is accomplished by minimizing the derived CRB's with respect to the TS parameters. Such methods have not been developed in earlier studies of these questions, and the results we obtain appear here for the first time.

1.3.4 Practical Synchronization and Channel Parameter Estimators

Following the ML approach, we derived several practical synchronization and channel parameter estimators using properties of Toeplitz matrices. The systolic structure is studied, which sheds insight on the VLSI implementation of several synchronization circuits.

This dissertation addresses the channel estimation problem for slow frequency-selective fading channels using training sequences and the ML approach. Traditional works assumed symbol period spaced delay-tapped line model and additive Gaussian noise (AWGN). Because of pre-filtering in the receiver front end, if the sampling rate is larger than one sample per symbol or the sampling epoch is unknown (i.e., the timing information is unavailable), the AWGN model is not valid anymore. A more general ML channel estimation method using the discrete Fourier transform (DFT) is derived given the colored Gaussian noise and over-sampling. A similar idea can be adopted to derive the ML joint timing and phase estimator.

A fundamental question addressed in this dissertation is the real-time implementation of the resulting algorithms with resulting good performance on relatively inexpensive hardware complexity. Although the algorithms we derive

and investigate were known before, we have provided useful extensions here. But primarily we have successfully addressed the hardware design problems already mentioned.

Based on the likelihood function, ML estimators were derived in the literature [12, 32] etc. Most estimators are computationally intense therefore unsuitable for VLSI implementations in practical systems in real-time. Several simplified quasi-ML estimators with VLSI implementations are proposed in this dissertation. For example, the carrier frequency estimation is conducted based on the auto-correlation of the input signal and on the linear regression of the auto-correlation phase [33, 34, 35].

Global maximum (*peak*) search is a key issue in many ML estimation problems. The central part around the global maximum of an objective function to be optimized can often be modeled by a quadratic function if it is close enough to the *true peak*. The *peak* of a quadratic function exists and is easy to compute. The *curve-fitting* algorithm is based on the observations: (1) the central part of an objective function is located through some coarse search method; (2) the quadratic function can be obtained through three adjacent samples on the objective curve around the *peak* using *Lagrange* interpolation; (3) the ML estimate can be computed through the coefficients of the quadratic function. A generic quasi-ML joint carrier phase and timing estimator based on the *curve-fitting* technique is proposed in this dissertation. Related publications resulting from the work described in this dissertation are [36, 34, 35].

These estimators exhibit good performance (in terms of near-zero bias and estimation variance approaching the CRB's at low signal to noise ratio (SNR)) with moderate implementation cost.

1.4 Dissertation Outline

The rest of this dissertation is organized as follows. Chapter 2 addresses the convergence properties of the inverse of Toeplitz matrices and their application in evaluating the likelihood function and signal processing. The CRB for joint carrier phase and timing offsets estimation, the MCRB for timing recovery in fading channel and training sequence design are proposed in Chapter 3. Chapter 4 derives a ML channel estimator for slow frequency-selective fading channel environments using the frequency domain approach introduced by the property of Toeplitz matrices. A simplified carrier frequency estimator and a joint carrier phase and timing offsets estimator are presented in Chapter 5. Systolic structure is also studied and the VLSI implementations of these estimators are discussed. Chapter 6 summarizes the dissertation and suggests future research.

Chapter 2

On the Convergence of the Inverse of Toeplitz Matrices and Its Applications

2.1 Introduction

Toeplitz matrices play a vital role in digital communications and signal processing. In fact many issues in these fields involve the analysis of the inverse of Toeplitz matrices. We are going to address this problem in this chapter.

A family of Toeplitz matrices T_n is defined by a sequence of complex numbers

$$\{t_i; i = \cdots, -1, 0, 1, \cdots\}$$

such that the element of T_n at the ith row and jth column is equal to t_{i-j}, i.e.,

$$T_n = \{t_{i-j}\}. \tag{2.1}$$

Furthermore, we restrict our discussion to the case that $t_{-i} = t_i^*$, the conjugate of t_i. With this restriction, T_n becomes Hermitian. Toeplitz matrices in this form play pivotal role in many signal processing issues. Often, what is really relevant is the inverse of such a matrix rather than the matrix itself. For instance, if t_i

represents the correlation of a stationary random process, the inverse of T_n is associated with the joint probability density function of n consecutive samples of the random process.

One of the difficulties in analyzing the inverse matrix arises from the fact that the inverse of a Toeplitz matrix is no longer Toeplitz, though it was shown in [20, 21] that such an inverse can be decomposed into multiplication and summation of Toeplitz matrices. One widely used technique to tackle the problem is to substitute the Toeplitz matrix T_n with a circular matrix. Such a circular matrix can be defined by the discrete Fourier transform (DFT) of the sequence $\{t_n\}$. Let $F(z)$ denote the z-Transform of $\{t_n\}$, i.e.,

$$F(z) = \sum_{k=-\infty}^{\infty} t_k z^{-k},$$

and $\mathcal{F}(\lambda) \triangleq F(e^{j\lambda})$ be the discrete-time Fourier transform (DTFT) of $\{t_n\}$. Let U_n denote the unitary matrix defined as

$$U_n = \frac{1}{\sqrt{n}} \begin{bmatrix} 1 & 1 & \cdots & 1 \\ 1 & e^{-j(2\pi/n)} & \cdots & e^{-j(2\pi(n-1)/n)} \\ \vdots & \vdots & \ddots & \vdots \\ 1 & e^{-j(2\pi(n-1)/n)} & \cdots & e^{-j(2\pi(n-1)(n-1)/n)} \end{bmatrix} \tag{2.2}$$

and D_n denote the diagonal matrix with the ith diagonal element $\mu_{i,n} = \mathcal{F}(2\pi i/n)$, i.e.,

$$D_n = \begin{bmatrix} \mu_{0,n} & 0 & \cdots & 0 \\ 0 & \mu_{1,n} & \cdots & 0 \\ \vdots & \vdots & \ddots & \vdots \\ 0 & 0 & \cdots & \mu_{n-1,n} \end{bmatrix}. \tag{2.3}$$

Then the matrix $C_n = U_n^H D_n U_n$ is a circular matrix [22, 23]. Substituting T_n with C_n is based on the well-known fact that T_n converges to C_n in the weak sense as long as $|F(z)|$ is bounded on the unit circle [22, 23]*. The weak convergence is based on the weak norm defined for an $n \times n$ matrix $A = \{a_{ij}\}$ as

$$\sqrt{n^{-1} \sum_{i=0}^{n-1} \sum_{j=0}^{n-1} |a_{ij}|^2}.$$

It has been observed that in many applications such a substitution leads to very useful and dramatic simplification to the problem at hand. This is due to the fact that the inverse of a circular matrix is still circular, whereas the inverse of a Toeplitz matrix is in general no longer Toeplitz. Furthermore, DFT-based eigendecomposition of C_n often leads to additional insight in the frequency domain.

However, the usefulness of this theorem is severely limited due to the following reasons. First, the convergence of T_n to C_n in the weak sense may not necessarily lead to the weak convergence of T_n^{-1} to C_n^{-1}. Secondly, many applications actually involve the quadratic form of T_n^{-1}. Even if T_n^{-1} converges to C_n^{-1} in the weak sense, substituting T_n^{-1} with C_n^{-1} may not warrant correct results since the convergence of quadratic forms can only be guaranteed if the convergence is in the strong sense, i.e., if the norm is defined for a Hermitian matrix A as

$$\| A \| = \max_x \frac{x^H A x}{x^H x},$$

where the maximum is over all the vectors of the same dimension as that of A.

*In [22], C_n is defined through the inverse discrete Fourier transform, i.e., the ith diagonal element of D_n is equal to $\mathcal{F}(-2\pi i/n)$ and U_n is replaced by U_n^H. The current notation is more consistent with engineering conventions.

It can be readily verified that in almost all practically interesting cases including the case that t_n has more than one but finite nonzero terms, we cannot strengthen the weak-sense convergence into the strong-sense convergence.

In many applications, the quadratic form $x^H T_n^{-1} x$ can be limited to the case that x has only finite nonzero terms in the middle of the vector, i.e.

$$x = (0, \cdots, 0, x_{-L}, \cdots, x_0, \cdots, x_L, 0, \cdots, 0)$$

and L does not increase with n. We refer to this structure as the *finite boundary quadratic form.*

The widely used assertion in the literature is that as long as the Toeplitz matrix T_n is of finite order, i.e., the associated sequence t_n has only finite nonzero terms, replacing T_n with C_n has negligible impact for large n on the evaluation of the finite boundary quadratic form associated with T_n^{-1} [12, 24].

In this dissertation, we first demonstrate by a simple example that this assertion is in general not correct. In this particular example it is shown that although T_n converge to the C_n in the weak sense and T_n is invertible for all n, T_n^{-1} does not converges to C_n^{-1}. In fact the example shows that T_n^{-1} cannot converge to a Toeplitz matrix in any sense under the given condition.

In section 2.3, we show that the T_n^{-1} converges to C_n^{-1} in the weak sense on the condition that there is no zero on the unit circle of the z-transform of t_n. Furthermore, under the same condition, we can strengthen the finite boundary quadratic form case from weak convergence to strong convergence; thus, asymptotically, replacing T_n^{-1} with C_n^{-1} yields correct results.

Section 2.4 illustrates some applications of the strong sense convergence on evaluating the probability density function of a random process with colored Gaussian noise and in digital communications. The frequency domain ap-

proaches endow us insights and simplify the problems dramatically.

2.2 An Example

We consider Toeplitz matrices $\{T_n\}$ by limiting the nonzero terms to t_0, t_1, t_{-1} and $t_1 = t_{-1}^*$. The closed-form T_n^{-1} is given by the following lemma.

Lemma 1 *Let T_n be a Hermitian Toeplitz matrix associated with the sequence $\{t_n\}$ of order three, i.e., $t_n = 0$ for $|n| \geq 2$, the element at the uth row and vth column of T_n^{-1} with $u, v = 0, \cdots, n-1$ is equal to*

$$(-1)^{u-v} \frac{t_1^{u-v} d_v d_{n-1-u}}{d_n} \qquad u \geq v \tag{2.4}$$

$$(-1)^{u-v} \frac{t_{-1}^{v-u} d_u d_{n-1-v}}{d_n} \qquad u < v \tag{2.5}$$

where d_n is the determinant of T_n, which is given by

$$d_n = \frac{\lambda_2^{n+1} - \lambda_1^{n+1}}{\lambda_2 - \lambda_1}, \tag{2.6}$$

with λ_1, λ_2 the roots of the following equation

$$x^2 - t_0 x - t_1 t_{-1} = 0. \tag{2.7}$$

Proof: It is straightforward to verify that the determinant d_n of T_n obeys the following recursive relation

$$d_n = t_0 d_{n-1} - t_1 t_{-1} d_{n-2} \tag{2.8}$$

with the initial condition $d_0 = 1, d_1 = t_0$. Solving the difference equation (2.8), we have

$$d_n = \frac{\lambda_2^{n+1} - \lambda_1^{n+1}}{\lambda_2 - \lambda_1},$$

where λ_1 and λ_2 are given by (2.7). Following the matrix inverse formula, we obtain (2.4, 2.5). ■

We consider the case $t_0 < 2|t_1|$. In this case, λ_2 and λ_1 are complex conjugates with the same magnitude equal to $|t_1|$. Let $\lambda_1 = |t_1|e^{j\theta}$ and $\lambda_2 = |t_1|e^{-j\theta}$. We further limit $\theta/(2\pi)$ to be an irrational number. In this case, $e^{(n+1)\theta} \neq e^{-(n+1)\theta}$ for any $n > 0$. Therefore, $\lambda_2^{n+1} \neq \lambda_1^{n+1}$, i.e., T_n is nonsingular. We can further verify that (2.4) becomes

$$\begin{aligned} &(-1)^{u-v} e^{j((u-v)\theta_t)} \frac{\sin(v+1)\theta \sin(n-u)\theta}{|t_1| \sin\theta \sin(n+1)\theta} \\ =&(-1)^{u-v} e^{j((u-v)\theta_t)} \frac{\cos(n-u-v-1)\theta - \cos(n-u+v+1)\theta}{2|t_1| \sin\theta \sin(n+1)\theta} \end{aligned} \tag{2.9}$$

given that θ_t is the phase of t_1. For fixed n and fixed $u-v$, the denominator and the last term of the nominator are constant. Thus, for fixed n, (2.9) varies with $\cos(n-u-v-1)\theta$. It can be shown that $\cos n\theta$ with $(n = 1, 2, \cdots)$ is densely populated over the interval $(-1, 1)$ as long as $\theta/(2\pi)$ is irrational. Therefore, $\cos(n-u-v-1)\theta$ will oscillate with u, v (see Appendix). For instance, the diagonal elements with $u = v$, $\cos(n-2v-1)\theta$ will not converge to a single value for different v and large n.

Figure 2.1 shows the central diagonal elements of T_n^{-1} with $t_0 = 1$, $t_1 = \sqrt{2}$ and $n = 200$. We observe that they oscillate, which implies that the central diagonal elements do not converge to a single value and the inverse matrix does not converge to a Toeplitz matrix at all. Figure 2.2 shows these elements with $t_0 = 1$, $t_1 = 0.35$ and $n = 200$. We can see that they converge to a single value except for the boundary leakage. This shows that the inverse of T_n in some scenarios cannot converge to a Toeplitz matrix in any sense since the diagonal elements oscillate over a wide range of values. Thus, the assertion made in [12, 24] is incorrect.

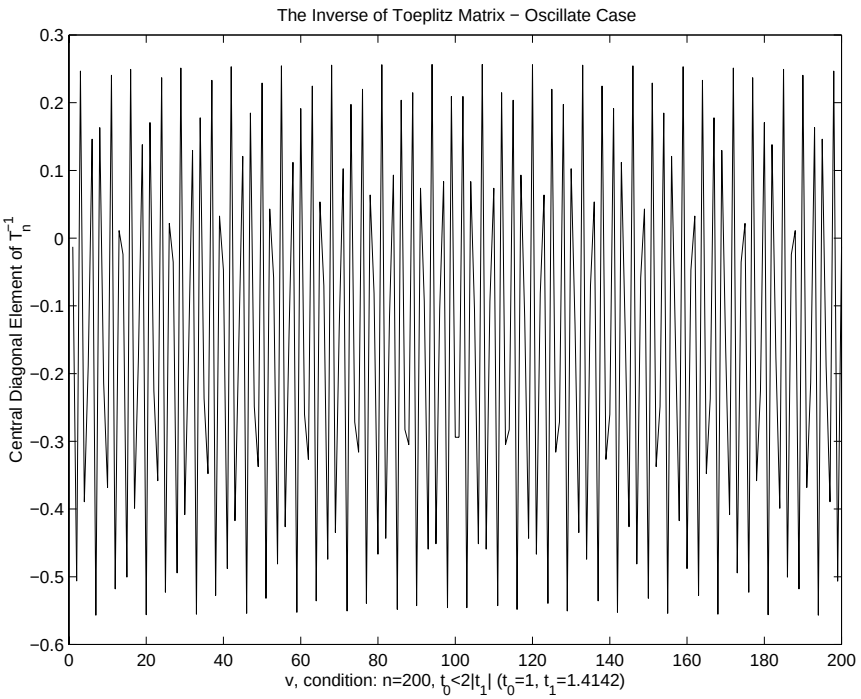

Figure 2.1: The Central Diagonal Elements of T_n^{-1} - Oscillate Case

In the following section, we will present a condition under which the convergence can be guaranteed.

2.3 A Condition for Convergence

Before presenting the main theorem, the finite boundary strong convergence is formally defined as follows.

Definition 1 *For two families of Hermitian matrices A_n, B_n, consider the quadratic form*

$$\max \left| \frac{x^H (A_n - B_n) x}{x^H x} \right|, \tag{2.10}$$

where the maximum is over all the n-dimensional vector of the form

$$x = (0, \cdots, 0, x_{-L}, \cdots, x_0, \cdots, x_L, 0, \cdots, 0).$$

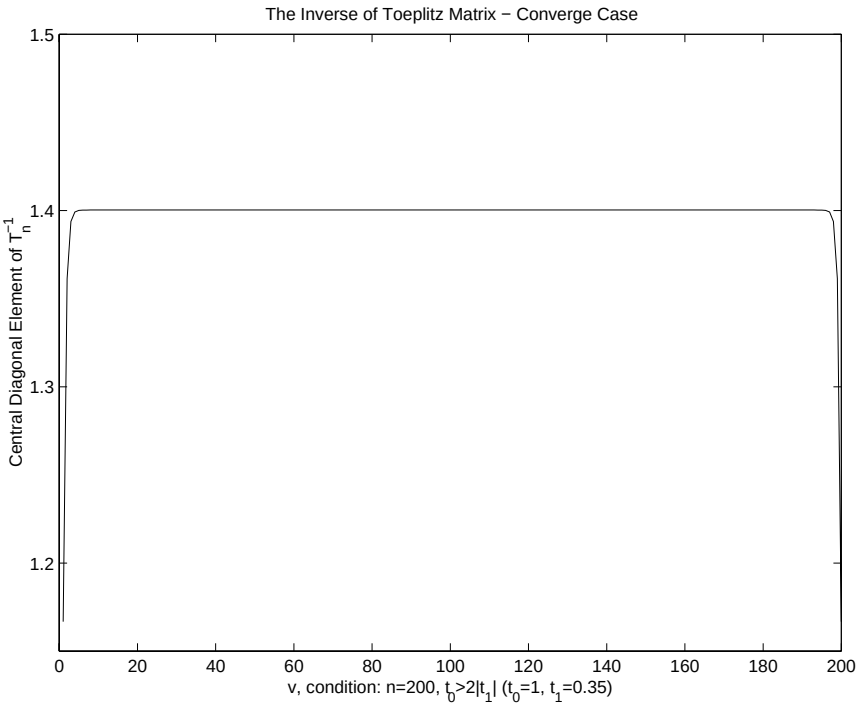

Figure 2.2: The Central Diagonal Elements of T_n^{-1} - Converge Case

If (2.10) converges to zero for any given L, we shall say that A_n converges to B_n in the finite boundary strong sense.

If x corresponds to an observation within the window $[-L, L]$ and with negligible leakage outside the observation window, we are able to replace A_n with B_n asymptotically in evaluating the quadratic forms. Many practical applications fall into this category.

In the remaining part of this section, we will present two conditions under which the inverse of a Toeplitz matrix converges to a circular matrix in the weak and strong sense for the finite boundary quadratic form respectively. The main objective is to derive the strong convergence theorem. For completeness, the weak convergence condition is also presented. We will start with the weak convergence since it is obtained by directly applying the theorems in [22].

Theorem 1 *Let $\{T_n\}$ be a family of Hermitian Toeplitz matrices associated with the sequence of $\{t_n\}$, and let $F(z)$ be the the z-Transform of t_n. If $|F(z)|$ is continuous and does not have any zero on the unit circle, T_n^{-1} converges to C_n^{-1} in the weak sense.*

Proof: Assume that the eigenvalues of T_n and C_n are respectively $\lambda_{k,n}$ and $\mu_{k,n}$ for $k = 0, \cdots, n-1$. Since $F(z)$ is continuous on the unit circle it is both upper and lower bounded. Assume that $m \leq F(z) \leq M$ over the unit circle. Note that $F(z)$ takes only real values due to the Hermitian constraint. Under this condition, it is well known that T_n converges to C_n in the weak sense [22, 23], i.e.,

$$\lim_{n\to\infty} \frac{\lambda_{0,n} + \cdots + \lambda_{n-1,n}}{n} = \lim_{n\to\infty} \frac{\mu_{0,n} + \cdots + \mu_{n-1,n}}{n}. \tag{2.11}$$

Actually, (2.11) implies that for any function $f(x)$ continuous over $[m, M]$, we have [22, p.65]

$$\lim_{n\to\infty} \frac{f(\lambda_{0,n}) + \cdots + f(\lambda_{n-1,n})}{n} = \lim_{n\to\infty} \frac{f(\mu_{0,n}) + \cdots + f(\mu_{n-1,n})}{n}. \tag{2.12}$$

Since $F(z)$ has no zero on the unit circle, this means that m and M are either both positive or both negative. Therefore, the function $f(x) = x^{-1}$ is continuous over $[m, M]$. Substituting this into (2.12), we obtain

$$\lim_{n\to\infty} \frac{\lambda_{0,n}^{-1} + \cdots + \lambda_{n-1,n}^{-1}}{n} = \lim_{n\to\infty} \frac{\mu_{0,n}^{-1} + \cdots + \mu_{n-1,n}^{-1}}{n}. \tag{2.13}$$

This means that T_n^{-1} converges to C_n^{-1} in the weak sense. ■

In order to present the more important strong sense convergence theorem, we need to introduce the concept of partial discrete time Fourier transform. For any integer w, we define

$$\mathcal{PF}(w, \lambda) = \sum_{k=w}^{\infty} t_k e^{-jk\lambda}. \tag{2.14}$$

In the sequel, $\mathcal{PF}(w, \lambda)$ will be termed as the partial DTFT of the sequence $\{t_k\}$ starting from w, based on the observation that $\mathcal{PF}(w, \lambda)$ is actually the DTFT of $\{\cdots, 0, t_w, t_{w+1}, \cdots\}$. Note that $\mathcal{PF}(-\infty, \lambda)$ is the DTFT of $\{t_k\}$, i.e., $\mathcal{F}(\lambda) = \mathcal{PF}(-\infty, \lambda)$. We further denote the ratio of partial DTFT to DTFT as $\mathcal{R}_f(w, \lambda)$, i.e.,

$$\mathcal{R}_f(w, \lambda) = \frac{\mathcal{PF}(w, \lambda)}{\mathcal{PF}(-\infty, \lambda)}. \tag{2.15}$$

Since $T_n^{-1} - C_n^{-1}$ is equal to $T_n^{-1}(I - T_n C_n^{-1})$, the norm of $T_n^{-1} - C_n^{-1}$ is highly related to $(I - T_n C_n^{-1})$. The inverse of the circular matrix can be expressed by using $\mu_{s,n}$, the samples of the DTFT of $\{t_k\}$. The following lemma gives the relation.

Lemma 2 *The element of $I - T_n C_n^{-1}$ at the wth row and vth column is equal to*

$$\begin{aligned}(I - T_n C_n^{-1})_{w,v} =& \frac{1}{n}\sum_{s=0}^{n-1} \mu_{s,n}^{-1} e^{j2\pi(w-v)s/n} \times (\mathcal{PF}(w+1, 2\pi s/n) + \\ & \mathcal{PF}(n-w, 2\pi s/n)^*).\end{aligned} \tag{2.16}$$

Furthermore, $(I - T_n C_n^{-1})_{w,v}$ is upper bounded by

$$\begin{aligned}|(I - T_n C_n^{-1})_{w,v}| \leq & \max_{0\leq s\leq n-1} \frac{1}{2}|\mathcal{R}_f(n-w, 2\pi(s+1)/n) - \mathcal{R}_f(n-w, 2\pi s/n)| + \\ & \max_{0\leq s\leq n-1} \frac{1}{2}|\mathcal{R}_f(w+1, 2\pi(s+1)/n) - \mathcal{R}_f(w+1, 2\pi s/n)| + \\ & (\max_{0\leq s\leq n-1} |\mathcal{R}_f(w+1, 2\pi s/n)| + \\ & \max_{0\leq s\leq n-1} |\mathcal{R}_f(n-w, 2\pi s/n)|) \times \\ & \frac{|2\pi(w-v+n/2)/n \mod 2\pi| n+2}{2n}\end{aligned} \tag{2.17}$$

Proof:

The (k,l)th element of C_n^{-1} is equal to

$$(C_n^{-1})_{k,l} = \frac{1}{n}\sum_{s=0}^{n-1} \mu_{s,n}^{-1} e^{j2\pi(k-l)s/n} \tag{2.18}$$

and therefore the (w,v)th element of $T_n C_n^{-1}$ is equal to

$$\begin{aligned}(T_n C_n^{-1})_{w,v} &= \frac{1}{n}\sum_{m=0}^{n-1} t_{w-m} \sum_{s=0}^{n-1} \mu_{s,n}^{-1} e^{j2\pi(m-v)s/n} \\ &= \frac{1}{n}\sum_{s=0}^{n-1} \mu_{s,n}^{-1} e^{j2\pi(w-v)s/n} \sum_{m=0}^{n-1} t_{w-m} e^{-j2\pi(w-m)s/n}.\end{aligned} \tag{2.19}$$

By the definition of $\mu_{s,n}$,

$$\mu_{s,n} = \sum_{k=-\infty}^{\infty} t_k e^{-j2\pi ks/n}$$

we have

$$\sum_{m=0}^{n-1} t_{w-m} e^{-j2\pi(w-m)s/n} = \mu_{s,n} - \sum_{k=-\infty}^{w-n} t_k e^{-j2\pi ks/n} - \sum_{k=w+1}^{\infty} t_k e^{-j2\pi ks/n}$$
$$= \mu_{s,n} - \mathcal{PF}(w+1, 2\pi s/n) - \mathcal{PF}(n-w, 2\pi s/n)^* \tag{2.20}$$

where $\mathcal{PF}(w,\lambda)$ is the partial DTFT, the second equality follows the Hermitian assumption $t_k^* = t_{-k}$. Equation (2.19) becomes

$$\frac{1}{n}\sum_{s=0}^{n-1} \mu_{s,n}^{-1} e^{j2\pi(w-v)s/n}(\mu_{s,n} - \mathcal{PF}(w+1, 2\pi s/n) - \mathcal{PF}(n-w, 2\pi s/n)^*)$$
$$= \delta[w-v] + \frac{1}{n}\sum_{s=0}^{n-1} \mu_{s,n}^{-1} e^{j2\pi(w-v)s/n}(\mathcal{PF}(w+1, 2\pi s/n) +$$
$$\mathcal{PF}(n-w, 2\pi s/n)^*). \tag{2.21}$$

The second equality follows from

$$\frac{1}{n}\sum_{s=0}^{n-1} e^{-j2\pi(w-v)s/n} = \delta[w-v] \triangleq \begin{cases} 1 & w = v, \\ 0 & \text{otherwise.} \end{cases}$$

Therefore, the first term of (2.21) corresponds to an identify matrix for $w, v = 0, \cdots, n-1$. This shows that the (w,v)th element of $I - T_n C_n^{-1}$ can be expressed as

$$(I - T_n C_n^{-1})_{w,v} = \frac{1}{n}\sum_{s=0}^{n-1} \mu_{s,n}^{-1} e^{j2\pi(w-v)s/n}(\mathcal{PF}(w+1, 2\pi s/n) + \mathcal{PF}(n-w, 2\pi s/n)^*). \tag{2.22}$$

It is interesting to observe that $\mathcal{PF}(w, 2\pi s/n)\mu_{s,n}^{-1}$ represents the ratio of the partial DTFT to the DTFT, i.e.,

$$\mathcal{PF}(w, 2\pi s/n)\mu_{s,n}^{-1} = \left.\frac{\mathcal{PF}(w,\lambda)}{\mathcal{F}(\lambda)}\right|_{\lambda = 2\pi s/n}. \tag{2.23}$$

For convenience, let $\mathcal{X}(w,\lambda)$ denote the following

$$\mathcal{X}(w,\lambda) \triangleq \frac{\mathcal{PF}(w+1,\lambda)}{\mathcal{F}(\lambda)} + \frac{\mathcal{PF}(n-w,\lambda)^*}{\mathcal{F}(\lambda)} \tag{2.24}$$

(2.24) is equal to

$$\mathcal{X}(w,\lambda) = \mathcal{R}_f(w+1,\lambda) + \mathcal{R}_f(n-w,\lambda)^*$$

With this notation, (2.22) can be written as

$$(I - T_n C_n^{-1})_{w,v} = \frac{1}{n}\sum_{s=0}^{n-1} \mathcal{X}(w, 2\pi s/n) e^{j2\pi(w-v)s/n} \tag{2.25}$$

Now consider the following summation obtained by replacing s in (2.25) with $2\lfloor s/2 \rfloor$:

$$\frac{1}{n}\sum_{s=0}^{n-1} \mathcal{X}(w, (2\pi)\cdot 2\lfloor s/2 \rfloor/n) e^{j2\pi(w-v)s/n}. \tag{2.26}$$

The terms of (2.26) with even index s are equal to those of (2.25). It can be readily verified that the difference between (2.25) and (2.26) is equal to

$$\frac{1}{n}\sum_{s=0}^{\lfloor (n-1)/2 \rfloor} (\mathcal{X}(w,(2\pi)\cdot(2s+1)/n) - \mathcal{X}(w,(2\pi)\cdot 2s/n)) e^{j2\pi(w-v)(2s+1)/n}. \tag{2.27}$$

Thus, the difference can be upper-bounded by

$$\max_{0\le s\le n-1} \frac{1}{2}|\mathcal{X}(w,(2\pi)\cdot(s+1)/n) - \mathcal{X}(w,(2\pi)\cdot s/n)|. \tag{2.28}$$

For even n, (2.26) is equal to

$$\frac{1}{n}\sum_{s=0}^{n/2-1} \mathcal{X}(w, 4\pi s/n) e^{j2\pi(w-v)2s/n}(1 + e^{j2\pi(w-v)/n}). \tag{2.29}$$

For odd n, (2.26) is equal to

$$\begin{aligned}&\frac{1}{n}\sum_{s=0}^{(n-1)/2-1} \mathcal{X}(w, 4\pi s/n) e^{j2\pi(w-v)2s/n}(1 + e^{j2\pi(w-v)/n}) + \\ &\frac{1}{n}\mathcal{X}(w,(2\pi)(n-1)/n) e^{j2\pi(w-v)(n-1)/n}.\end{aligned} \tag{2.30}$$

By using the inequality that $|1-e^{jx}| \leq |x \mod 2\pi|$, where $(x \mod 2\pi)$ is within $[-\pi, \pi)$, we obtain that

$$|1+e^{j2\pi(w-v)/n}| = |1-e^{j2\pi(w-v+n/2)/n}| \leq |2\pi(w-v+n/2)/n \mod 2\pi|. \quad (2.31)$$

Substituting (2.31) into (2.29), (2.29) can be upper-bounded by

$$\frac{1}{2} \max_{0\leq s\leq n-1} |\mathcal{X}(w, 2\pi s/n)| \times |2\pi(w-v+n/2)/n \mod 2\pi| \quad (2.32)$$

Similarly, (2.30) can be upper-bounded by

$$\begin{aligned} &\frac{n-1}{2n} \max_{0\leq s\leq n-1} |\mathcal{X}(w, 2\pi s/n)| \times |2\pi(w-v+n/2)/n \mod 2\pi| + \\ &\frac{1}{n} \max_{0\leq s\leq n-1} |\mathcal{X}(w, 2\pi s/n)| \quad (2.33) \\ =& \max_{0\leq s\leq n-1} |\mathcal{X}(w, 2\pi s/n)| \times \frac{|2\pi(w-v+n/2)/n \mod 2\pi|(n-1)+2}{2n}. \end{aligned}$$

Both (2.32) and (2.33) are smaller than

$$\max_{0\leq s\leq n-1} |\mathcal{X}(w, 2\pi s/n)| \times \frac{|2\pi(w-v+n/2)/n \mod 2\pi|n+2}{2n}. \quad (2.34)$$

Therefore, $(I - T_n C_n^{-1})_{w,v}$ is upper bounded by the summation of (2.28) and (2.34). ■

Lemma 3 *If* $|\mathcal{R}_f(w,\lambda)| \leq B_1(w)$ *and* $|d\mathcal{R}_f(w,\lambda)/d\lambda)| \leq B_2(w)$, *let* $B_1(w) \triangleq \max_\lambda |\mathcal{R}_f(w,\lambda)|$ *and* $B_2(w) \triangleq \max_\lambda |d\mathcal{R}_f(w,\lambda)/d\lambda|$ *we have*

$$\begin{aligned} |(I - T_n C_n^{-1})_{w,v}| \leq& \frac{\pi(B_2(w+1)+B_2(n-w))}{n} + (B_1(w+1)+B_1(n-w)) \times \\ & \frac{|2\pi(w-v+n/2)/n \mod 2\pi|n+2}{2n}. \end{aligned} \quad (2.35)$$

Proof: This readily follows (2.16). ■

Lemma 4 *The variables $B_1(w)$ defined in Lemma 3 is bounded by the following:*

$$B_1(w) \leq \frac{\sum_{k=w}^{\infty} |t_k|}{\min_{\lambda\in[0,2\pi)} |\mathcal{F}(\lambda)|}. \tag{2.36}$$

Proof: According to the definition of $B_1(w)$ that is the upper bound of $|\mathcal{R}_f(w,\lambda)|$, we have

$$\begin{aligned} |\mathcal{R}(w,\lambda)| &= \left| \frac{\sum_{k=w}^{\infty} t_k e^{-jk\lambda}}{\mathcal{F}(\lambda)} \right| \\ &\leq \sum_{k=w}^{\infty} \left| \frac{t_k e^{-jk\lambda}}{\mathcal{F}(\lambda)} \right|, \end{aligned} \tag{2.37}$$

equation (2.36) follows handily. ■

If we restrict the condition on the sequence $\{t_n\}$ further, more useful properties on $B_1(w)$ and $B_2(w)$ can be obtained.

Lemma 5 *If the sequence $\{t_n\}$ satisfies the following conditions: 1) $|t_n| = O(1/|n|^p)$ with $p > 2$; 2) its DTFT $\mathcal{F}(\lambda) \neq 0,\ \forall\lambda \in [0, 2\pi)$, then $B_2(w)$ is bounded, and*

$$B_1(w) < O(1/w), w \geq 2. \tag{2.38}$$

Proof: First we address $B_2(w)$. For arbitrary $w \in [0, n-1]$,

$$\begin{aligned} \left| \left(\frac{\sum_{n=w}^{\infty} t_n e^{-j\lambda n}}{\sum_{n=-\infty}^{\infty} t_n e^{-j\lambda n}} \right)' \right| &= \left| \frac{\sum_{n=w}^{\infty} \sum_{k=-\infty}^{\infty} t_k t_n (k-n) e^{-j\lambda(n+k)}}{(\sum_{n=-\infty}^{\infty} t_n e^{-j\lambda n})^2} \right| \\ &\leq \frac{1}{\min_{\lambda\in[0,2\pi)} |\mathcal{F}(\lambda)|^2} \times (\sum_{n=w}^{\infty} \sum_{k=-\infty}^{\infty} (|t_k t_n||k| + |t_k t_n|n)) \\ &\leq \frac{1}{\min_{\lambda\in[0,2\pi)} |\mathcal{F}(\lambda)|^2} \times (2 \sum_{k=-\infty}^{\infty} |t_k| C_t). \end{aligned} \tag{2.39}$$

The third inequality holds because $|t_n| = O(1/|n|^p)$ and $p - 1 > 1$

$$\begin{aligned} \sum_{k=-\infty}^{\infty} |t_k||k| &= \sum_{k=-\infty}^{\infty} O(1/|k|^{p-1}) \\ &\leq C_t, \end{aligned}$$

which follows from the fact that the series of $O(1/|k|^q)$ with $q > 1$ converges. C_t is a finite number, therefore $B_2(w)$ is upper bounded by some fixed finite number B_{2max}.

Next we address $B_1(w)$. According to Lemma 4,

$$\begin{aligned} B_1(w) &\leq \frac{\sum_{k=w}^{\infty} |t_k|}{\min_{\lambda\in[0,2\pi)} |\mathcal{F}(\lambda)|} \\ &< \sum_{k=w}^{\infty} \frac{G}{\min_{\lambda\in[0,2\pi)} |\mathcal{F}(\lambda)|} \times \frac{1}{k^2} \\ &< \frac{G}{\min_{\lambda\in[0,2\pi)} |\mathcal{F}(\lambda)|} \times \left(\sum_{k=w}^{\infty} \frac{1}{k^2-1} \right) \\ &= \frac{G}{\min_{\lambda\in[0,2\pi)} |\mathcal{F}(\lambda)|} \times \left(\frac{1}{2(w-1)} + \frac{1}{2w} \right) \\ &< \frac{G}{\min_{\lambda\in[0,2\pi)} |\mathcal{F}(\lambda)|} \times \frac{1}{w-1} \end{aligned} \tag{2.40}$$

where G is a finite positive constant such that $|t_n| < G/|n|^2$, which gives the second inequality in (2.40); the fourth equality follows from the following partial series sum formula with $w \geq 2$

$$\sum_{k=2}^{n} \frac{1}{k^2-1} = \frac{3}{4} - \frac{1}{2n} - \frac{1}{2(n+1)}.$$

Hence, we have $B_1(w) < C_{B1}/(w-1)$ with $w \geq 2$ and C_{B1} a positive constant.

■

Theorem 2 *Let T_n be a family of Hermitian Toeplitz matrices associated with the sequence $\{t_n\}$, and $F(z)$ be the z-transform of $\{t_n\}$. If $|F(z)|$ does not have any zero on the unit circle, and $|t_n| \leq O(1/|n|^p)$ with $p > 2$, T_n^{-1} converges to C_n^{-1} in the finite boundary strong sense and*

$$\| T_n^{-1} - C_n^{-1} \| \leq O(1/\sqrt{n}). \tag{2.41}$$

Proof: Let $m = \min_{|z|=1} F(z)$ and $M = \max_{|z|=1} F(z)$, then all the eigenvalues of T_n are bounded in between m and M [22, p.64]. Thus, all the eigenvalues of T_n^{-1} are bounded by $B = 1/m$. The number B must be finite since there is no zero on the unit circle and $F(z)$ is continuous on the unit circle. Therefore, $\| T_n^{-1} \|$, the strong norm of T_n^{-1}, is bounded by B.

Let us define the vector norm $\| x \| = \sqrt{x^H x}$ for a vector x, and the spectral norm $\| A \|_s$ of a matrix A as

$$\| A \|_s = \max_{\|x\|=1} \| Ax \| .$$

and

$$\| A \|_s = \max\{\sqrt{\lambda} : \lambda \text{ is an eigenvalue of } A^H A\} \tag{2.42}$$

(2.42) follows [37, p.295]. It is readily verified that if A is a Hermitian matrix $\| A \| = \| A \|_s$ [37, p.176], which is the largest eigenvalue of A and is a matrix norm.

Then inequality:

$$\begin{aligned} \| T_n^{-1} - C_n^{-1} \| &= \max_{\|x\|=1} \| (T_n^{-1} - C_n^{-1})x \| \\ &= \max_{\|x\|=1} \| T_n^{-1}(I - T_n C_n^{-1})x \| \\ &\le \| T_n^{-1} \| \cdot \max_{\|x\|=1} \| (I - T_n C_n^{-1})x \| \end{aligned} \tag{2.43}$$

where the first equality follows the fact that T_n^{-1} and C_n^{-1} are Hermitian, the third inequality is due to the property of the matrix norm. We further obtain

$$\| T_n^{-1} - C_n^{-1} \| \le B \| (I - T_n C_n^{-1}) \|_s . \tag{2.44}$$

Since we are interested in the case that x is limited to $n-$dimensional vectors of type $x = (0, \cdots, 0, x_{-L}, \cdots, x_0, \cdots, x_L, 0, \cdots, 0)$, which is equivalent to setting the first and the last $\lfloor \frac{n-(2L+1)}{2} \rfloor$ columns of $(I - T_n C_n^{-1})$ to 0 in evaluating

$\| (I - T_n C_n^{-1})x \|$ for arbitrary x with vector norm 1. Denote the matrix obtained in this way as Q_n, i.e.,

$$Q_n = \begin{bmatrix} \mathbf{0} & \boldsymbol{D} & \mathbf{0} \end{bmatrix} \tag{2.45}$$

Block $\boldsymbol{D}$ ranges from Column $\lfloor \frac{n-(2L+1)}{2} \rfloor$ to Column $\lfloor \frac{n+(2L-1)}{2} \rfloor$.

In order to prove that we can strengthen the weak convergence into strong convergence for finite boundary problem, we only need to show that $\| Q_n \|_s \to 0$ as $n \to \infty$, which is equivalent to showing that the maximum eigenvalue of $Q_n^H Q_n$ goes to 0 as $n \to \infty$. We have

$$Q_n^H Q_n = \begin{bmatrix} \mathbf{0} \\ \boldsymbol{D}^H \\ \mathbf{0} \end{bmatrix} \begin{bmatrix} \mathbf{0} & \boldsymbol{D} & \mathbf{0} \end{bmatrix} = \begin{bmatrix} \mathbf{0} & \mathbf{0} & \mathbf{0} \\ \mathbf{0} & \boldsymbol{D}^H \boldsymbol{D} & \mathbf{0} \\ \mathbf{0} & \mathbf{0} & \mathbf{0} \end{bmatrix} \tag{2.46}$$

Using the theorem in [37, p.346], let q_{wv} be the $\{w, v\}$th element of $Q_n^H Q_n$. The largest eigenvalue of $Q_n^H Q_n$ is bounded by

$$\| Q_n^H Q_n \| \leq \min \left\{ \max_i \sum_{j=0}^{n-1} |q_{ij}|, \max_j \sum_{i=0}^{n-1} |q_{ij}| \right\} \tag{2.47}$$

There are only $(2L+1)^2$ nonzero elements in $\boldsymbol{D}^H \boldsymbol{D}$, the number does not increase as n increases. Therefore, if we can show that all the nonzero elements of Q_n converge to zero, this leads to the conclusion that the summation of all the elements of $Q_n^H Q_n$ converges to zero. It further leads to the result that $\| Q_n \|$ converges to zero.

To complete the proof, the (q, r)th element of $\boldsymbol{D}^H \boldsymbol{D}$ is upper bounded by

the following (using Lemma 3),

$$|(\boldsymbol{D}^H\boldsymbol{D})|_{q,r} \leq \sum_{w=0}^{n-1}\left(\frac{\pi(B_2(w+1)+B_2(n-w))}{n}+(B_1(w+1)+B_1(n-w))\times \frac{|2\pi(w-q+n/2)/n \mod 2\pi|n+2}{2n}\right)\times \left(\frac{\pi(B_2(w+1)+B_2(n-w))}{n}+(B_1(w+1)+B_1(n-w))\times \frac{|2\pi(w-r+n/2)/n \mod 2\pi|n+2}{2n}\right), \tag{2.48}$$

where $q, r = \lfloor\frac{n-(2L+1)}{2}\rfloor \cdots \lfloor\frac{n+(2L-1)}{2}\rfloor$.

Therefore it is readily verified that for large n (compared with L) the summations in (2.48) are bounded by the following (using Lemma 4 and 5)

$$\sum_{w=0}^{n-1}\left(\frac{\pi(B_2(w+1)+B_2(n-w))}{n}\right)^2 \leq O(1/n)$$

and

$$\sum_{w=0}^{n-1}\frac{\pi(B_2(w+1)+B_2(n-w))}{n}\times(B_1(w+1)+B_1(n-w))\times \frac{|2\pi(w-r+n/2)/n \mod 2\pi|n+2}{2n} < O(1/n)$$

and

$$\sum_{w=0}^{n-1}(B_1(w+1)+B_1(n-w))^2 \times \frac{|2\pi(w-q+n/2)/n \mod 2\pi|n+2}{2n}\times \frac{|2\pi(w-r+n/2)/n \mod 2\pi|n+2}{2n} < O(1/n).$$

That means

$$|(\boldsymbol{D}^H\boldsymbol{D})_{q,r}| \leq O(1/n) \tag{2.49}$$

which implies

$$\sum_{j=0}^{n-1}|q_{ij}|, \sum_{i=0}^{n-1}|q_{ij}| \leq (2L+1)O(1/n). \tag{2.50}$$

Since L does not increase with n, we have

$$\| Q \|_s = \sqrt{\| Q^H Q \|} \leq O(1/\sqrt{n})$$

and

$$\| T_n^{-1} - C_n^{-1} \| \leq O(1/\sqrt{n}). \tag{2.51}$$

The above shows that the summation of the absolute value of the elements of $Q^H Q$ approaches to zero for large n, which means that Q_n converges to the all-zero matrix in the strong sense. This concludes the proof. ■

If the sequence $\{t_n\}$ is finite order, we have the following corollary.

Corollary 1 *Let $\{T_n\}$ be a family of Hermitian Toeplitz matrices associated with the sequence $\{t_n\}$ of finite order, i.e., $t_s = 0$ for $|s| > W$ [23, p.23], and $F(z)$ be the z-transform. If $|F(z)|$ does not have any zero on the unit circle, T_n^{-1} converges to C_n^{-1} in the finite boundary strong sense and*

$$\| T_n^{-1} - C_n^{-1} \| \leq O(1/n). \tag{2.52}$$

Proof: Follow the same strategy of Theorem 2, use the observation $B_1(w) = 0$ and $B_2(w) = 0$ for $w > W$. ■

Remarks: Clearly, the condition on the sequence $\{t_n\}$ ($O(1/|n|^p)$ or finite order) is sufficient but not necessary. Theorem 2 and Corollary 1 provide the upper bound of the residue error of the circular matrix approximation. In fact, it may converge much faster.

Example: Consider again the example given in Section 2.2. The z-transform of t_n becomes

$$t_{-1} z + t_0 + t_1 z^{-1}$$

The transform has a zero on the unit circle if and only if $t_0 \leq 2|t_1|$. Under this condition, we have shown in Section 2.2 that T_n^{-1} cannot converge to a Toeplitz matrix. Note that only in the case that $t_0 = 2|t_1|$, T_n becomes singular.

2.4 Some Applications

In this section, we discuss a few potential applications. The theorems presented in the previous section provide us with a simple way to diagonalize the inverse of a Toeplitz matrix. In fact, in the literature, the substitution of the inverse of a Toeplitz matrix by a circular matrix has been widely used and yielded many useful results. The theorems fill the gap in this applications and avoid potential erroneous results by ignoring the condition that the z-transform of the sequence which defines a Toeplitz matrix has no zero on the unit circle. They also provide the upper bound of the residue error as a function of the rank of the Toeplitz matrix, which could serve as a guideline in some applications.

2.4.1 Evaluating the Likelihood Function of a Discrete-Time Stationary Process

Statistical techniques play a pivotal role in designing state-of-the-art communication systems. In contemporary digital transceivers, almost all the signals are represented in digital forms. The input analog signals are sampled at certain sampling rate to obtain discrete-time samples. If the noise incurred in the channel is modeled as general additive Gaussian noise, not necessarily white, it is often mathematically intractable to design good algorithms. The difficulty lies in the fact that the likelihood function for the non-white Gaussian noise is

complicated. The convergence theorem provides us a tool to simplify it.

Assume the received signal is modeled as the follows:

$$y(t) = s(A,t) + N(t), \tag{2.53}$$

where $y(t)$ is the received signal, $s(A,t)$ is the transmitted signal, A is the information of interest, $N(t)$ is noise, typically modeled as general Gaussian noise with zero mean and auto-correlation function $g_N(t-u)$ given that the Gaussian process is stationary. The signal $y(t)$ is sampled every T_s seconds; we obtain the following vectors

$$\underline{y} = \underline{s}(A) + \underline{N}, \tag{2.54}$$

where

$$\underline{y} = [y_{-n/2}, \cdots, y_{n/2-1}]$$

$$\underline{s}(A) = [s_{-n/2}(A), \cdots, s_{n/2-1}(A)]$$

$$\underline{N} = [N_{-n/2}, \cdots, N_{n/2-1}]$$

with $y_k = y(kT_s)$, $s_k(A) = S(A, kT_s)$ and $N_k = N(kT_s)$. The $n \times n$ auto-correlation matrix K of the noise vector $\underline{N}$ is Toeplitz based on the stationary assumption. The $\{w,v\}$th element of K is equal to $g_N((w-v)T_s)$. In practice, the autocorrelation function usually decreases exponentially; let us assume $g_N(nT_s) = O(1/|n|^p)$ $(p > 2)$ here. The likelihood function of $\underline{s}(A)$ is given by

$$f(\underline{r}|\underline{s}(A)) = \frac{\exp\left\{-\frac{1}{2}(\underline{y} - \underline{s}(A))^H K^{-1} (\underline{y} - \underline{s}(A))\right\}}{(2\pi)^{n/2}|K|^{1/2}}. \tag{2.55}$$

It was difficult to evaluate (2.55) because K^{-1} is hard to obtain analytically. It is natural to diagonalize the matrix K so that the coefficients in the new coordinates are independent [16]. The circular matrix approximation of K^{-1}

is desired because it is well known that the eigendecomposition of a circular matrix is equivalent to the DFT which provides a frequency domain approach to evaluate the likelihood function. Sometimes it is reasonable to assume that the signal $s(A,t)$ is very small when $|t| > t_s$ (i.e., the finite boundary condition for the quadratic form) because it could be under the system designers' control. We have the following corollary.

Corollary 2 *If the z-transform $F(z)$ of the sequence $\{g_N(kT_s)\}$ is continuous and has no zeros on the unit circle, i.e.,*

$$F(z) = \sum_{k=-\infty}^{\infty} g_N(kT_s) z^{-k}$$

as n becomes large enough the likelihood function (2.55) can be approximated by the following

$$\begin{aligned} &\lim_{n\to\infty} f(\underline{y}|\underline{s}(A)) \sim \\ &\quad \lim_{n\to\infty} (2\pi)^{-n/2} |K|^{-1/2} \exp\left\{ -\frac{1}{2} (U_n(\underline{y} - \underline{s}(A)))^H D_n^{-1} (U_n(\underline{y} - \underline{s}(A))) \right\} \end{aligned} \tag{2.56}$$

where

$$D_n = \mathrm{diag}(\mathcal{F}(2\pi 0/\mathrm{n}), \cdots, \mathcal{F}(2\pi(\mathrm{n}-1)/\mathrm{n}))$$

$$\mathcal{F}(\lambda) = \sum_{k=-\infty}^{\infty} g(kT_s) e^{-j\lambda k}.$$

$\mathcal{F}(\lambda)$ is the discrete-time Fourier transform of $\{g(kT_s)\}$, $U_n(\underline{y} - \underline{s}(A))$ is the n point DFT of $(\underline{y} - \underline{s}(A))$.

Proof: Applying the finite boundary strong convergence theorem of the inverse of a Toeplitz matrix, we have

$$K^{-1} \sim U_n^H D_n^{-1} U_n,$$

(2.56) holds handily. ■

Remarks:

- A hidden assumption, that $\underline{y}$ satisfies the finite boundary condition is adopted during the proof above. It sounds unreasonable to neglect the received signal (that accommodates noise information) outside the observation window. Actually it does not matter in communication receiver design when we use maximum likelihood (ML) or maximum a posteriori (MAP) approaches. Because we are only interested in the information in $\underline{s}(A)$, the term $\underline{y}^H K^{-1} \underline{y}$ in the RHS of (2.56) does not affect the final result. The following inequality (property of vector norm) holds

$$\| \underline{y}^H K^{-1} \underline{s}(A) \| \leq \| y \| \| K^{-1} \underline{s}(A) \|,$$

  where $\| \underline{y} \|$ is bounded, and for large n

$$\| K^{-1} \underline{s}(A) \| \sim \| U_n^H D_n^{-1} U_n \underline{s}(A)) \|,$$

  and we have

$$\underline{y}^H K^{-1} \underline{s}(A) \sim (U_n \underline{y})^H D_n^{-1} (U_n \underline{s}(A)).$$

- According to Theorem 2, Corollary 1, (2.47) and (2.48), the quadratic form's $(\underline{s}(A)^H K^{-1} \underline{s}(A))$ convergence speed is lower-bounded. It could also be obtained from numerical evaluation. The convergence speed is an important factor during system design when the DFT diagonalization is desired. It provides us the necessary number of zeros to be packed with the useful information $\underline{s}(A)$ to make the leakage tolerable. From our numerical evaluation, if K is modeled as a finite order Toeplitz matrix with small W, the effective length $(2L+1)$ of the finite boundary vector $\underline{s}(A)$ is large $(2L+1 > W)$, the quadratic form converges quickly as $n > (2L+1)$, i.e., the number of packed zeros is small or unnecessary.

- Since $g_N(t)$ is the auto-correlation function, its Fourier transform is the power spectrum density (PSD) of the noise process $N(t)$ and is non-negative. One question comes up naturally: if $y(t)$ is over-sampled, $F(z)$ has zeros on the unit circle though $\mathcal{F}(\lambda)$ does not have zeros in the frequency band of interests, does Corollary 2 still hold? The answer is positive. It is a classical question related to the likelihood function. If $y(t)$ is over-sampled, K is singular for large n, which implies that some rows are the linear combination (interpolation in digital signal processing) of other rows, and K^{-1} does not exist. To prevent such situation from happening, decimation (down-sampling) or the technique mentioned in [16, p.289] can be applied to give us mathematical convenience and guarantee our operations will be meaningful. We are only interested in the passband of $\mathcal{F}(\lambda)$. For those processes that have zeros in the passband, a similar technique (adding small white noise) could be applied with the cost being slow convergence.

2.4.2 Application on Digital Communications in Nonwhite Gaussian Noise

The DFT in (2.56) associated with the eigendecomposition of a circular matrix leads naturally to the frequency domain analysis, which often yields additional insight and simplification. In a communication system, in addition to the desired signal at the receiver, there is always noise that can be characterized as a Gaussian process. Due to the pre-filter in the receiver front-end for eliminating out of band noise and interference, the noise $n(t)$ in digital receiver is nonwhite (colored) in general, especially when there is more than one sample per sym-

bol (over-sampling). In fact over-sampling is widely used in the receiver front-end [12], such as synchronization, detection, channel estimation, fractionally-spaced equalizer, etc. In order to simplify the calculations, some analyses simply assume that the noise is white. This may lose potential insight or even lead to erroneous results. Another approach is to exploit pre-whitening [16]. However, pre-whitening the noise may lead to large inter-symbol interference and needs the pre-knowledge of the correlation properties of the random process. Furthermore, digital filters are often one of the most power consuming components in the digital receiver. The eigendecomposition in (2.56) decorrelates the noise in the frequency domain. This eliminates the need for pre-whitening.

Furthermore, the DFT matrix is not varied with a particular Toeplitz matrix. This means that the decorrelation can be achieved without pre-knowledge of the random process. It is useful in linear estimation and predication problems [19], because the DFT approximation often leads to a simple and robust estimator structure. A similar idea was adopted in the robust channel estimation algorithm for OFDM systems when solving the Yule-Walker equations [38]. Furthermore, the theorems derived here provide an analytic tool to design the training signal and to calculate the upper bound of the approximation residue error.

In addition, sometimes transmitted signals are some kind of convolution between the data sequence and the shaping pulse, the frequency domain approach transforms this convolution to multiplication in some data-aided applications [12]. The following chapters illustrate its applications on the computation of the Cramer-Rao lower Bound for the data-aided estimation and the derivation of channel estimation algorithms in wireless communications.

2.5 Conclusions

The convergence issue of the inverse of Toeplitz matrices was addressed in this chapter. Through a simple example, we illustrated that a widely used assertion is incorrect in general and therefore we propose a related convergence problem. We showed that under the condition that the z-transform of the sequence with which the Toeplitz matrices are associated has no zero on the unit circle, the inverse converges in the weak sense to a circular matrix. What is more, for the finite boundary quadratic form problem, the convergence can be strengthened into strong sense.

The eigendecomposition of a circular matrix is equivalent to DFT, which introduces the frequency domain approach in statistical signal processing and digital communications.

Appendix

This appendix shows that $\{m\theta \bmod 1; m = 1, 2, \cdots\}$ are densely populated over $[0, 1]$ for irrational θ. This assertion can be proved as follows. First of all, for any integer $m \neq n$, $(m-n)\theta \bmod 1$ cannot be zero, otherwise, $(m-n)\theta = k$ for some integer k, i.e, $\theta = (m-n)/k$, a rational number. This means that $n\theta \bmod 1$ takes infinite possible values between 0 and 1. Therefore, for any small number ϵ, we can find m,n such that $|(m-n)\theta mod 1| \leq \epsilon$. Note that $k((m-n)\theta mod 1)$ partitions $(0, 1)$ at equal spacing less than ϵ. This implies that for any number between 0 and 1, there is an integer k such that $k(m-n)\theta \bmod 1$ is less than ϵ. This proves the assertion.

Chapter 3

Performance Limits of the Data-Aided Synchronization and Training Sequence Design

3.1 Introduction

The Cramer-Rao lower bound (CRB) is a general lower bound on the minimum mean square error (MMSE) of any unbiased estimator [16]. The CRB usually serves as a benchmark for the performance of an actual unbiased estimator. Therefore it has received considerable attention in the literature. In some practical systems, synchronization parameters such as timing and carrier phase offsets are acquired with the help of a training sequence (TS) that is known to the receiver, which is called *DA* estimation. In the DA case, the CRB generally varies with the TS, which implies that different training sequences offer fundamentally different performance. Therefore it is very important to compute the CRB for any particular TS to understand the fundamental limit that a particular TS has.

However, in the literature [12, 28, 29, 30, 31, 18, 39], the closed-form CRB

for DA timing and/or carrier phase recovery for an arbitrary TS is not available. The authors of [12] gave a summary of the CRB for carrier frequency, phase and timing offsets estimation. The CRB for joint timing and carrier phase recovery was first introduced by Moeneclaey in [29, 30], and it was further discussed in his publications [31] and [28]. It is difficult to evaluate the bound when the TS is arbitrary. Moeneclaey simplified the calculation by the adoption of the strong law of large numbers and the assumption that the TS is zero mean, i.i.d., and sufficiently long. This method reduces the calculation dramatically, but it also hides the interaction between the TS and the estimation performance, therefore limiting the usage of the CRB. In order to deal with the estimation problem in the presence of nuisance parameters, D'Andrea *et al.* proposed the *modified* CRB (MCRB) in [18]. It was pointed out in [28] that the CRB's derived previously in [29, 31] are actually MCRB's. A modified CRB that considers the case where the symbol timing estimate is restricted to a finite interval of one symbol duration and the inter-symbol interference (ISI) is omitted was derived in [39].

In principle, it is possible to use brute-force numerical approach to compute the CRB for any given TS. Such brute-force computation involves the evaluation of derivative numerically and matrix inversion. Besides the computational complexity, the brute-force approach does not provide any insight on the interaction between a TS and the resultant CRB. In this chapter, a closed-form CRB for the DA joint carrier phase and timing offsets estimation is derived with respect to arbitrary TS. The only assumption is that the derivative of the shaping pulse exists (i.e., the pulse is sufficiently smooth). The bound reveals the close relation between the TS and the performance limit on timing and phase recovery, and therefore it provides insight on sequence design. The research result on the

inverse of Toeplitz matrices of Chapter 2 is applied in the computation. The frequency domain approach introduced by the eigendecomposition of the circular matrix expedites the calculation of the bound.

Similar methods can be applied in computing the performance limit for DA synchronization in a fading channel. Fading noise that is a nuisance parameter gives extra burden. Fortunately the *modified* CRB (MCRB) [13, 18] can be computed instead in this scenario. The MCRB for timing estimation in Rayleigh flat fading channel is derived in chapter as well.

The rest of the chapter is organized as follows. In Section 3.2, the research results on Toeplitz matrices are revisited, the DA CRB (denoted as $\mathrm{CRB}_{\mathrm{DA}}$) for joint timing and carrier phase estimation is derived. Section 3.3 evaluates the bound. We show that the CRB's derived in [12, 28, 29, 30, 31] are special cases of the CRB derived here. Section 3.4 presents the MCRB for timing estimation in a flat fading channel. Training sequence design for timing acquisition is proposed in Section 3.5. Optimal training sequences for timing recovery under the energy constraint are derived for both over and under sampling scenarios. A DA maximum likelihood (ML) joint carrier phase and timing offsets estimator will be discussed in Chapter 4. Computer simulation shows that the estimation variance meets the $\mathrm{CRB}_{\mathrm{DA}}$ (derived here) with different shaping functions and training sequences. The timing estimation variance with some training sequences is significantly lower than the CRB derived in the literature [12, 28, 29, 30, 31] (the performance difference is several dB sometimes).

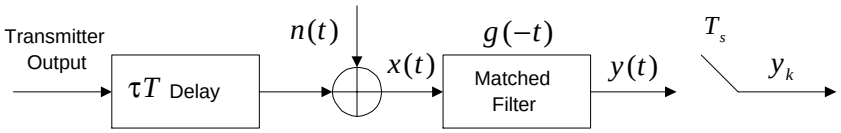

Figure 3.1: Modeling of Channel and Matched Filter

3.2 The Calculation of the DA Cramer-Rao Lower Bound in a Gaussian Channel

The baseband received signal is modeled as:

$$x(t) = \sqrt{E_s} \sum_{m=-N/2}^{N/2-1} a_m g(t - mT - \tau T) e^{j\phi} + n(t) \tag{3.1}$$

where $g(t) = g_T(t) \otimes c(t) \otimes f(t)$ (without loss of generality let us assume that $g(t)$ is real), $g_T(t)$ is the transmitter shaping function, $c(t)$ is the channel response, $f(t)$ is the prefilter, $n(t)$ is the additive white Gaussian noise (AWGN) with two-sided power spectral density (PSD) $N_0/2$, T is the symbol interval, $\{a_m\}$, $m \in \mathcal{Z}$ ($\mathcal{Z}$ the set of integers) is the training sequence drawn from the complex plane with $E[a_m] = 0$ and $E[|a_m|^2] = 1$. ϕ is the carrier phase offset. The delay jitter τT models the absence of symbol synchronization between transmitter and receiver, it is assumed that $\tau \in [-0.5, 0.5)$. Table 3.1 summarizes these notations. The received signal $x(t)$ is passed through a matched filter with response $g(-t)$ as shown in Figure 3.1. We assume that channel and prefilter are perfect, i.e., $g(t)$ is equal to the transmitter shaping function $g_T(t)$. The output $y(t)$ of the matched filter is sampled at the rate of $1/T_s$, typically $T = LT_s$, with L an integer. In the DA case, the TS $\{a_m\}$ ($m = -N/2, \cdots, N/2 - 1$) is known between the transmitter and receiver. The implicit assumption is that the timing offset τ remains fixed over the duration of observation.

$g_T(t)$	transmitter shaping function
$c(t)$	channel response
$f(t)$	prefilter response
$n(t)$	AWGN noise with PSD $N_0/2$
T	symbol interval
$\{a_m\}$	data sequence with $E[a_m] = 0$ and $E[\|a_m\|^2] = 1$
ϕ	carrier phase offset
τ	timing offset
N	training sequence length
L	sampling rate in samples per symbol

Table 3.1: Notations

3.2.1 Problem Formulation

The output of the matched filter is

$$y(t) = \sqrt{E_s} \sum_{m=-N/2}^{N/2-1} a_m r(t - mT - \tau T) e^{j\phi} + N(t), \tag{3.2}$$

where

$$\begin{aligned} r(t) &= \int_{-\infty}^{\infty} g(t+u)g(u)du \\ N(t) &= \int_{-\infty}^{\infty} n(t+u)g(u)du. \end{aligned}$$

Therefore,

$$y_k = \sqrt{E_s} \sum_{m=-N/2}^{N/2-1} a_m r(kT_s - mT - \tau T) e^{j\phi} + N_k \tag{3.3}$$

with $N_k = N(kT_s)$ that is a sequence of Gaussian random variables with zero mean and the auto-correlation function

$$R_y[k-l] = E[N_k N_l^*] = \frac{N_o}{2} r((k-l)T_s). \tag{3.4}$$

We can rewrite (3.3) in terms of matrix and vector product. First let us define the following vectors

$$\begin{aligned} \underline{y} &= [\ y_{-K/2} \ \cdots \ y_0 \ \cdots \ y_{K/2-1}\ ]^T \\ \underline{a} &= [\ a_{-N/2} \ \cdots \ a_0 \ \cdots \ a_{N/2-1}\ ]^T \\ \underline{N} &= [\ N_{-K/2} \ \cdots \ N_0 \ \cdots \ N_{K/2-1}\ ]^T \end{aligned} \tag{3.5}$$

where $K = L(N+R)$, R models the signal $y(t)$ beyond the TS portion in the ideal case in which a shaping pulse $r(t)$ modulated *only* by the TS $\underline{a}$ is transmitted and used to estimate the parameters. The observation window K is long enough to store the statistical information of $y(t)$. Because the CRB is a performance lower bound, therefore the estimation performance should not be better than the *ideal case*. Let us define a $K \times N$ matrix $R(\tau)$ with the $\{m,n\}$th element equal to $r((m-K/2)T_s - (n-N/2)T - \tau T)$, for $m = 0, 1, \cdots, K-1$, $n = 0, 1, \cdots, N-1$. With these notations, (3.3) can be written as

$$\underline{y} = \sqrt{E_s} R(\tau)\underline{a}e^{j\phi} + \underline{N}. \tag{3.6}$$

The likelihood function for ϕ and τ is formulated as follows. The mean of $\underline{y}$ given $\underline{a}$, ϕ and τ is

$$\underline{m}_y(\underline{a},\phi,\tau) = E[\underline{y}|\underline{a},\phi,\tau] = \sqrt{E_s} R(\tau)\underline{a}e^{j\phi}. \tag{3.7}$$

The auto-covariance matrix of the vector $\underline{y}$ is

$$\mathrm{cov}[\underline{y}|\underline{a},\phi,\tau] = \frac{N_o}{2}\Lambda, \tag{3.8}$$

where Λ is a $K \times K$ matrix defined as

$$\Lambda = \begin{bmatrix} r(0T_s) & r(-T_s) & \cdots & r(-(K-1)T_s) \\ r(T_s) & r(0T_s) & \cdots & r(-(K-2)T_s) \\ \vdots & \vdots & \ddots & \vdots \\ r((K-1)T_s) & r((K-2)T_s) & \cdots & r(0T_s) \end{bmatrix} \tag{3.9}$$

where the $\{k,m\}$th element is equal to $r_{km} = r[(k-m)T_s]$. Therefore Λ is a Toeplitz matrix (for a stationary random process). The likelihood function for ϕ, τ given $\underline{a}$ is

$$f(\underline{y}|\underline{a},\phi,\tau) = \frac{\exp\left\{-\frac{1}{2}(\underline{y}-\underline{m}_y)^H \left(\frac{N_o}{2}\Lambda\right)^{-1}(\underline{y}-\underline{m}_y).\right\}}{(2\pi)^{K/2}|\frac{N_o}{2}\Lambda|^{1/2}} \tag{3.10}$$

The log likelihood function is given by

$$\begin{aligned} l(\underline{y}|\underline{a},\phi,\tau) &= \log(f(\underline{y}|\underline{a},\phi,\tau)) \\ &= -\frac{1}{N_o}\left[-\underline{y}^H Q\underline{m}_y - \underline{m}_y^H Q\underline{y} + \underline{m}_y^H Q\underline{m}_y\right] \\ &\quad -\left(\frac{1}{N_o}\underline{y}^H Q\underline{y} + \log\left[(2\pi)^{K/2}\left|\frac{N_o}{2}\Lambda\right|^{1/2}\right]\right), \end{aligned} \tag{3.11}$$

where Q is the inverse matrix of Λ with the assumption that its inverse exists.

The $\mathrm{CRB}_{\mathrm{DA}}$'s are the diagonal elements of the inverse of the Fisher information matrix J [16] for the joint estimation $\{\phi,\tau\}$, where J is defined as

$$J = \begin{bmatrix} J_{\phi\phi} & J_{\phi\tau} \\ J_{\tau\phi} & J_{\tau\tau} \end{bmatrix} \tag{3.12}$$

whose element is given by (let $\underline{\theta} = [\theta_1\ \theta_2]$ with $\theta_1 = \phi$ and $\theta_2 = \tau$)

$$J_{\theta_i\theta_j} = E\left[-\frac{\partial^2 l(\underline{y}|\underline{a},\phi,\tau)}{\partial\theta_i\partial\theta_j},\right] \tag{3.13}$$

where E denotes the expectation with respect to $\underline{y}$, τ and ϕ if τ and ϕ are random, or it denotes the expectation with respect to $\underline{y}$ if they are deterministic

[16]. Let us average $J_{\theta_i\theta_j}$ with respect to $\underline{y}$ first. If the result depends on ϕ and τ then we shall compute them further based on the condition whether ϕ and τ are deterministic or not. The variable $J_{\theta_i\theta_j}$ is as follows (see Appendix)

$$\begin{aligned} J_{\theta_i\theta_j} &= \frac{1}{N_0}\left[\frac{\partial \underline{m}_y^H}{\partial\theta_i}Q\frac{\partial \underline{m}_y}{\partial\theta_j}+\frac{\partial \underline{m}_y^H}{\partial\theta_j}Q\frac{\partial \underline{m}_y}{\partial\theta_i}\right] \\ &= \frac{2}{N_0}\Re\left[\frac{\partial \underline{m}_y^H}{\partial\theta_i}Q\frac{\partial \underline{m}_y}{\partial\theta_j}\right]. \end{aligned} \tag{3.14}$$

According to (3.7), the following holds

$$\begin{aligned} \frac{\partial \underline{m}_y}{\partial\phi} &= j\sqrt{E_s}R(\tau)\underline{a}e^{j\phi} \\ \frac{\partial \underline{m}_y}{\partial\tau} &= \sqrt{E_s}\frac{\partial R(\tau)}{\partial\tau}\underline{a}e^{j\phi}. \end{aligned}$$

Therefore from (3.13), we can get

$$J_{\phi\phi} = \frac{2E_s}{N_0}\underline{a}^H R(\tau)^H Q R(\tau)\underline{a} \tag{3.15}$$

$$J_{\phi\tau} = \frac{2E_s}{N_0}\Re\left[(-j)\underline{a}^H R(\tau)^H Q\frac{\partial R(\tau)}{\partial\tau}\underline{a}\right] \tag{3.16}$$

$$J_{\tau\phi} = J_{\phi\tau} \tag{3.17}$$

$$J_{\tau\tau} = \frac{2E_s}{N_0}\underline{a}^H\frac{\partial R(\tau)^H}{\partial\tau}Q\frac{\partial R(\tau)}{\partial\tau}\underline{a}. \tag{3.18}$$

The $\mathrm{CRB}_{\mathrm{DA}}$'s for the DA joint estimation of carrier phase and timing offsets are given by

$$E\left[(\phi-\hat{\phi})^2\right] \geq \mathrm{CRB}_{\mathrm{DA}}(\phi) \triangleq \frac{J_{\tau\tau}}{J_{\phi\phi}J_{\tau\tau}-J_{\phi\tau}^2} \tag{3.19}$$

$$E\left[(\tau-\hat{\tau})^2\right] \geq \mathrm{CRB}_{\mathrm{DA}}(\tau) \triangleq \frac{J_{\phi\phi}}{J_{\phi\phi}J_{\tau\tau}-J_{\phi\tau}^2}. \tag{3.20}$$

3.2.2 Results from Toeplitz Matrices

Computing (3.15 -3.18) with an arbitrary TS $\underline{a}$ is quite difficult. In order to simplify the computation, $J_{\theta_i\theta_j}$ is approximated by being averaged over the TS $\underline{a}$

Figure 3.2: Packing Zero's with the Training Sequence $\{a_m\}$

when $\underline{a}$ is zero mean, i.i.d. and the number of training symbols N large enough in the literature [12, 28, 29, 31, 18], which follows from the strong law of large number.

We are intrigued by the fact that y_k is some sort of convolution of the TS $\underline{a}$ and the shaping pulse $r(kT_s)$, which implies multiplication in the frequency domain, therefore the frequency domain approach seems to be a natural solution. Before we introduce this method, let us reexamine the results about Toeplitz matrices derived in Chapter 2 and [25].

The auto-covariance matrix Λ (defined in (3.9)) is a Toeplitz matrix for a stationary random process. The evaluation of (3.15 -3.18) involves the convergence issue of the inverse of the Toeplitz matrix Λ in the strong sense (quadratic form). The finite boundary strong sense convergence theorem (Theorem 2), Corollary 1 and 2 can be applied here. Before we apply the theorems, let us examine the conditions of these theorems first:

- In our problem, $r(t)$ is the autocorrelation function of the noise process $N(t)$, e.g., $r(t)$ is a raised-cosine shaping pulse. The discrete-time Fourier transform (DTFT) of the sequence $\{r(kT_s)\}$ should be non-negative in its passband, in fact it is positive for the raised-cosine shaping pulse.

- In a typical communication receiver, the shaping pulse $\{r(kT_s)\}$ usually degrades faster than $O(1/|k|^2)$, e.g., the magnitude of the raised-cosine pulse converges to zero at a speed faster than $O(1/|k|^3)$. In engineering

practice, it is under the system designer's control to make the training portion (i.e., $\underline{m}_y$ (3.7)) satisfy the finite boundary condition through packing zeros along with the training sequence $\{a_m\}$. As explained in Chapter 2 and [25], the value of R is determined by the residue error of the (circular matrix) approximation. Figure 3.2 shows the training signal for timing and phase recovery. In Chapter 2 an upper bound for the quadratic-form-approximation error is derived. One reason we introduce R is for mathematical convenience and it coincidentally models the ideal case in which all the information about $y(t)$ is collected to estimate the parameters. The training sequence length N can be relaxed to an arbitrary number with the help of R. In the literature, Moeneclaey assumed large N in order to apply the strong law of large numbers.

Therefore the scenario meets the conditions to apply the strong sense convergence theorem.

3.2.3 The Derivation of the Cramer-Rao Lower Bound

According to Theorem 2, the inverse matrix Q can be approximated by a circular matrix $U_K^H D^{-1} U_K$. The matrix U_K is the discrete Fourier transform (DFT) matrix (defined in (2.2)), which introduces the frequency domain approach in which we are interested. The matrix D is a diagonal matrix with the ith diagonal element equal to $\mathcal{F}(2\pi i/K)$ and we introduce a new variable W with $W \triangleq U_K$. The DTFT $\mathcal{F}(\omega)$ of $r(kT_s)$ $(k = \cdots, -1, 0, 1, \cdots)$ is redefined as:

$$\mathcal{F}(\omega) = \sum_{k=-\infty}^{\infty} r(kT_s) e^{-j\omega k} \tag{3.21}$$

First, let us consider $WR(\tau)\underline{a}$, with its mth element equal to

$$\frac{1}{\sqrt{K}} \sum_{k=-K/2}^{K/2-1} \sum_{n=-N/2}^{N/2-1} r(kT_s - nT - \tau T) a_n e^{-j2\pi mk/K} e^{j\theta(m)}, \tag{3.22}$$

where $\theta(m)$ is a fixed phase shift independent of both ϕ and τ. According to our assumption that $r(kT_s)$ is assumed to be zero for large $|k|$ with negligible leakage, the summation with respect to k in (3.22) can be extended to $-\infty$ and ∞ for large K. Thus, the mth element of $WR(\tau)\underline{a}$ becomes

$$\frac{1}{\sqrt{K}} \sum_{n=-N/2}^{N/2-1} \sum_{k=-\infty}^{\infty} r(kT_s - nT - \tau T) a_n e^{-j2\pi mk/K} e^{j\theta(m)}. \tag{3.23}$$

Let $\mathcal{R}(\omega)$ be the Fourier transform of $r(t)$, i.e.,

$$\mathcal{R}(\omega) = \int_{-\infty}^{\infty} r(t) e^{-j\omega t} dt$$

and we observe that $\mathcal{R}(\omega)$ is the power spectrum density (PSD) of the noise process $N(t)$ and is non-negative. Then $\hat{\mathcal{R}}_{n,\tau}(\omega)$, the DTFT of $r(kT_s - nT - \tau T), k = \cdots, -1, 0, 1, \cdots$, is given by

$$\hat{\mathcal{R}}_{n,\tau}(\omega) = \frac{1}{T_s} \sum_{k=-\infty}^{\infty} \mathcal{R}\left(\frac{\omega}{T_s} - \frac{2\pi k}{T_s}\right) e^{-j(\tau+n)T(\omega/T_s - 2\pi k/T_s)}. \tag{3.24}$$

Clearly, $\hat{\mathcal{R}}_{0,0}(\omega) = \mathcal{F}(\omega)$ as previously defined by (3.21). Equation (3.23) becomes

$$\begin{aligned} &\frac{1}{\sqrt{K}} \sum_{n=-N/2}^{N/2-1} \hat{\mathcal{R}}_{n,\tau}\left(\frac{2\pi m}{K}\right) a_n e^{j\theta(m)} \\ =&\frac{1}{T_s\sqrt{K}} \sum_{k=-\infty}^{\infty} \mathcal{R}\left(\frac{2\pi m}{KT_s} - \frac{2\pi k}{T_s}\right) \mathcal{A}\left(\frac{2\pi m}{N+R} - 2\pi kL\right) \\ &e^{-j(\tau(2\pi m/(N+R) - 2\pi kL) + \theta(m))}, \end{aligned} \tag{3.25}$$

where $\mathcal{A}(\omega)$ is the DTFT of $\underline{a}$, which is defined by $\mathcal{A}(\omega) = \sum_{-N/2}^{N/2-1} a_n e^{-j\omega n}$. Similarly, the DTFT of $\dot{r}(kT_s - nT - \tau T)$ (where the derivative is with respect

to τ) is

$$\hat{\mathcal{R}}'_{n,\tau}(\omega) = \frac{-T}{T_s} \sum_{k=-\infty}^{\infty} j\left(\frac{\omega}{T_s} - \frac{2\pi k}{T_s}\right) . \mathcal{R}\left(\frac{\omega}{T_s} - \frac{2\pi k}{T_s}\right) e^{-j(\tau+n)T(\omega/T_s - 2\pi k/T_s)} \quad (3.26)$$

Let us define a new variable

$$\mathcal{RA}(m,k) \triangleq \frac{1}{T_s}\mathcal{R}\left(\frac{2\pi m}{KT_s} - \frac{2\pi k}{T_s}\right)\mathcal{A}\left(\frac{2\pi m}{N+R} - 2\pi kL\right). \quad (3.27)$$

The variable $J_{\phi\phi}$ from (3.15) becomes

$$J_{\phi\phi} = \frac{2E_s}{N_0 K}\sum_{m=0}^{K-1}\frac{\sum_{k,l=-\infty}^{\infty}\mathcal{RA}(m,k)\mathcal{RA}(m,l)^* e^{j2\pi\tau(k-l)L}}{\mathcal{F}(2\pi m/K)}, \quad (3.28)$$

$J_{\phi\tau}$ from (3.16) becomes

$$J_{\phi\tau} = -\frac{2E_s T}{N_0 K} \Re\left\{\sum_{m=0}^{K-1}\frac{\sum_{k,l=-\infty}^{\infty}\left(\frac{2\pi m}{KT_s} - \frac{2\pi k}{T_s}\right)\mathcal{RA}(m,k)\mathcal{RA}(m,l)^* e^{j2\pi\tau(k-l)L}}{\mathcal{F}(2\pi m/K)}\right\} \quad (3.29)$$

and $J_{\tau\tau}$ from (3.18) becomes

$$J_{\tau\tau} = \frac{2E_s T^2}{KN_0} \sum_{m=0}^{K-1}\frac{\sum_{k,l=-\infty}^{\infty}\left(\frac{2\pi m}{KT_s} - \frac{2\pi k}{T_s}\right)\left(\frac{2\pi m}{KT_s} - \frac{2\pi l}{T_s}\right)\mathcal{RA}(m,k)\mathcal{RA}(m,l)^* e^{j2\pi\tau(k-l)L}}{\mathcal{F}(2\pi m/K)}. \quad (3.30)$$

Let us discuss different scenarios according to the sampling rate L. We are interested in the case when L is an integer, because of its popularity.

The Over-Sampling Case

In the over-sampling case, L is no less than the Nyquist frequency, i.e., $1/T_s \geq 2B$ for B the bandwidth of $r(t)$. There is no aliasing in $\mathcal{F}(\omega)$ in the frequency domain. It is straightforward to verify that $J_{\phi\phi}$, $J_{\phi\tau}$ and $J_{\tau\tau}$ (3.28-3.30) are independent of ϕ and τ, therefore they are the same whether ϕ and τ are deterministic

or not. They are given by

$$J_{\phi\phi} = \frac{2E_s}{N_0 K} \sum_{m=-K/2}^{K/2-1} \mathcal{RA}_o(m) \tag{3.31}$$

$$J_{\phi\tau} = -\frac{2E_s}{N_0 K} \sum_{m=-K/2}^{K/2-1} \left(\frac{2\pi m}{N+R}\right) \mathcal{RA}_o(m) \tag{3.32}$$

$$J_{\tau\tau} = \frac{2E_s}{N_0 K} \sum_{m=-K/2}^{K/2-1} \left(\frac{2\pi m}{N+R}\right)^2 \mathcal{RA}_o(m) \tag{3.33}$$

where $\mathcal{RA}_o(m)$ (the subscript o refers to *over-sampling*) is defined as

$$\mathcal{RA}_o(m) \triangleq \frac{1}{T_s} \mathcal{R}\left(\frac{2\pi m}{KT_s}\right) \left|\mathcal{A}\left(\frac{2\pi m}{N+R}\right)\right|^2. \tag{3.34}$$

Basically $\mathcal{RA}_o(\omega) \triangleq \mathcal{R}(\omega)|\mathcal{A}(\omega)|^2$ is the PSD of the signal output from the matched filter.

The Under-Sampling Case

In the under-sampling case, L is less than the Nyquist frequency, i.e., $1/T_s < 2B$, There is aliasing in the frequency domain. In this scenario $J_{\phi\phi}$, $J_{\phi\tau}$ and $J_{\tau\tau}$ (3.28-3.30) are independent of ϕ but depend on τ, and they should be averaged with respect to $\underline{y}$ and τ. In practice, τ can be modeled by a uniformly distributed random variable in the receiver front-end. In a typical communication system, one-sample-per-symbol sampling rate ($L = 1$, $K = N + R$) is usually used. The following holds for arbitrary integers k and l

$$\int_{-1/2}^{1/2} e^{j2\pi\tau(k-l)} d\tau = \delta[k-l],$$

where $\delta[n] = 1$, if $n = 0$, and $\delta[n] = 0$, otherwise. Therefore $J_{\phi\phi}$, $J_{\phi\tau}$ and $J_{\tau\tau}$ in the under-sampling case become

$$J_{\phi\phi} = \frac{2E_s}{N_0 K} \sum_{m=-K/2}^{K/2-1} \frac{\mathcal{RA}_u(m)}{\mathcal{F}(2\pi m/K)} \tag{3.35}$$

$$J_{\phi\tau} = -\frac{2E_s}{N_0 K} \sum_{m=-K/2}^{K/2-1} \left(\frac{2\pi m}{N+R}\right) \frac{\mathcal{RA}_u(m)}{\mathcal{F}(2\pi m/K)} \tag{3.36}$$

$$J_{\tau\tau} = \frac{2E_s}{N_0 K} \sum_{m=-K/2}^{K/2-1} \left(\frac{2\pi m}{N+R}\right)^2 \frac{\mathcal{RA}_u(m)}{\mathcal{F}(2\pi m/K)} \tag{3.37}$$

where $\mathcal{RA}_u(m)$ (the subscript u refers to *under-sampling*) is defined as

$$\mathcal{RA}_u(m) \triangleq \sum_{k=-\infty}^{\infty} \frac{1}{T_s^2} \mathcal{R}\left(\frac{2\pi m}{KT_s} - \frac{2\pi k}{T_s}\right)^2 \left|\mathcal{A}\left(\frac{2\pi m}{N+R}\right)\right|^2. \tag{3.38}$$

In the calculation of (3.38), we use the fact that $\mathcal{A}(\omega - 2\pi k) = \mathcal{A}(\omega)$ with k an integer, therefore we can separate $\mathcal{A}(\omega)$ and the aliased $\mathcal{R}(\omega)^2$. In practice, a shaping pulse is always band-limited. Typically its effective bandwidth B ranges from $1/2T$ to $1/T$, therefore the variable k in (3.24) is usually from -1 to 1. If the sampling rate L is not an integer, the computation becomes more complicated because $\mathcal{A}(\omega)$ can not be separated from the aliased $\mathcal{R}(\omega)^2$.

3.3 Evaluating the Bounds

The $\mathrm{CRB}_{\mathrm{DA}}$ for phase and timing estimation is given by (3.19) (3.20). In the following presentation, we evaluate the bounds through evaluating $J_{\phi\phi}$, $J_{\phi\tau}$ and $J_{\tau\tau}$ separately.

3.3.1 $J_{\phi\tau}$: the Cost of Two Unknown Parameters

Since $J_{\phi\tau}^2 \geq 0$, from (3.19-3.20) it is clear that

$$\frac{J_{\tau\tau}}{J_{\phi\phi}J_{\tau\tau} - J_{\phi\tau}^2} \geq \frac{J_{\tau\tau}}{J_{\phi\phi}J_{\tau\tau}} = \frac{1}{J_{\phi\phi}} \tag{3.39}$$

$$\frac{J_{\phi\phi}}{J_{\phi\phi}J_{\tau\tau} - J_{\phi\tau}^2} \geq \frac{J_{\phi\phi}}{J_{\phi\phi}J_{\tau\tau}} = \frac{1}{J_{\tau\tau}} \tag{3.40}$$

It is easy to verify that the CRB for timing/phase estimation with known phase/timing offset is equal to $1/J_{\tau\tau}$ ($1/J_{\phi\phi}$) respectively, therefore $J_{\phi\tau}$ serves as the *cost* when both phase and timing offsets are unknown. There are two observations:

- The cost could be reduced to zero in the following manner. In the over-sampling case $J_{\phi\tau}$ is given by (3.32). According to the assumption that $r(t)$ is real, which means that $\mathcal{R}(\omega)$ is an even function; $(2\pi m/(N+R))$ is an odd function; if $|\mathcal{A}(\omega)|$ is an even function, which is a sufficient condition, $J_{\phi\tau} = 0$. In the under-sampling case, the same result holds.

- As pointed in [12, p.329], the random data TS could make $J_{\phi\tau} = 0$. A more general sufficient condition is proposed here. In fact, any real TS $\underline{a}$ could make $J_{\phi\tau}$ be equal to zero.

In the following presentation, we assume that $J_{\phi\tau}$ is equal to zero.

3.3.2 The $\mathrm{CRB}_{\mathrm{DA}}$ for Phase Estimation

The CRB for phase estimation is equal to

$$\mathrm{CRB}_{\mathrm{DA}}(\phi) = \frac{1}{J_{\phi\phi}} \tag{3.41}$$

where $J_{\phi\phi}$ is given by (3.31) and (3.35).

In the over-sampling case $J_{\phi\phi}$ is given by (3.31). According to Parseval's relation, for an orthogonal transform like K-point DFT, $\mathcal{RA}_o(m)$ becomes

$$\sum_{m=-K/2}^{K/2-1} \frac{1}{T_s}\mathcal{R}\left(\frac{2\pi m}{KT_s}\right)\left|\mathcal{A}\left(\frac{2\pi m}{N+R}\right)\right|^2 = K\sum_{l=-K/2}^{K/2-1} R(l)A(l) \tag{3.42}$$

where $R(l)$ and $A(l)$ are the inverse DFT (IDFT) of $\mathcal{R}(2\pi m/KT_s)$ and $\mathcal{A}(2\pi m/(N+R))$ respectively. It is straightforward to show that

$$R(l) = \frac{1}{K}\sum_{m=-K/2}^{K/2-1}\frac{1}{T_s}\mathcal{R}\left(\frac{2\pi m}{KT_s}\right)e^{j2\pi ml/K} = r(lT_s). \tag{3.43}$$

Similarly $A(l)$ is given by

$$\begin{aligned} A(l) &= \frac{1}{K}\sum_{k=-K/2}^{K/2-1}\left|\sum_{n=-N/2}^{N/2-1} a_n e^{-j2\pi kn/N}\right|^2 e^{j2\pi kl/K} \\ &= \sum_{n=-N/2}^{N/2-1}\sum_{m=-N/2}^{N/2-1} a_n a_m^* \delta[l-L(n-m)]. \end{aligned} \tag{3.44}$$

Therefore $J_{\phi\phi}$ is equal to

$$\begin{aligned} J_{\phi\phi} &= \frac{2E_s}{N_0}\sum_{l=-K/2}^{K/2-1} r(lT_s)\sum_{n=-N/2}^{N/2-1}\sum_{m=-N/2}^{N/2-1} a_n a_m^*\delta[l-L(n-m)] \\ &= \frac{2E_s}{N_0}\sum_{n=-N/2}^{N/2-1}|a_n|^2. \end{aligned} \tag{3.45}$$

The second quality in (3.45) follows for the Nyquist shape $r(lT_s)$ that is given by the following

$$r(lT_s) = \begin{cases} 1 & l=0 \\ 0 & l \text{ is other multiple of } L. \end{cases}$$

For PSK type modulation, (3.45) becomes

$$\mathrm{CRB}_{\mathrm{DA}}(\phi) = \left\{\frac{2E_sN}{N_0}\right\}^{-1} \tag{3.46}$$

From (3.46), the $\mathrm{CRB}_{\mathrm{DA}}(\phi)$ is independent of the specific shaping pulse and TS if the Nyquist shaping pulse and PSK modulation are applied. Actually $\mathrm{CRB}_{\mathrm{DA}}(\phi)$ is the same as the bound for phase estimation in the literature [12]. However the literature [12] does not address the CRB for phase estimation when both phase and timing are unknown in the under-sampling case.

We still focus our discussion on one sample per symbol ($L = 1$) and the Nyquist shaping pulse that has the following Fourier transform (FT)

$$\sum_k \mathcal{R}(\omega - 2\pi k/T) = T,$$

which implies the DTFT of $\{r(kT)\}$ $\mathcal{F}(\omega) = 1$. Because of its popularity, let us limit our discussion on the raised-cosine shaping pulse whose FT is

$$\mathcal{R}(\omega) = \begin{cases} T & 0 \le |\omega| \le \pi(1-\alpha)/T, \\ \frac{T}{2}\left[1 - \sin\left(\frac{T|\omega|-\pi}{2\alpha}\right)\right] & \pi(1-\alpha)/T \le |\omega| \le \pi(1+\alpha)/T, \\ 0 & \text{otherwise} \end{cases} \tag{3.47}$$

when rolloff factor α ranges from 0 to 1, the effective bandwidth of $r(t)$ ranges from $1/2T$ to $1/T$. Therefore for the Nyquist shaping pulse in the under-sampling case, from (3.35) we have

$$\begin{aligned} &\mathrm{CRB}_{\mathrm{DA}}(\phi) \\ &= \left\{ \frac{2E_s}{N_0(N+R)} \sum_{m=0}^{K-1} \sum_{k=0}^{1} \frac{1}{T^2} \mathcal{R}\left(\frac{2\pi m}{(N+R)T} - \frac{2\pi k}{T}\right)^2 \left|\mathcal{A}\left(\frac{2\pi m}{N+R}\right)\right|^2 \right\}^{-1} \end{aligned} \tag{3.48}$$

In summary, we have the following theorem:

Theorem 3 *In a DA joint timing and carrier phase offsets estimator, let* $\{a_n\}$ *(*$n = -N/2, \cdots, N/2-1$*) be the training sequence,* $r(t)$ *be the shaping pulse,* $\mathcal{A}(\omega)$ *be the discrete-time Fourier transform of* $\{a_n\}$*, and* $\mathcal{R}(\omega)$ *be the Fourier transform of* $r(t)$*.*

If the shaping pulse $r(t)$ is a Nyquist pulse with the maximum frequency between half symbol rate and one symbol rate, the mean square estimation error for phase ϕ is lower bounded by the following CRB:

$$E[(\hat{\phi}-\phi)^2] \geq \left\{ \frac{2E_s}{N_0} \sum_{n=-N/2}^{N/2-1} |a_n|^2 \right\}^{-1} \tag{3.49}$$

when the sampling rate is no less than two samples per symbol, or

$$E[(\hat{\phi}-\phi)^2] \geq \left\{ \frac{2E_s}{N_0 K} \sum_{m=-K}^{K-1} \frac{1}{T^2} \mathcal{R}\left(\frac{2\pi m}{KT}\right)^2 \left| \mathcal{A}\left(\frac{2\pi m}{K}\right) \right|^2 \right\}^{-1} \tag{3.50}$$

when the sampling rate is one sample per symbol. In (3.50) $K = N + R$, where R is a large number needed for (3.50) to converge.

The following observations can be made:

- The bound $\mathrm{CRB}_{\mathrm{DA}}(\phi)$ in the under-sampling case (3.50) with unknown timing information depends on both rolloff factor (shaping pulse) and the TS $\underline{a}$.

- Because $\sum_k \mathcal{R}(\omega - 2\pi k/T) \geq \mathcal{R}(\omega)$, therefore $\mathcal{R}(\omega)/T \leq 1$ holds for the Nyquist pulse. Compared with $J_{\phi\phi}$ in the over-sampling case (3.31), $\mathrm{CRB}_{\mathrm{DA}}(\phi)$ with $L = 1$ is larger than that with $L \geq 2$, i.e., the phase estimation has worse performance limit due to the aliasing in the frequency domain.

- Increasing the rolloff factor introduces more aliasing in the frequency domain, then the phase estimation performance degrades. As a special case, when $\alpha = 0$, $\mathrm{CRB}_{\mathrm{DA}}(\phi)$ with $L = 1$ is the same as that of over-sampling case ($L \geq 2$) because there is no aliasing at this point.

- Because R models the ideal case, in the numerical evaluation of the bound, it should be chosen to make the bound converge, i.e., when R is larger than some value the bound should not change.

3.3.3 The $\mathrm{CRB}_{\mathrm{DA}}$ for Timing Estimation

The $\mathrm{CRB}_{\mathrm{DA}}$ for timing estimation in the joint estimation is given by

$$\mathrm{CRB}_{\mathrm{DA}}(\tau) = \frac{1}{J_{\tau\tau}} \tag{3.51}$$

where $J_{\tau\tau}$ is given by (3.33) and (3.37). Similarly, we have the following theorem with the assumption that $\{a_n\}$ and $r(t)$ are real.

Theorem 4 *In a DA joint timing and phase offset estimator, let* $\{a_n\}$ $(n = -N/2, \cdots, N/2-1)$ *be the training sequence,* $r(t)$ *be the shaping pulse,* $\mathcal{A}(\omega)$ *be the discrete-time Fourier transform of* $\{a_n\}$*,* $\mathcal{R}(\omega)$ *be the Fourier transform of* $r(t)$*, and* L *be the sampling rate in samples per symbol.*

If the shaping pulse $r(t)$ *is a Nyquist pulse with the maximum frequency between half symbol rate and one symbol rate, the mean square estimation error for timing offset* τ *is lower bounded by the following CRB:*

$$E[(\hat{\tau}-\tau)^2] \geq \left\{ \frac{2E_s}{N_0(N+R)} \left[\sum_{m=-K/2}^{K/2-1} \left(\frac{2\pi m}{N+R}\right)^2 \frac{1}{T} \mathcal{R}\left(\frac{2\pi m}{(N+R)T}\right) \left| \mathcal{A}\left(\frac{2\pi m}{N+R}\right) \right|^2 \right] \right\}^{-1} \tag{3.52}$$

when the sampling rate is no less than two sample per symbol, where $K = L(N+$

R); or

$$E[(\hat{\tau}-\tau)^2] \geq$$
$$\left\{ \frac{2E_s}{N_0(N+R)} \left[\sum_{m=-K}^{K-1} \left(\frac{2\pi m}{N+R} \right)^2 \frac{1}{T^2} \mathcal{R}\left(\frac{2\pi m}{(N+R)T} \right)^2 \left| \mathcal{A}\left(\frac{2\pi m}{N+R} \right) \right|^2 \right] \right\}^{-1} \tag{3.53}$$

when the sampling rate is one sample per symbol, and $K = N + R$, where R is a large number that makes (3.52, 3.53) converge.

Similarly because $\mathcal{R}(\omega)/T \leq 1$ for the Nyquist pulse, $\mathrm{CRB}_{\mathrm{DA}}(\tau)$ with $L \geq 2$ (3.52) is smaller than that with $L = 1$ (3.53) because there is no aliasing.

In previous works, the CRB for timing estimation was derived in the literature [31] for both over and under-sampling cases. When the sampling rate $L \geq 2$, the CRB (denoted as $\mathrm{CRB}_{\mathrm{RD}}(\tau)$) with the assumption that the TS is i.i.d. random data and the sequence length N is long enough is given by

$$\mathrm{CRB}_{\mathrm{RD}}(\tau) = \frac{1}{T^2} \left\{ \frac{2E_s}{N_0} N \int_{-\infty}^{\infty} 4\pi^2 f^2 \mathcal{R}(2\pi f) df \right\}^{-1} \tag{3.54}$$

In the under-sampling case with $L = 1$ and the Nyquist pulse, $\mathrm{CRB}_{\mathrm{RD}}(\tau)$ is given by

$$\mathrm{CRB}_{\mathrm{RD}}(\tau) = \frac{1}{T^2} \left\{ \frac{2E_s}{N_0} N \frac{1}{T} \int_{-\infty}^{\infty} \dot{r}^2(t) dt \right\}^{-1}. \tag{3.55}$$

In the following subsection, we shall show that (3.51) and (3.54) are special cases of our bound with the same i.i.d. random data and large N assumption. Equations (3.51) and (3.54) provide people little insight on the effects of TS on the bound.

3.3.4 The Ideal Case: $R \to \infty$

Let $\Delta f = 1/(N+R)$, because N and R are bounded, as either of them goes to ∞, we have the following integral expressions for the bounds. When $L = 1$, $\mathrm{CRB}_{\mathrm{DA}}(\phi)$ is

$$\mathrm{CRB}_{\mathrm{DA}}(\phi) = \left\{ \frac{2E_s}{N_0 T^2} \int_{-\infty}^{\infty} \mathcal{R}\left(\frac{2\pi f}{T}\right)^2 |\mathcal{A}(2\pi f)|^2 \, df \right\}^{-1}, \tag{3.56}$$

$\mathrm{CRB}_{\mathrm{DA}}(\tau)$ is

$$\mathrm{CRB}_{\mathrm{DA}}(\tau) = \left\{ \frac{2E_s}{N_0 T^2} \int_{-\infty}^{\infty} 4\pi^2 f^2 \mathcal{R}\left(\frac{2\pi f}{T}\right)^2 |\mathcal{A}(2\pi f)|^2 df \right\}^{-1}. \tag{3.57}$$

For $L \geq 2$, because the phase bound has closed form in (3.46), we only address the timing bound that is

$$\mathrm{CRB}_{\mathrm{DA}}(\tau) = \left\{ \frac{2E_s}{N_0 T} \int_{-\infty}^{\infty} 4\pi^2 f^2 \mathcal{R}\left(\frac{2\pi f}{T}\right) |\mathcal{A}(2\pi f)|^2 df \right\}^{-1}. \tag{3.58}$$

Equations (3.56-3.57) are actually the ultimate bounds for arbitrary TS with length N and infinite observation length, i.e., R goes to ∞. Equations (3.48-3.53) provide a way to evaluate the bounds numerically. The difference between the bounds obtained from (3.48-3.53) and the asymptotic ones from (3.56-3.58) reveals the residue error caused by finite R. In practice, R should be chosen to make (3.48-3.53) converge. In our numerical evaluation of the bounds $R \geq 100$ is sufficient in most cases.

Let us revisit the bounds derived by Moeneclaey. For zero mean, i.i.d. TS $\underline{a}$,

as the length N goes to ∞, the PSD of $\underline{a}$ is

$$\begin{aligned}\left|\mathcal{A}\left(\frac{2\pi m}{N+R}\right)\right|^2 &= \sum_{n=-N/2}^{N/2-1}\sum_{k=-N/2}^{N/2-1} a_n a_k^* e^{-j(2\pi m(n-k)/(N+R))} \\ &\approx \sum_{n=-N/2}^{N/2-1}\sum_{k=-N/2}^{N/2-1} E[a_n a_k^*] e^{-j(2\pi m(n-k)/(N+R))} \\ &= \sum_{n=-N/2}^{N/2-1}\sum_{k=-N/2}^{N/2-1} \delta[n-k] e^{-j(2\pi m(n-k)/(N+R))} \\ &= N.\end{aligned} \tag{3.59}$$

The second equality in (3.59) follows from the strong law of large numbers. Substituting $|\mathcal{A}(2\pi f)|^2$ with N in (3.58), we can see that the $\mathrm{CRB}_{\mathrm{RD}}(\tau)$ in the over-sampling case is equivalent to (3.58) with the long random data assumption. In the under-sampling case, applying Parseval's relation, for real $r(t)$ we get

$$\frac{1}{T}\int_{-\infty}^{\infty} \dot{r}(t)^2 dt = \int_{-\infty}^{\infty} \left(2\pi f \mathcal{R}\left(\frac{2\pi f}{T}\right)\right)^2 df.$$

Therefore the $\mathrm{CRB}_{\mathrm{RD}}(\tau)$ for both cases derived in the previous literature are the special cases of our bound derived in this paper with zero mean, i.i.d. and long random data assumption.

3.3.5 Several Example Cases

The $\mathrm{CRB}_{\mathrm{DA}}$'s give us insight on the effect of the training data pattern on the estimation performance limit. We are going to address several data patterns based on QPSK signaling.

- CW Pattern

  The continuous wave (CW) pattern is the TS with data pattern $a_k = \sqrt{2}/2(1+j)$, (for $k = -N/2-1, \cdots, N/2$). It is usually used in the

rolloff factor α	$J_{\tau\tau}/(2E_s/N_0)$
0.25	2.8328
0.50	3.0417
0.75	3.5326
1.00	5.5439

Table 3.2: Normalized $\mathrm{CRB}_{\mathrm{DA}}(\tau)$ of CW with $N = 20$ and $L = 2$

rolloff factor α	$J_{\tau\tau}/(2E_s/N_0)$
0.25	2.8330
0.50	3.0416
0.75	3.5329
1.00	5.5449

Table 3.3: Normalized $\mathrm{CRB}_{\mathrm{DA}}(\tau)$ of CW with $N = 50$ and $L = 2$

rolloff factor α	$J_{\tau\tau}/(2E_s/N_0)$
0.25	2.8330
0.50	3.0416
0.75	3.5329
1.00	5.5450

Table 3.4: Normalized $\mathrm{CRB}_{\mathrm{DA}}(\tau)$ of CW with $N = 100$ and $L = 2$

burst preamble in TDMA networks to expedite carrier acquisition. Equation (3.33) is adopted to calculate $J_{\tau\tau}$ in the over-sampling case. Table 3.2, 3.3 and 3.4 show the normalized $J_{\tau\tau}$. We can see that $J_{\tau\tau}/(2E_s/N_o)$ is independent of the sequence length N, e.g., as rolloff factor $\alpha = 0.5$, $J_{\tau\tau}/(2E_s/N_o) = 3.04$, which does not increase as N increases. As N goes to ∞, if we ignore R when calculating $\mathcal{A}(\omega)$, we can get the following DFT,

$$\left|\mathcal{A}\left(\frac{2\pi m}{N}\right)\right| \approx \begin{cases} N & \text{if } m = 0, \\ 0 & \text{if } m = -N/2, \cdots, -1, 1, \cdots, N/2 - 1. \end{cases} \tag{3.60}$$

Therefore $J_{\tau\tau} \approx 0$, i.e., $\mathrm{CRB}_{\mathrm{DA}}(\tau) \approx \infty$, the CW pattern provides little timing information. We have two observations:

- As heuristically explained in [12, p.336], the CW pattern is not suitable for timing recovery. The bound $\mathrm{CRB}_{\mathrm{DA}}(\tau)$ provides an analytical explanation.
- If we consider the finite TS length N case, with the help of the extended observation window length R the transition from pure noise to CW portion in $y(t)$, and from CW to fade gives us *some* timing information. This explains the reason why $J_{\tau\tau} \neq 0$, and $J_{\tau\tau}$ doesn't increase as N increases.

- Alternating One-Zero Pattern

  The alternating one zero pattern is the TS with data pattern $a_k = \sqrt{2}/2(1+j)$, k is even, and $a_k = -\sqrt{2}/2(1+j)$, k is odd. It is widely used as the preamble in TDMA frame structure for timing recovery. The $\mathrm{CRB}_{\mathrm{DA}}(\tau)$ supports it through the fact that it has much smaller estimation variance

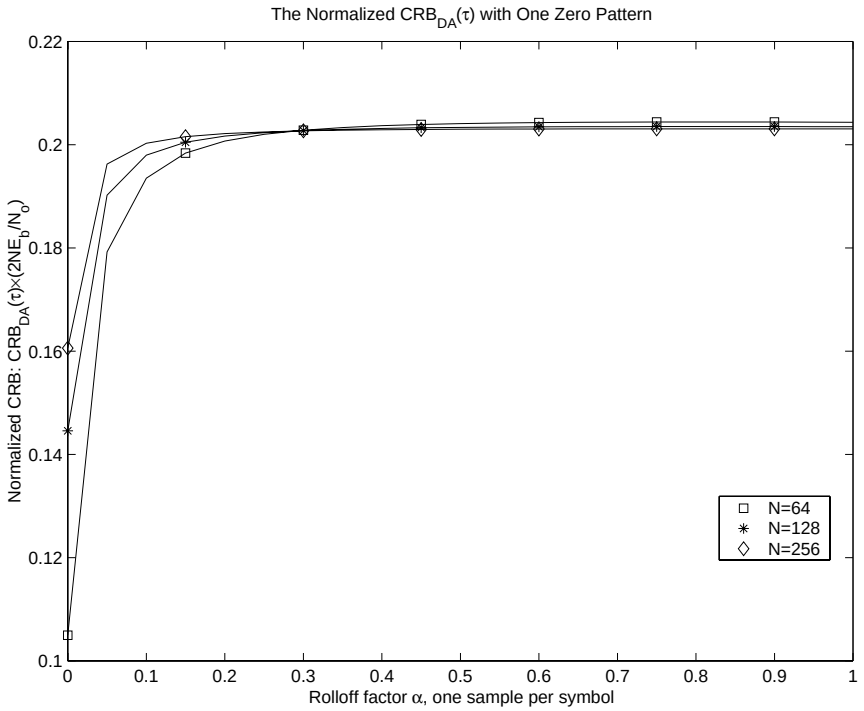

Figure 3.3: The Normalized $\mathrm{CRB}_{\mathrm{DA}}(\tau)$ for One-Zero Pattern, One Sample per Symbol

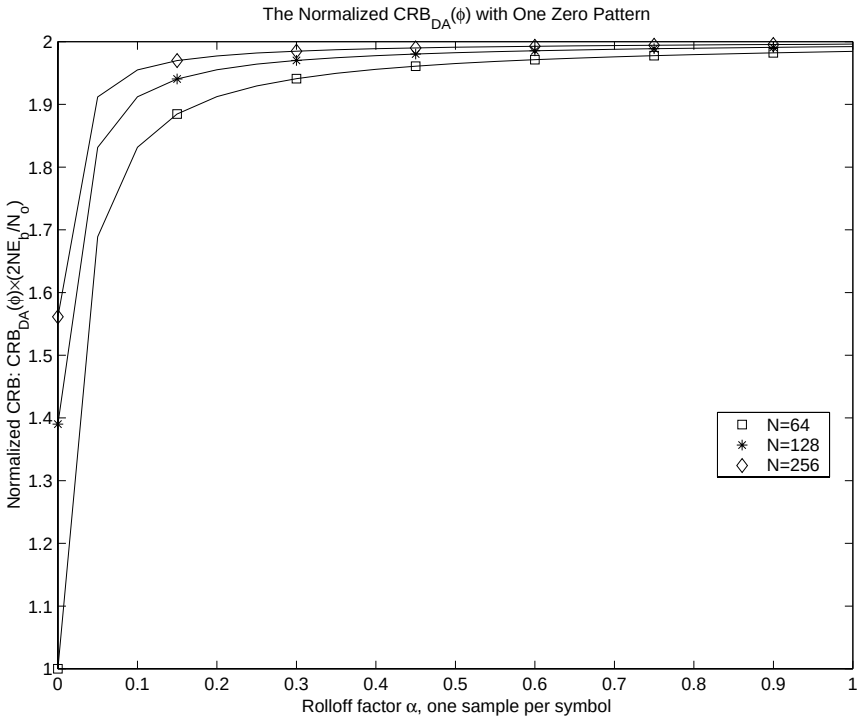

Figure 3.4: The Normalized $\mathrm{CRB}_{\mathrm{DA}}(\phi)$ for One-Zero Pattern, One Sample per Symbol

compared with the pseudo-random data pattern. Equations (3.52-3.53) are applied to evaluate the bound. The spectrum $|\mathcal{A}(\omega)|$ of $\underline{a}$ is a tone type with central frequency at half symbol rate. When the sequence length N is small, the side-lobe around half symbol rate is significant; as N increase, the side-lobe reduces. Hence for very sharp rolloff factor (i.e., $\alpha \approx 0$), the CRB is very sensitive to the interpolation length R. As N goes to ∞, for $\forall \alpha > 0$ we can drop R and obtain $|\mathcal{A}(\omega)|$ that is equal to the following

$$\left|\mathcal{A}\left(\frac{2\pi m}{N}\right)\right| \approx \begin{cases} N & \text{if } m = N/2, \\ 0 & \text{if } m = 0, \cdots, N/2-1, N/2+1, \cdots, N-1. \end{cases} \tag{3.61}$$

For the raised cosine shape $1/T\mathcal{R}(1/2T) = 1/2$ with $\forall \alpha$. Hence for N large enough and $L \geq 2$, the CRB for timing estimation is

$$\mathrm{CRB}_{\mathrm{DA}}(\tau) \approx \left\{2\pi^2 \frac{E_s}{N_0} N\right\}^{-1} \tag{3.62}$$

When the sampling rate $L = 1$, the CRB for timing estimation is 3dB worse than that with $L \geq 2$ (3.61):

$$\mathrm{CRB}_{\mathrm{DA}}(\tau) \approx \left\{\pi^2 \frac{E_s}{N_0} N\right\}^{-1} \tag{3.63}$$

the CRB for phase estimation is

$$\mathrm{CRB}_{\mathrm{DA}}(\phi) \approx \left\{\frac{E_s}{N_0} N\right\}^{-1}. \tag{3.64}$$

Figure 3.3 shows the normalized CRB for timing estimation ($\mathrm{CRB}_{\mathrm{DA}}(\tau) \times (2NE_s/N_0)$) with $L = 1$. As N increase the normalized $\mathrm{CRB}_{\mathrm{DA}}(\tau)$ converges to $2/\pi^2$ (≈ 0.203, according to (3.63)) for $\alpha > 0$. The $\mathrm{CRB}_{\mathrm{DA}}(\tau)$ with $L = 1$ is close to the bound with $L \geq 2$ as $\alpha \approx 0$ (because there is little aliasing in the frequency domain). Since the *side-lobe* effect reduces

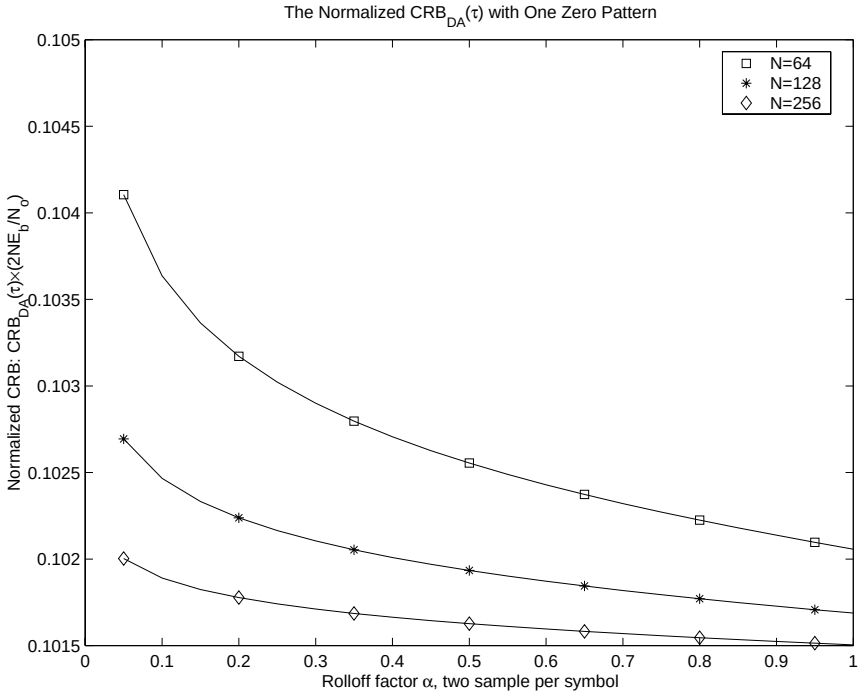

Figure 3.5: The Normalized $\mathrm{CRB}_{\mathrm{DA}}(\tau)$ for One-Zero Pattern, Two Samples per Symbol

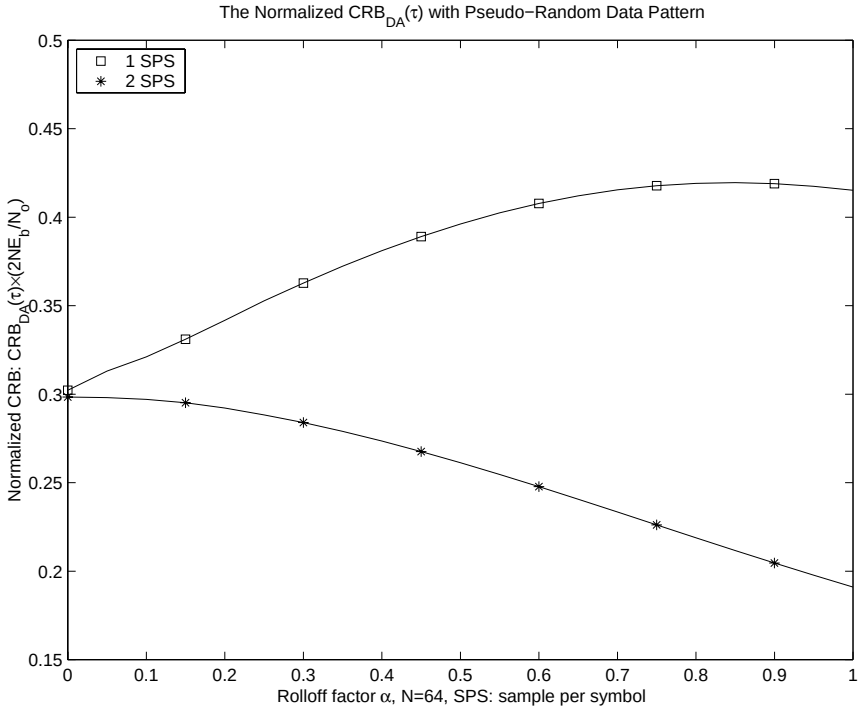

Figure 3.6: The Normalized $\mathrm{CRB}_{\mathrm{DA}}(\tau)$ for Pseudo-Random Data Pattern

as N increases for $\alpha > 0$, the normalized $\mathrm{CRB}_{\mathrm{DA}}(\tau)$ converges to 0.203 quickly, which is shown in Figure 3.3. Figure 3.4 shows the normalized CRB for phase estimation ($\mathrm{CRB}_{\mathrm{DA}}(\phi) \times (2NE_s/N_0)$) with $L = 1$. Similarly, as N increases the normalized $\mathrm{CRB}_{\mathrm{DA}}(\phi)$ converges to 2 (according to (3.64)) for $\alpha > 0$. Figure 3.5 shows the normalized $\mathrm{CRB}_{\mathrm{DA}}(\tau)$ in the over-sampling case with $L = 2$. First we observe that the performance increases as rolloff factor α increases (increasing signal bandwidth). It also shows that as N increases, the side-lobe of $|\mathcal{A}(\omega)|$ reduces, the normalized $\mathrm{CRB}_{\mathrm{DA}}(\tau)$ converges to $1/\pi^2$ (≈ 0.101, according to (3.62)).

- Pseudo-Random Data Pattern

  The pseudo-random data pattern (e.g., M-sequence, unique word (UW)) is used to do joint timing and phase estimation in some systems. A 64-

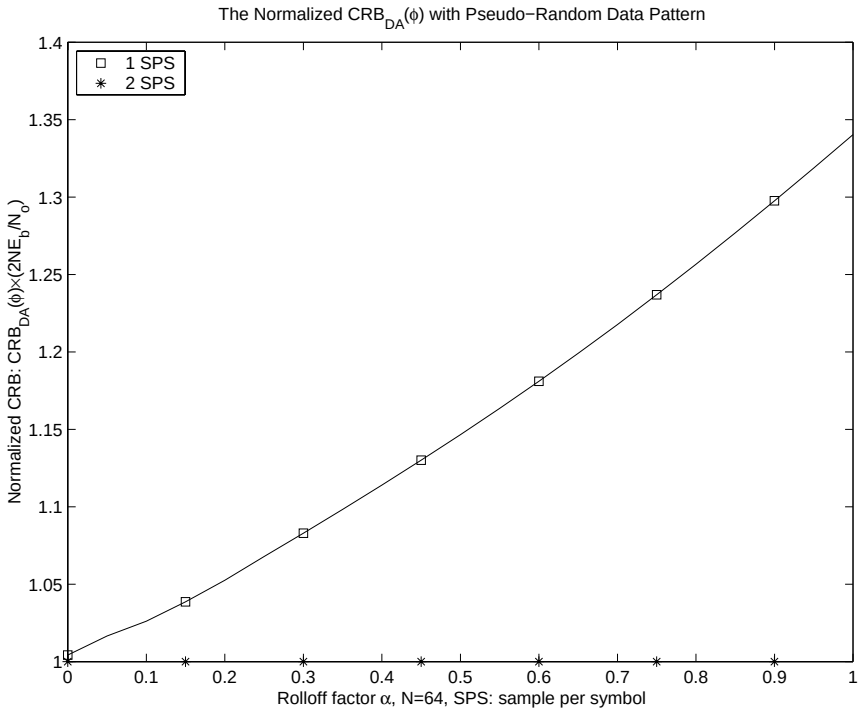

Figure 3.7: The Normalized $\mathrm{CRB}_{\mathrm{DA}}(\phi)$ for Pseudo-Random Data Pattern

symbol UW is selected to evaluate the CRB. The normalized $\mathrm{CRB}_{\mathrm{DA}}(\tau)$ is shown in Figure 3.6 for $L = 1, 2$. There are several observations based on this result:

- The timing estimation performance of the pseudo-random data pattern is worse than that of the one-zero pattern in both the over and under-sampling cases. For example, when $L = 1$ and $\alpha = 0.5$, the normalized $\mathrm{CRB}_{\mathrm{DA}}(\tau)$ of the one-zero pattern is 0.203 and that of the UW pattern is 0.396.
- In the under-sampling case, unlike the one-zero pattern whose $|\mathcal{A}(\omega)|$ is a tone in the frequency domain, the PSD of the pseudo-random pattern is relatively flat. As the rolloff factor α increases, there are two factors influencing performance: increasing α increases bandwidth,

which tends to improve performance; however at the same time, increasing α results in more aliasing, which tends to decrease performance. Hence there is a certain α which causes worst performance.

– In the over-sampling case, the estimation performance increases as the rolloff factor increases because there is no aliasing.

Figure 3.7 shows the normalized $\mathrm{CRB}_{\mathrm{DA}}(\phi)$. In the under-sampling case, according to (3.48) increasing the rolloff factor increases aliasing therefore decreases the estimation performance. One interesting issue is that the phase estimation performance of the UW is better than that of the one-zero pattern in this case. In the over-sampling case, the performance is independent of the rolloff factor and the TS for the Nyquist pulse (3.46).

3.4 The MCRB for DA Timing Estimation in Flat Fading Channel

In this section, we are going to address the performance limit of timing estimation in fading channels. The derivation of the bound for joint timing and phase estimation follows the same strategy as before.

3.4.1 Problem Formulation

The complex baseband signal is modeled as:

$$x(t) = \sqrt{E_s} \sum_{n=-N/2}^{N/2-1} h(t) a_m g(t - mT - \tau T) + n(t) \tag{3.65}$$

where $h(t)$ is the fading induced multiplicative noise, other signals are the same as those defined in Table 3.1. There is an assumption on $h(t)$: $h(t)$ is a complex-valued stationary Gaussian process with zero mean and unit variance. The autocorrelation function of $h(t)$ is defined as $r_h(v) = E[h(t)h(t-v)^*]$, and its PSD $S_h(\omega)$ is the Fourier transform of $r_h(v)$.

Similarly the received signal $x(t)$ is passed through a matched filter with response $g(-t)$ as shown in Figure 3.1. The output $y(t)$ of the matched filter is sampled at the rate of $1/T_s$ with $T = LT_s$. In this section, we assume that the sampling rate L is no less than the Nyquist sampling rate because of its popularity; the under-sampling case follows the same methodology applied in this section and Section 3.2. The signal $y(t)$ is equal to

$$\begin{aligned} y(t) =& x(t) \otimes g(-t) \\ \approx& \sqrt{E_s} \sum_{n=-N/2}^{N/2-1} h(t) a_m r(t - mT - \tau T) + N(t) \end{aligned} \tag{3.66}$$

where $r(t) = g(t) \otimes g(-t)$ and $N(t) = n(t) \otimes g(-t)$. Since the vast majority of wireless systems operating over fading channels are designed so that fading rates remain well below the symbol rate, the approximation $h(t+u) \approx h(t)$ can be taken to be valid within the duration of the pulse $g(-t)$ whose main lobe spans the region $-T < t < T$ [12, p.589]. Use the notations $\underline{y}$, $\underline{a}$, $\underline{N}$ and $R(\tau)$, and define a diagonal matrix H as

$$H = diag[h_{-K/2}, \cdots, h_{K/2-1}]$$

where $h_k = h(kT_s)$.

Our objective is to estimate the timing offset τ from $K = L(N+R)$ samples of $y(t)$ without knowing $h(t)$. In this case, $h(t)$ is a nuisance parameter. Before

deriving the performance limit, let us address the *modified* Cramer-Rao lower bound (MCRB) first.

3.4.2 The Modified Cramer-Rao Lower Bound

In our problem because $h(t)$ is a nuisance parameters, it is mathematically intractable to calculate the CRB. To cope with this situation, the *modified* CRB (MCRB) [13] [18] was proposed. First, let us revisit the definition of the CRB when a nuisance parameter is present. The CRB is defined as

$$\mathrm{CRB}(\lambda) = \frac{1}{E_{\underline{r}}\left[-\dfrac{\partial^2}{\partial\lambda^2}\ln f(\underline{r};\lambda)\right]} \tag{3.67}$$

where $\underline{r}$ is the observation vector, λ is a deterministic/random parameter we want to estimate, $\underline{r} = s(\lambda, \underline{u}) + \underline{n}$, $\underline{u} = [u_0, \cdots, u_{P-1}]$ is a random nuisance vector parameter with *a priori* $f(\underline{u})$. The expectation $E_{\underline{r}}[\cdot]$ is with respect to the pdf $f(\underline{r};\lambda)$, which is obtained as

$$f(\underline{r};\lambda) = E_{\underline{u}}[f(\underline{r}|\underline{u};\lambda)], \tag{3.68}$$

where $E_{\underline{u}}[\cdot]$ denotes the expectation with respect to the *a priori* $f(\underline{u})$. In the equations above $f(\underline{r};\lambda)$ and $f(\underline{r}|\underline{u};\lambda)$ are the likelihood functions of λ and of λ and $\underline{u}$ respectively. Because of the expectation in (3.67) and (3.68), the CRB is often very hard to compute in the case of the estimation in the presence of nuisance parameters. In [18], the MCRB has been investigated. This bound on the variance of any unbiased estimator is given by

$$E_{\underline{r}}[(\hat{\lambda}(\underline{r}) - \lambda)^2] \geq \mathrm{MCRB}(\lambda) \tag{3.69}$$

where

$$\mathrm{MCRB}(\lambda) = \left\{ E_{\underline{u}} \left[E_{\underline{r}|\underline{u}} \left[-\frac{\partial^2}{\partial \lambda^2} \ln f(\underline{r}|\underline{u};\lambda) \right] \right] \right\}^{-1} \tag{3.70}$$

and $E_{\underline{r}|\underline{u}}[\cdot]$ denotes the expectation with respect to $f(\underline{r}|\underline{u};\lambda)$. It has been shown that

$$\mathrm{MCRB}(\lambda) \leq \mathrm{CRB}(\lambda) \tag{3.71}$$

in [18], which indicates that $\mathrm{MCRB}(\lambda)$ is a looser lower bound than $\mathrm{CRB}(\lambda)$.

3.4.3 The Calculation of the MCRB

In our problem, $\underline{y}$ is the $\underline{r}$ in (3.67), H is the nuisance variable $\underline{u}$, and τ is the variable λ we want to estimate. The mean of $\underline{y}$ given $\underline{a}$, H and τ is

$$\underline{m}_y(\underline{a}, H, \tau) = E[\underline{y}|\underline{a}, H, \tau] = \sqrt{E_s} H R(\tau) \underline{a}. \tag{3.72}$$

The log likelihood function is the same as (3.11) except for different $\underline{m}_y$ (3.72).

The modified Fisher information is given by

$$\begin{aligned} J_\tau &= E_H \left[E_{\underline{y}|H} \left[-\frac{\partial^2}{\partial \tau^2} l(\underline{y}|\underline{a}, H, \tau) \right] \right] \\ &= E_H \left[\frac{2}{N_0} \Re \left[\frac{\partial \underline{m}_y^H}{\partial \tau} Q \frac{\partial \underline{m}_y}{\partial \tau} \right] \right] \\ &= E_H[J_\tau{}']. \end{aligned} \tag{3.73}$$

Substituting (3.72) into (3.73), we get

$$J_\tau^{'} = \frac{2E_s}{N_0} \underline{a}^H \frac{\partial R(\tau)^H}{\partial \tau} H^H Q H \frac{\partial R(\tau)}{\partial \tau} \underline{a}. \tag{3.74}$$

Apply the finite boundary strong sense convergence theorem, replace Q with $W^H D^{-1} W$, where D and W remain the exactly same as those in Section 3.2, rewrite (3.74) as the following

$$J_\tau^{'} = \frac{2E_s}{N_0} \underline{a}^H \frac{\partial R(\tau)^H}{\partial \tau} H^H W^H D^{-1} W H \frac{\partial R(\tau)}{\partial \tau} \underline{a}. \tag{3.75}$$

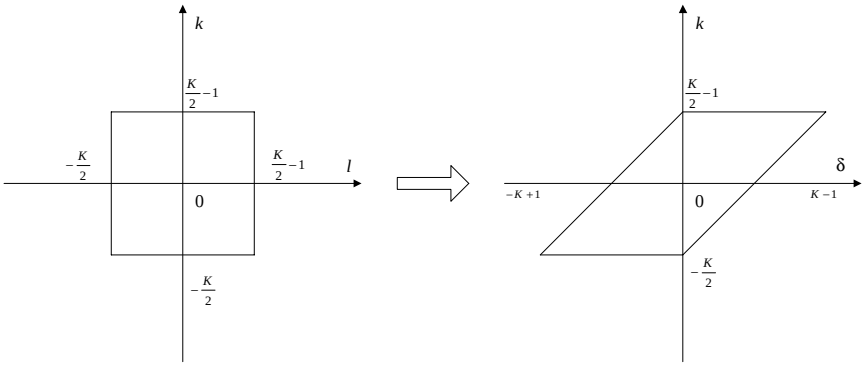

Figure 3.8: Variable Change: $l \to \delta$

The modified Fisher information becomes

$$J_\tau = \sum_{m=0}^{K-1} \frac{2E_s T^2}{KN_0 \mathcal{F}(2\pi m/K)} E_H \left[\left| \sum_{k=-K/2}^{K/2-1} \sum_{n=-N/2}^{N/2-1} h(kT_s)\dot{r}(kT_s - nT - \tau T) a_n e^{-j2\pi mk/K} \right|^2 \right] \tag{3.76}$$

where the derivative is with respect to t, and $\mathcal{F}(\omega)$ is the DTFT of $\{r(kT_s)\}$. The expectation in (3.76) is equal to

$$\begin{aligned}
&\sum_{n,p=-N/2}^{N/2-1} \sum_{k,l=-K/2}^{K/2-1} E_H[h(kT_s)h^*(lT_s)]\dot{r}(kT_s - nT - \tau T) \\
&\dot{r}(lT_s - pT - \tau T) a_n a_p^* e^{-j2\pi(k-l)m/K} \\
&= \sum_{n,p=-N/2}^{N/2-1} \sum_{\delta=-K+1}^{K-1} \sum_{k \in f(\delta)} r_h(\delta T_s)\dot{r}(kT_s - nT - \tau T) \\
&\dot{r}((k-\delta)T_s - pT - \tau T) a_n a_p^* e^{-j2\pi\delta m/K} \\
&\approx \sum_{n,p=-N/2}^{N/2-1} \sum_{\delta=-K+1}^{K-1} r_h(\delta T_s) q(\delta T_s - (n-p)T) a_n a_p^* e^{-j2\pi\delta m/K} \\
&= \sum_{\delta=-K+1}^{K-1} r_h(\delta T_s) \left[\sum_{n,p=-N/2}^{N/2-1} q(\delta T_s - (n-p)T) a_n a_p^* \right] e^{-j2\pi\delta m/K}
\end{aligned} \tag{3.77}$$

where $\delta = k - l$ and the function $f(\delta)$ in the first equality is equal to

$$f(\delta) = \begin{cases} [-K/2, \delta + K/2 - 1] & -(K-1) \le \delta < 0 \\ [\delta - K/2, K/2 - 1] & 0 \le \delta \le (K-1) \end{cases} \tag{3.78}$$

which is shown in Figure 3.8. The variable $q(t)$ in (3.77) is defined as

$$q(t) = \dot{r}(t) \otimes \dot{r}(-t) = \int_{-\infty}^{\infty} \dot{r}(\tau)\dot{r}(\tau - t)d\tau.$$

The second equality follows from the equivalence theorem of digital and analog signal processing [12, p.259,p.337] for large K (i.e., R), Nyquist sampling rate $L \ge 2$ and time-limited shaping pulse $r(t)$ with negligible boundary leakage, i.e.,

$$\begin{aligned} & \sum_{k \in f(\delta)} \dot{r}(kT_s - nT - \tau T)\dot{r}(kT_s - \delta T_s - pT - \tau T) \\ \approx & \sum_{k=-\infty}^{\infty} \dot{r}(kT_s - nT - \tau T)\dot{r}(kT_s - \delta T_s - pT - \tau T) \\ = & q(\delta T_s - (n-p)T). \end{aligned}$$

The DFT $\mathcal{I}(m)$ of the inner summation in the third equality of (3.77) is equal to

$$\begin{aligned} \mathcal{I}(m) = & \sum_{\delta=-K+1}^{K-1} \left[\sum_{n,p=-N/2}^{N/2-1} a_n a_p^* q(\delta T_s - (n-p)T) \right] e^{-j2\pi\delta m/K} \\ \approx & \sum_{n,p=-N/2}^{N/2-1} a_n a_p^* \sum_{\delta=-\infty}^{\infty} q(\delta T_s - (n-p)T) e^{-j2\pi\delta m/K} \\ = & \mathcal{Q}\left(\frac{2\pi m}{K}\right) \sum_{n=-N/2}^{N/2-1} a_n e^{-j2\pi nmL/K} \sum_{p=-N/2}^{N/2-1} a_p^* e^{j2\pi pmL/K} \\ = & \mathcal{Q}\left(\frac{2\pi m}{K}\right) \left| \mathcal{A}\left(\frac{2\pi mL}{K}\right) \right|^2 \end{aligned} \tag{3.79}$$

where we use the fact that L is no less than the Nyquist sampling rate, $\mathcal{A}(\omega)$ is

the DTFT of $\{a_n\}$, and $\mathcal{Q}(\omega)$ is the DTFT of $\{q(\delta T_s)\}$, i.e.,

$$\begin{aligned}\mathcal{Q}(\omega) &= \sum_{\delta=-\infty}^{\infty} q(\delta T_s) e^{-j\omega\delta} \\ &= \left|\mathcal{R}^{'}(\omega)\right|^2 \\ &= \left(\sum_{k=-\infty}^{\infty} \left(\frac{\omega}{T_s} - \frac{2\pi k}{T_s}\right) \frac{1}{T_S} \mathcal{R}\left(\frac{\omega}{T_s} - \frac{2\pi k}{T_s}\right)\right)^2\end{aligned}$$

where $\mathcal{R}^{'}(\omega)$ is the DTFT of $\{\dot{r}(kT_s)\}$. Let the DFT of $\{r_h(\delta T_s)\}$ be

$$\mathcal{H}(m) = \frac{1}{T_s} \sum_{k=-\infty}^{\infty} S_h\left(\frac{2\pi m}{KT_s} - \frac{2\pi k}{T_s}\right)$$

According to the property of DFT, the DFT of a product of two sequences is the circular convolution of their respective DFT [40, p.546], therefore (3.77) is equal to

$$\mathcal{J}(m) \triangleq \frac{1}{K} \sum_{l=-K/2}^{K/2-1} \mathcal{Q}\left(\frac{2\pi l}{K}\right) \mathcal{A}\left(\frac{2\pi l}{N+R}\right) \mathcal{H}[((m-l))_K]. \tag{3.80}$$

The MCRB for timing estimation is

$$\mathrm{MCRB}(\tau) = \left\{\frac{2E_s T^2}{KN_0} \sum_{m=-K/2}^{K/2-1} \frac{\mathcal{J}(m)}{\mathcal{F}(2\pi m/K)}\right\}^{-1}. \tag{3.81}$$

Typically the PSD of fading noise $h(t)$ is a narrow low-pass function in the frequency domain. From Jakes' model [14]

$$r_n(v) = J_0(v\omega_d)$$

where $J_0(x)$ is the zeroth-order Bessel function of the first kind, and its Fourier transform is

$$S_h(\omega) = \begin{cases} \frac{2}{\omega_d} \frac{1}{\sqrt{1-(\omega/\omega_d)^2}} & \text{if } |\omega| \le \omega_d \\ 0 & \text{otherwise} \end{cases} \tag{3.82}$$

In the above expression $\omega_d = 2\pi f_d$, and f_d is the *Doppler frequency*, which is related to the vehicle speed v and the carrier frequency f_c by

$$f_d = \frac{v f_c}{c}$$

where c is the speed of light. For example, for a system with carrier frequency $f_c = 2\text{GHz}$, $f_d = 184\text{Hz}$ when the user is moving at 60 mi/h. In a more simplified case, the time-domain correlation could be ideal ω_d-band-limited, i.e.,

$$S_h(\omega) = \begin{cases} \frac{\pi}{\omega_d} & \text{if } |\omega| \leq \omega_d \\ 0 & \text{otherwise} \end{cases} \tag{3.83}$$

Any ω_d-band-limited function $S_h(\omega)$ should satisfy

$$\frac{1}{2\pi} \int_{-\omega_d}^{\omega_d} S_h(\omega) d\omega = 1$$

3.5 Training Sequence Design for Timing Acquisition

Because $\text{CRB}_{\text{DA}}(\tau)$ reveals the close relation between the TS and the fundamental limit of timing estimation performance, therefore it sheds insight on the TS design. Our goal is to find a certain data pattern $\underline{a}$ that minimizes $\text{CRB}_{\text{DA}}(\tau)$ under some constraints. Minimizing $\text{CRB}_{\text{DA}}(\tau)$ is equivalent to maximizing $J_{\tau\tau}$. The sequel illustrates a simple example on the TS design with energy constraint. Because $J_{\phi\tau}$ is equal to zero if the TS is real, we limit our discussion in a real sequence.

Suppose that the sequence length N is long enough, which means that we can drop R with negligible loss, the sequence $\{a_n\}$ has the following energy

constraint:

$$\sum_{n=-N/2}^{N/2-1} |a_n|^2 = E_a \tag{3.84}$$

i.e.,

$$\sum_{m=-N/2}^{N/2-1} \left| \mathcal{A}\left(\frac{2\pi m}{N}\right) \right|^2 = NE_a$$

The variable $J_{\tau\tau}$ is different in under and over sampling cases, therefore, we are going to address the TS design in two scenarios.

Theorem 5 *If the sampling rate of a timing recovery system with the Nyquist pulse is one sample per symbol, the optimal TS under the condition of (3.84) is the sequence* $\{a_n\}$ *that has the following* N*-point DFT*

$$\left| \mathcal{A}\left(\frac{2\pi m}{N}\right) \right| = \begin{cases} \sqrt{NE_a/2} & \text{if } m = \pm m_v \\ 0 & \text{otherwise} \end{cases} \tag{3.85}$$

where $m_v \in [0, N/2]$ *is defined as*

$$m_v \triangleq \arg\max_m \sum_{k=0}^{1} \frac{1}{T^2} \left(\frac{2\pi m}{N} - 2\pi k\right)^2 \mathcal{R}\left(\frac{2\pi m}{NT} - \frac{2\pi k}{T}\right)^2 \tag{3.86}$$

Proof: In the under-sampling case, the optimal sequence should be equal to

$$\underline{a}|_{op} = \arg\max \sum_{m=0}^{N-1} \sum_{k=0}^{1} \frac{1}{T^2} \left(\frac{2\pi m}{N} - 2\pi k\right)^2 \mathcal{R}\left(\frac{2\pi m}{NT} - \frac{2\pi k}{T}\right)^2 \left| \mathcal{A}\left(\frac{2\pi m}{N}\right) \right|^2 \tag{3.87}$$

When the sampling rate L is equal to one, the sampling period 2π of $r(t)$ is equal to the period of $\mathcal{A}(\omega)$ in the DFT spectrum.

Because both $r(t)$ and $\{a_n\}$ are real, $(2\pi m/N)^2\mathcal{R}(2\pi m/NT)^2$ and $|\mathcal{A}(2\pi m/N)|$

are both non-negative and even. It is easy to verify that

$$\begin{aligned}&\sum_{k=0}^{1}\left(\frac{2\pi m}{N}-2\pi k\right)^2\mathcal{R}\left(\frac{2\pi m}{NT}-\frac{2\pi k}{T}\right)^2\\=&\sum_{k=0}^{1}\left(\frac{2\pi(N-m)}{N}-2\pi k\right)^2\mathcal{R}\left(\frac{2\pi(N-m)}{NT}-\frac{2\pi k}{T}\right)^2\end{aligned}$$

for $m \in [0, N/2]$, i.e., the function above is symmetric about $N/2$. Let m_v be the m defined in (3.86) and the maximum be $\mathcal{R}_{max}$, then the following holds

$$\begin{aligned}\text{RHS of (3.87)} &\leq \sum_{m=0}^{N-1}\mathcal{R}_{max}\left|\mathcal{A}\left(\frac{2\pi m}{N}\right)\right|^2\\&= \mathcal{R}_{max}NE_a\end{aligned} \tag{3.88}$$

Therefore the optimal sequence should be a tone with the normalized frequency at m_v/N; (3.85) can be derived readily. ■

In the over-sampling scenario, it is a little bit different. We have the following theorem:

Theorem 6 *If the sampling rate of a timing recovery system is larger than the Nyquist sampling rate, the optimal TS under the condition of (3.84) is the sequence* $\{a_n\}$ *that has the following* N*-point DFT*

$$\left|\mathcal{A}\left(\frac{2\pi m}{N}\right)\right| = \begin{cases}\sqrt{NE_a/2} & \text{if } m = \pm m_v\\ 0 & \text{otherwise}\end{cases} \tag{3.89}$$

where $m_v \in [0, N/2]$ *is defined as*

$$m_v \triangleq \arg\max_m \sum_{k=0}^{1}\frac{1}{T}\left(\frac{2\pi m}{N}-2\pi k\right)^2\mathcal{R}\left(\frac{2\pi m}{NT}-\frac{2\pi k}{T}\right) \tag{3.90}$$

Proof: In over-sampling case (e.g., $L = 2$), the optimal should be equal to

$$\underline{a}|_{op} = \arg\max \sum_{m=-K/2}^{K/2-1}\frac{1}{T}\left(\frac{2\pi m}{N}\right)^2\mathcal{R}\left(\frac{2\pi m}{NT}\right)\left|\mathcal{A}\left(\frac{2\pi m}{N}\right)\right|^2 \tag{3.91}$$

The proof is similar to that of Theorem 5. When the sampling rate L is larger than the Nyquist sampling frequency, the period of $\mathcal{A}(\omega)$ is equal to the normalized symbol rate (that is normalized to the sampling rate) in the DFT spectrum. Since $\{a_n\}$ is real, $|\mathcal{A}(\omega)|$ is an even function, i.e.,

$$\left|\mathcal{A}\left(\frac{2\pi m}{N}\right)\right| = \left|\mathcal{A}\left(\frac{2\pi(N-m)}{N}\right)\right|$$

we have

$$\begin{aligned}
&\sum_{m=-K/2}^{K/2-1}\left(\frac{2\pi m}{N}\right)^2 \mathcal{R}\left(\frac{2\pi m}{NT}\right)\left|\mathcal{A}\left(\frac{2\pi m}{N}\right)\right|^2 \\
=&\sum_{m=0}^{N-1}\sum_{k=0}^{1}\left(\frac{2\pi m}{N}-2\pi k\right)^2 \mathcal{R}\left(\frac{2\pi m}{NT}-\frac{2\pi k}{T}\right)\left|\mathcal{A}\left(\frac{2\pi m}{N}-2\pi k\right)\right|^2 \qquad (3.92)\\
=&\sum_{m=0}^{N-1}\sum_{k=0}^{1}\left(\frac{2\pi m}{N}-2\pi k\right)^2 \mathcal{R}\left(\frac{2\pi m}{NT}-\frac{2\pi k}{T}\right)\left|\mathcal{A}\left(\frac{2\pi m}{N}\right)\right|^2
\end{aligned}$$

where the first equality holds because:(1) the sampling rate $L \geq 2$; (2) the term of the summation is equal to zero when $m = 0$; (3) $r(t)$ is real and band-limited, $\mathcal{R}(2\pi/T) = 0$.

The remaining of the proof follows the proof idea of Theorem 5. ■

If the shaping pulse $r(t)$ is a low-pass Nyquist pulse, we have the following *important* corollary.

Corollary 3 *In the over-sampling case, if the shaping pulse $r(t)$ is a band-limited low-pass Nyquist pulse, the optimal TS under the condition of (3.84) is the alternating one-zero sequence, i.e., $\{a_n\}$ is equal to*

$$a_n = \sqrt{\frac{E_a}{N}}(-1)^n \qquad (3.93)$$

Proof: According to Theorem 6, the optimal sequence $\{a_n\}$ should be a tone with the normalized frequency at $\pm m_v/N$ with m_v defined in (3.90), i.e.,

m_v is the $m \in [0, N/2]$ that maximizes

$$\left(\frac{2\pi m}{N}\right)^2 \mathcal{R}\left(\frac{2\pi m}{NT}\right) + \left(\frac{2\pi(N-m)}{N}\right)^2 \mathcal{R}\left(\frac{2\pi(N-m)}{NT}\right). \tag{3.94}$$

In this corollary, we are going to prove that $m_v = N/2$ for band-limited (within $1/2T$ and $1/T$) low-pass Nyquist pulse. If $r(t)$ is a Nyquist pulse, the following holds

$$\sum_{k=-\infty}^{\infty} \mathcal{R}(\omega - 2\pi k) = T$$

for band-limited real $r(t)$, we have

$$\mathcal{R}\left(\frac{2\pi m}{NT}\right) + \mathcal{R}\left(\frac{2\pi(N-m)}{NT}\right) = T$$

which implies that we can define a function $w(m) \triangleq \mathcal{R}(2\pi m/NT) - T/2$ for $m \in [0, N/2]$, and

$$\begin{aligned} \mathcal{R}\left(\frac{2\pi m}{NT}\right) &= \frac{T}{2} + w(m) \\ \mathcal{R}\left(\frac{2\pi(N-m)}{NT}\right) &= \frac{T}{2} - w(m) \end{aligned}$$

Equation (3.94) becomes

$$\left(\frac{2\pi}{N}\right)^2 \left[(m^2 + (N-m)^2)\frac{T}{2} + w(m)(m^2 - (N-m)^2))\right] \tag{3.95}$$

For $0 \le m \le N/2$, the first item in the parenthesis in (3.95) has the maximum value when $m = N/2$, i.e.,

$$\arg\max_m m^2 + (N-m)^2 = N/2,$$

and $w(m) \ge 0$ since $r(t)$ is a low-pass function with $\mathcal{R}(2\pi m/NT)|_{m=N/2} = T/2$, therefore the second item is bounded by zero, i.e.,

$$w(m)(m^2 - (N-m)^2) \le 0$$

with equality at $m = N/2$. Therefore, we have proven that

$$m_v = N/2$$

and the optimal TS is the alternating one-zero sequence defined in (3.93). ■

This corollary tells us that the alternating one-zero pattern is the optimal TS for low-pass Nyquist pulses that are widely used in contemporary digital receivers for timing recovery purpose. The one zero pattern can achieve the minimum estimation variance. Therefore we have the following theorem.

Theorem 7 *In a DA timing recovery system, if the shaping pulse $r(t)$ is a band-limited low-pass Nyquist pulse and the sampling rate is no less than the Nyquist sampling rate, the mean square estimation error of timing offset τ for long TS with length N is lower bounded by the following*

$$E[(\hat{\tau} - \tau)^2] \geq \left\{ 2\pi^2 \frac{E_s}{N_0} N \right\}^{-1} \tag{3.96}$$

given any TS, the equality is achievable when the TS is the alternating one-zero sequence.

Table 3.5 shows the m_v and $\mathcal{R}_{max}$ that is the maximum value of

$$\frac{1}{T^2} \sum_{k=0}^{1} \left(\frac{2\pi m}{N} - 2\pi k \right)^2 \mathcal{R}\left(\frac{2\pi m}{NT} - \frac{2\pi k}{T} \right)^2 \tag{3.97}$$

where the raised-cosine shaping pulse is adopted. Figure 3.9 shows (3.97) with different rolloff factors, where 1 on the x axis corresponds to one symbol rate. From these numerical results we can see that the optimal TS in the under-sampling case should be a tone with the normalized frequency ranging from 0.40 symbol rate to 0.50 symbol rate.

rolloff factor α	m_v/N	R_{max}
0.1	0.45	7.99
0.2	0.42	6.64
0.3	0.40	5.56
0.4	0.44	4.96
0.5	0.50	4.94
0.6	0.50	4.94
0.7	0.50	4.94
0.8	0.50	4.94
0.9	0.50	4.94
1.0	0.50	4.94

Table 3.5: The Normalized Frequency that Maximizes $\sum_{k=0}^{1}(2\pi(f-k))^2\mathcal{R}(2\pi f/T - 2\pi k/T)^2$ with $L = 1$ $(1/T \sim 1)$

rolloff factor α	Normalized m_v	R_{max}
0.1	0.50	9.87
0.2	0.50	9.87
0.3	0.50	9.87
0.4	0.50	9.87
0.5	0.50	9.87
0.6	0.50	9.87
0.7	0.50	9.87
0.8	0.50	9.87
0.9	0.50	9.87
1.0	0.50	9.87

Table 3.6: The Normalized Frequency that Maximizes $\sum_{k=0}^{1}(2\pi(f - k))^2\mathcal{R}(2\pi f/T - 2\pi k/T)$ with $L = 2$ $(1/T \sim 1)$

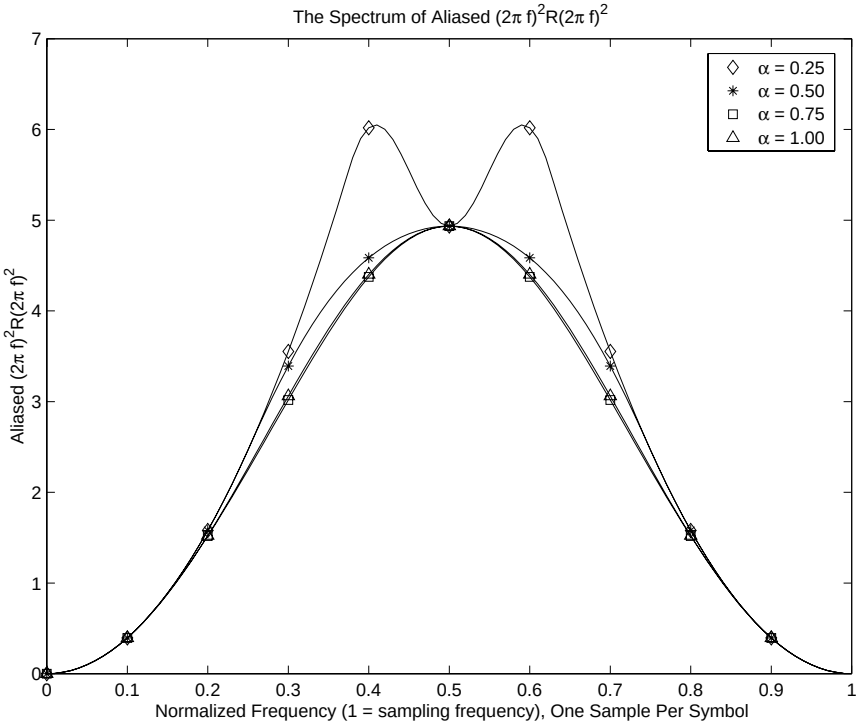

Figure 3.9: The Spectrum of Aliased $(2\pi f)^2/T\mathcal{R}(2\pi f/T)^2$ with $L = 1$

Figure 3.10 shows the spectrum of $(2\pi f)^2\mathcal{R}(2\pi f/T)$ with the raised-cosine shaping pulse and different rolloff factors. According to Corollary 3, the optimal TS for the low-passed Nyquist shaping pulse is the alternating one-zero sequence, Table 3.6 supports it through numerical evaluation. This example explains the reason why the one-zero pattern outperforms the pseudo-random data pattern in timing acquisition.

The TS design method illustrated above is simplified. In practice, there are several important factors that have to be taken into account, e.g., other constraints besides energy constraint; the sequence $\underline{a}$ obtained from these methods is generally non-binary, quantization is an important issue; if N is not long enough, R has to be included, the side-lobe effects need further attention.

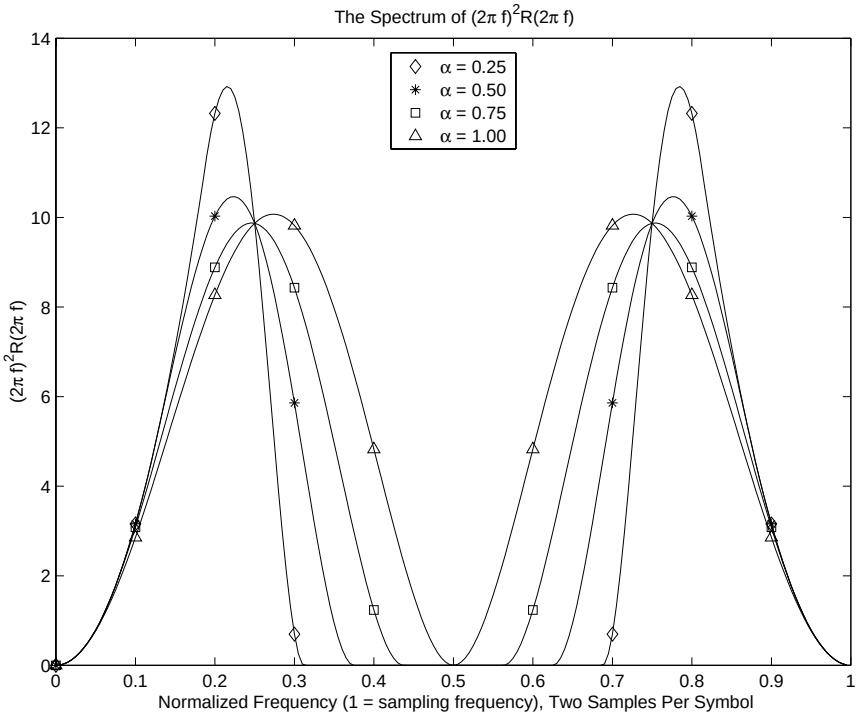

Figure 3.10: The Spectrum of $(2\pi f)^2/T\mathcal{R}(2\pi fT)$ with $L = 2$

3.6 Conclusions

The performance limits - the CRB and MCRB for the DA synchronization parameter estimation were derived and discussed in depth in this chapter. Both Gaussian channel and flat fading channel cases were addressed. It will be shown in Chapter 5 that there is a joint timing and phase estimator whose performance approaches the CRB proposed in this chapter for different rolloff factors and TS's.

The close relation between the TS and the fundamental performance limits sheds insight on the TS design for synchronization. The optimal TS's for timing acquisition in different scenarios were proposed. In this work, we have proven that the alternating one-zero TS pattern could achieve minimum timing

estimation variance for the band-limited low-pass Nyquist shaping pulses in the over-sampling case, which is widely encountered in modern digital receivers.

Appendix

Calculating J_{ij}

According to (3.13), we can get the following

$$\begin{aligned}\frac{\partial^2 l(\underline{y}|\underline{a},\phi,\tau)}{\partial\theta_i\partial\theta_j} &= -\frac{1}{N_0}\left[-\underline{y}^H Q\frac{\partial^2 \underline{m}_y}{\partial\theta_i\partial\theta_j} - \frac{\partial^2 \underline{m}_y^H}{\partial\theta_i\partial\theta_j}Q\underline{y} + \frac{\partial^2 \underline{m}_y^H}{\partial\theta_i\partial\theta_j}Q\underline{m}_y + \right. \\ &\left. \frac{\partial \underline{m}_y^H}{\partial\theta_i}Q\frac{\partial \underline{m}_y}{\partial\theta_j} + \frac{\partial \underline{m}_y^H}{\partial\theta_j}Q\frac{\partial \underline{m}_y}{\partial\theta_i} + \underline{m}_y^H Q\frac{\partial^2 \underline{m}_y^H}{\partial\theta_i\partial\theta_j}\right],\end{aligned} \tag{3.98}$$

follow (3.7),

$$E_{\underline{y}}[\underline{y}] = \underline{m}_y \tag{3.99}$$

J_{ij} is given by the following equation

$$\begin{aligned}J_{ij} &= E_{\underline{y}}\left[-\frac{\partial^2 l(\underline{y}|\underline{a},\phi,\tau)}{\partial\theta_i\partial\theta_j}\right] \\ &= \frac{1}{N_0}\left[\frac{\partial \underline{m}_y^H}{\partial\theta_i}Q\frac{\partial \underline{m}_y}{\partial\theta_j} + \frac{\partial \underline{m}_y^H}{\partial\theta_j}Q\frac{\partial \underline{m}_y}{\partial\theta_i}\right]\end{aligned} \tag{3.100}$$

Because the auto-covariance matrix Λ is a Hermitian matrix, its inverse Q is also Hermitian [37, p.169], the following holds

$$\left(\frac{\partial \underline{m}_y^H}{\partial\theta_i}Q\frac{\partial \underline{m}_y}{\partial\theta_j}\right)^* = \frac{\partial \underline{m}_y^H}{\partial\theta_j}Q\frac{\partial \underline{m}_y}{\partial\theta_i} \tag{3.101}$$

finally

$$J_{ij} = \frac{2}{N_0}\Re\left[\frac{\partial \underline{m}_y^H}{\partial\theta_i}Q\frac{\partial \underline{m}_y}{\partial\theta_j}\right] \tag{3.102}$$

Chapter 4

ML Slow Frequency-Selective Fading Channel Estimation Using the Frequency Domain Approach

For burst-transmission digital communication systems, channel estimation is required for maximum-likelihood sequence estimation receivers [12] [41]. A typical data burst consists of several blocks of user data and a predetermined training sequence (TS) which is used to estimate the channel impulse response. Channel estimation problems are widely addressed in the literature [42, 43, 44, 45, 46]. Estimation can be implemented using a Wiener filter or the discrete Fourier transform (DFT). For example, [42, 43, 44] consider channel estimation given a known TS. The authors of [42] addressed the problem of selecting the optimum TS for channel estimation by processing in the frequency domain. Optimum unbiased channel estimation given white noise is considered in [43] following a maximum-likelihood approach. Following the least-squares (LS) philosophy, [44] presents algorithms for optimal unbiased channel estimation with aperiodic spread spectrum signals for white or nonwhite noise.

Previous works [42] - [44] assumed a symbol period delay-tapped line model or AWGN noise [42]. Because of pre-filtering in the receiver front end, this model is not accurate enough and will cause aliasing or leakage on the spectrum. Since typical pulse shaping rolloff factors in wireless communication range between 0.2 and 0.7, a sampling frequency larger than one symbol rate is required to prevent aliasing. Typically a nominal sampling rate of two samples per symbol period is used in wireless receivers [12]. When the sampling rate is higher than one sample per symbol or timing information is unknown, AWGN model is not valid. Therefore a more general model is desired to accommodate the colored Gaussian noise and a higher sampling rate. Felhauer proposed a whitening matched filter approach in [44] to deal with the colored noise, which actually follows the general idea in Van Trees' classical work in [16]. In this paper, we will show that a direct optimum estimator can be derived without preliminary processing [16, p.289].

In what follows we take a ML approach and derive an optimal channel estimation algorithm in the frequency domain. Since we know the auto-covariance matrix of a colored Gaussian noise is a Toeplitz matrix which was thoroughly studied in Chapter 2. Let us revisit some of the results we obtained in that chapter. It is well known that the inverse of a Toeplitz matrix is not Toeplitz generally. Kobayashi showed that the inverse of a Toeplitz matrix was asymptotically Toeplitz [24], and a similar methodology was adopted in Meyr's book [12]. However we found that it was incorrect in general and that there were some conditions required in order to apply this idea in our work [25, 26]. The condition is that the z transform of the sequence with which a Toeplitz matrix is associated has no zeros on the unit circle. In another word, the discrete time Fourier transform (DTFT) of this function has no zeros within the frequency

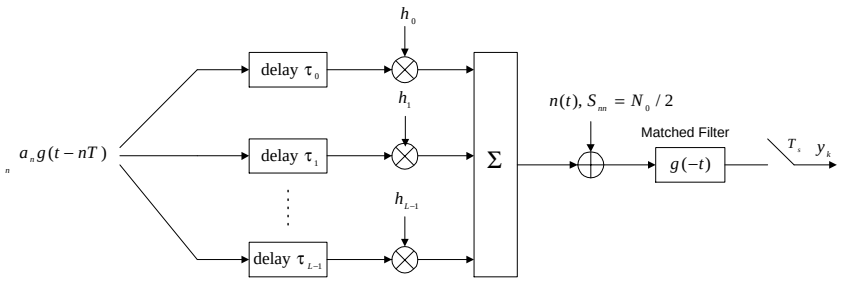

Figure 4.1: Modeling of Slow Frequency-Selective Fading Channel and Matched Filter

band that is smaller than the sampling rate. If the above condition is satisfied, the inverse of a Toeplitz matrix converges to a circular matrix in the "finite boundary strong sense". It is well understood that the eigendecomposition of a circular matrix is equivalent to discrete Fourier transform (DFT).

This chapter illustrates the application of the eigendecomposition of the Toeplitz inverse matrix in wireless communications. The DFT approximation introduces the frequency domain approach that can simplify the design significantly. The rest of the chapter is organized as follows. Section 4.1 describes the channel model and derives the likelihood function. The ML channel estimator is presented in Section 4.2. Section 4.3 addresses one special case, the ML joint carrier phase and timing offset estimator. Some computer simulation results are shown in Section 4.3 too. Section 4.4 concludes this chapter.

4.1 Problem Formulation

Without limitations on the number of paths and delay of each path in our problem, the following channel model is assumed:

$$h(t) = \sum_{l=0}^{M-1} h_l \delta(t - \tau_l T) \tag{4.1}$$

where M is the total number of paths, which is unknown, h_l and τ_l are the attenuation and delay factor of path l respectively, T is the symbol period. In our model, a slow and frequency selective fading channel is assumed, i.e., h_l and τ_l remain constant within the observation window, τ_l is comparable with symbol period. The baseband received signal is modeled as the following:

$$x(t) = \sqrt{E_s} \sum_{l=0}^{M-1} \sum_{n=-N/2}^{N/2-1} h_l a_n g(t - nT - \tau_l T) + n(t) \tag{4.2}$$

where $\{a_n\}$ is the TS, $n(t)$ is the AWGN noise with two-sided power spectrum density (PSD) $N_0/2$. The received signal $x(t)$ is passed through a matched filter with response $g(-t)$, then sampled at the rate $1/T_s$ with $T_s = T/L$ (L is the sampling rate in samples per symbol). The output of the matched filter is defined as $y(t)$ that is given by:

$$y(t) = \sqrt{E_s} \sum_{l=0}^{M-1} \sum_{n=-N/2}^{N/2-1} h_l a_n r(t - nT - \tau_l T) + N(t) \tag{4.3}$$

where $r(t) = g(t) \otimes g(-t)$, $N(t) = n(t) \otimes g(-t)$.

The likelihood function of $\{h_l, \tau_l\}$ is the pdf of a Gaussian random variable. The mean of y_k given $\{h_l, \tau_l\}$ is

$$m_y(k) = \sqrt{E_s} \sum_{l=0}^{M-1} \sum_{n=-N/2}^{N/2-1} h_l a_n r(kT_s - nT - \tau_l T) + N(kT_s), \tag{4.4}$$

where $k \in [-K/2, K/2 - 1]$, and $K = L(N + R)$ is the total number of digital samples, N is used to model the central portion of the TS, R is used to model the signal $y(t)$ beyond the TS portion in the ideal case in which a shaping pulse $r(t)$ modulated only by the TS is transmitted and used to estimate the channel

response, which is shown in Figure 3.2. Define vectors $\underline{y}$, $\underline{a}$ and $\underline{N}$ as (3.5), i.e.,

$$\begin{aligned}
\underline{y} &= [\ y_{-K/2} \quad \cdots \quad y_0 \quad \cdots \quad y_{K/2-1}\ ]^T \\
\underline{a} &= [\ a_{-N/2} \quad \cdots \quad a_0 \quad \cdots \quad a_{N/2-1}\ ]^T \\
\underline{N} &= [\ N_{-K/2} \quad \cdots \quad N_0 \quad \cdots \quad N_{K/2-1}\ ]^T
\end{aligned}$$

The auto-covariance matrix of vector $\underline{y}$ is

$$\mathrm{cov}[\underline{y}|\underline{h},\underline{\tau}] = \frac{N_0}{2}\Lambda \tag{4.5}$$

where Λ is a K by K Hermitian and Toeplitz matrix defined as (3.9).

Similarly, the log likelihood function is given by

$$\begin{aligned}
l(\underline{y}|\underline{h},\underline{\tau}) &= \log(f(\underline{y}|\underline{h},\underline{\tau})) \qquad (4.6)\\
&= -\frac{1}{N_o}\left[-\underline{y}^H Q\underline{m}_y - \underline{m}_y^H Q\underline{y} + \underline{m}_y^H Q\underline{m}_y\right] \\
&\quad -\left(\frac{1}{N_o}\underline{y}^H Q\underline{y} + \log\left[(2\pi)^{K/2}\left|\frac{N_o}{2}\Lambda\right|^{1/2}\right]\right)
\end{aligned}$$

where Q is the inverse of Λ.

4.2 ML Channel Estimator in the Frequency Domain

The auto-covariance matrix Λ (defined in (3.9)) is a Toeplitz matrix for a stationary random process. The derivation of the ML channel estimator involves the convergence issue of the inverse of the Toeplitz matrix Λ in the strong sense (quadratic form). The finite boundary strong sense convergence theorem (Theorem 2), Corollary 1 and 2 can be applied here. As explained in Chapter 3, in typical communication receivers, the shaping pulse $\{r(kT_s)\}$ usually degrades

faster than $O(1/|k|^2)$, e.g., the magnitude of the raised-cosine pulse converges to zero at the speed faster than $O(1/|k|^3)$. In engineering practice, it is under the system designer's control to make the training portion $\underline{m}_y$ satisfy the finite boundary condition through packing zeros along with the training sequence $\{a_n\}$.

Following the finite strong sense convergence theorem, we can replace the inverse matrix Q by a circular matrix $C^{-1} \triangleq U_K^H D^{-1} U_K$. The matrix U_K is the DFT matrix (defined in (2.2)), which introduces the frequency domain approach. The matrix D is a diagonal matrix with the ith diagonal element equal to $\mathcal{F}(2\pi i/K)$. The DTFT $\mathcal{F}(\omega)$ of $r(kT_s)$ $(k = \cdots, -1, 0, 1, \cdots)$ is defined as:

$$\mathcal{F}(\omega) = \sum_{k=-\infty}^{\infty} r(kT_s) e^{-j\omega k}. \tag{4.7}$$

In order to emphasize the digital implementation, we use the notation $\mathcal{G}[m]$ to stand for the mth element of the DFT of the sequence $\{g_k\}$, which is different from last two chapters. Define a new variable $\mathcal{F}_r[k]$ as the kth diagonal element of D $(k = 0, \cdots, K-1)$, i.e.,

$$\mathcal{F}_r[k] = \frac{1}{T_s} \sum_{l=-\infty}^{\infty} \mathcal{R}\left(\frac{2\pi k}{KT_s} - \frac{2\pi l}{T_s}\right) \tag{4.8}$$

where $\mathcal{R}(\omega)$ is the Fourier transform of $r(t)$.

The ML estimate of the channel response $\{\underline{h}, \underline{\tau}\}$ is

$$(\underline{h}, \underline{\tau}) = \arg \max_{\underline{h}, \underline{\tau}} l(\underline{y} | \underline{h}, \underline{\tau}). \tag{4.9}$$

Because all the information related to the channel response is in $\underline{m}_y$, therefore

$$(\underline{h}, \underline{\tau}) = \arg \max_{\underline{h}, \underline{\tau}} \left\{ -\frac{1}{N_o} \left[-\underline{y}^H Q \underline{m}_y - \underline{m}_y^H Q \underline{y} + \underline{m}_y^H Q \underline{m}_y \right] \right\} \tag{4.10}$$

After some arithmetic, we get

$$U_K \underline{m}_y = \sqrt{\frac{E_s}{K}}\Pi \tag{4.11}$$

where Π is a $K \times 1$ vector with mth element equal to (when K is large enough, and the sampling rate L satisfies the Nyquist sampling theorem)

$$\begin{aligned}
\pi[m] &= \sum_{k=-K/2}^{K/2-1} \sum_{l=0}^{M-1} \sum_{n=-N/2}^{N/2-1} h_l a_n r(kT_s - nT - \tau_l T) e^{-j2\pi mk/K} \\
&\approx \sum_{l=0}^{M-1} \sum_{n=-N/2}^{N/2-1} h_l a_n \mathcal{F}_r[m] e^{-j2\pi m(n+\tau_l)/(N+R)} \\
&= \sum_{l=0}^{M-1} \mathcal{F}_r[m]\mathcal{A}[m] h_l e^{-j2\pi m\tau_l/(N+R)} \\
&= \mathcal{F}_r[m]\mathcal{A}[m]H[m]
\end{aligned} \tag{4.12}$$

where $\mathcal{A}[m]$ ($\mathcal{A}[m] = \sum_{n=-N/2}^{N/2-1} a_n e^{-j2\pi mn/(N+R)}$) is the $N+R$ point DFT of the TS $\{a_n\}$, $H[m] = \sum_{l=0}^{M-1} h_l e^{-j2\pi m\tau_l/(N+R)}$ that is the DFT of the channel response.

Similarly, we can get

$$\begin{aligned}
\underline{y}^H Q \underline{m}_y &= \frac{\sqrt{E_s}}{K} \sum_{m=-K/2}^{K/2-1} \frac{\mathcal{F}_y[m]^* \mathcal{F}_r[m]\mathcal{A}[m]H[m]}{\mathcal{F}_r[m]} \\
&= \frac{\sqrt{E_s}}{K} \sum_{m=-K/2}^{K/2-1} \mathcal{F}_y[m]^* \mathcal{A}[m]H[m]
\end{aligned} \tag{4.13}$$

where $\mathcal{F}_y[m]$ is the K-point DFT of $\underline{y}$, i.e.,

$$\mathcal{F}_y[m] = \sum_{k=-K/2}^{K/2-1} y(kT_s) e^{-j2\pi mk/K}. \tag{4.14}$$

Also we have

$$\underline{m}_y^H Q \underline{m}_y = \frac{E_s}{K} \sum_{m=-K/2}^{K/2-1} \mathcal{F}_r[m] |\mathcal{A}[m]|^2 |H[m]|^2. \tag{4.15}$$

Therefore, the ML estimate of the channel response is given by

$$(\underline{h},\underline{\tau}) = \arg \max_{\underline{h},\underline{\tau}} \{ \frac{\sqrt{E_s}}{N_0 K} \sum_{m=-K/2}^{K/2-1} [\mathcal{F}_y[m]\mathcal{A}[m]^* H[m]^* + \mathcal{F}_y[m]^* \mathcal{A}[m] H[m] - \sqrt{E_s}\mathcal{F}_r[m]|\mathcal{A}[m]|^2 |H[m]|^2] \} \tag{4.16}$$

The summation in the parenthesis on the RHS of (4.16) can be reorganized as

$$\begin{aligned} RHS &= \sum_{m=-K/2}^{K/2-1} [\mathcal{F}_y[m]\mathcal{A}[m]^* H[m]^* + \mathcal{F}_y[m]^* \mathcal{A}[m] H[m] \\ &\quad - \sqrt{E_s}\mathcal{F}_r[m]|\mathcal{A}[m]|^2 |H[m]|^2 - \frac{|\mathcal{F}_y[m]|^2}{\sqrt{E_s}\mathcal{F}_r[m]} + \frac{|\mathcal{F}_y[m]|^2}{\sqrt{E_s}\mathcal{F}_r[m]}] \\ &= \sum_{m=-K/2}^{K/2-1} \left[\frac{|\mathcal{F}_y[m]|^2}{\sqrt{E_s}\mathcal{F}_r[m]} - \left(E_s^{1/4}\sqrt{\mathcal{F}_r[m]}\mathcal{A}[m]H[m] - \frac{\mathcal{F}_y[m]}{E_s^{1/4}\sqrt{\mathcal{F}_r[m]}} \right) \cdot \right. \\ &\quad \left. \left(E_s^{1/4}\sqrt{\mathcal{F}_r[m]}\mathcal{A}[m]^* H[m]^* - \frac{\mathcal{F}_y[m]^*}{E_s^{1/4}\sqrt{\mathcal{F}_r[m]}} \right) \right] \\ &= \sum_{m=-K/2}^{K/2-1} \left[\frac{|\mathcal{F}_y[m]|^2}{\sqrt{E_s}\mathcal{F}_r[m]} - \left| E_s^{1/4}\sqrt{\mathcal{F}_r[m]}\mathcal{A}[m]H[m] - \frac{\mathcal{F}_y[m]}{E_s^{1/4}\sqrt{\mathcal{F}_r[m]}} \right|^2 \right] \end{aligned} \tag{4.17}$$

Because $\mathcal{F}_y[m]$ and $\mathcal{F}_r[m]$ are not related to $\{\underline{h},\underline{\tau}\}$, therefore, the ML estimate of channel response becomes

$$\begin{aligned} (\underline{h},\underline{\tau}) &= \arg \min_{\underline{h},\underline{\tau}} \sum_{m=-K/2}^{K/2-1} \left| E_s^{1/4}\sqrt{\mathcal{F}_r[m]}\mathcal{A}[m]H[m] - \frac{\mathcal{F}_y[m]}{E_s^{1/4}\sqrt{\mathcal{F}_r[m]}} \right|^2 \\ &= \arg \min_{\underline{h},\underline{\tau}} \sum_{m=-K/2}^{K/2-1} \left| \frac{\sqrt{E_s}\mathcal{F}_r[m]\mathcal{A}[m]H[m] - \mathcal{F}_y[m]}{E_s^{1/4}\sqrt{\mathcal{F}_r[m]}} \right|^2 . \end{aligned} \tag{4.18}$$

In summary, the ML estimate of $\{\underline{h},\underline{\tau}\}$ is the $\{\underline{h},\underline{\tau}\}$ that has the following DFT

$$H[m] = \begin{cases} \mathcal{F}_y[m]/(\sqrt{E_s}\mathcal{F}_r[m]\mathcal{A}[m]) & \text{if } \mathcal{F}_r[m] \neq 0, \\ 0 & \text{if } \mathcal{F}_r[m] = 0. \end{cases} \tag{4.19}$$

We have the following *Remarks*:

- People are only interested in the channel response within the passband of the shaping function, i.e., when $\mathcal{F}_r[m] \neq 0$, (4.19) follows.

- If there is no noise, i.e., $N_0 = 0$, it is straightforward to verify that the real channel response $H[m]$ is exactly equal to (4.19). Therefore the channel estimator (4.19) is unbiased.

- Because $H[m]$ is just the DTFT of $\underline{h}$ and $\underline{\tau}$, there are a lot of possible $\underline{h}$ and $\underline{\tau}$ that have the same $H[m]$. If the time domain response is more important, $H[m]$ can be treated as an intermediate result. With the help of some physical modeling on $\underline{h}$ and $\underline{\tau}$, the time domain response can be obtained from $H[m]$.

- According to the finite boundary strong sense convergence theorem, when $K \to \infty$, the inverse matrix Q approaches a circular matrix. How to handle it in practice? Two observations based on (4.19) can be made: (1) if the sampling rate L is larger than the Nyquist sampling rate, all the information related to the channel response is preserved; (2) the DFT $\mathcal{F}_y[m]$ of $\underline{y}$ is given by (4.14), y_k can be approximated as zero with negligible leakage when $|k|$ is outside the training window ($[-N/2, N/2-1]$) if the TS length N is long enough, i.e., R can be dropped with negligible performance loss. In practice, when N is not large enough to make $\underline{y}$ contain most information about $\underline{h}$, $\underline{\tau}$ and noise $\underline{N}$, proper number (R) of zeros can be packed along with the TS to provide the channel estimator enough statistical information of the noise process $\underline{N}$.

- If the PSD of $\underline{N}$ has no cross zero points within the frequency band of interests, the ML channel estimator is given by (4.19). Compared with

other frequency domain estimation methods mentioned in [42], a higher sampling rate is adopted in our algorithm, and the colored noise is compensated in the denominator in (4.19). We also observe that the TS length N has to be large enough to apply the old estimation algorithms.

4.3 A Special Case and Simulation Results

The frequency domain approach introduced by the circular matrix approximation simplifies the estimator design. The sequel illustrates a special case of the channel estimator - joint timing and carrier phase offsets estimator.

4.3.1 The Data-Aided ML Joint Timing and Carrier Phase Offsets Estimator

As a special case, let us assume:(1) $M = 1$, which means there is only one path; (2) $h_0 = e^{j\phi}$. With these assumptions, the frequency-selective fading channel estimation problem becomes the joint carrier phase and timing offsets estimation problem. Timing and carrier phase recoveries are very important synchronization functions in coherent demodulation. The variables ϕ and τ are used to model the carrier phase and timing offsets between the transmitter and receiver respectively.

The channel response $H[m]$ is equal to $e^{j\phi}e^{-j2\pi\tau m/(N+R)}$. If there is no noise the following holds

$$e^{-j(2\pi\tau m/(N+R)+\phi)} = \frac{\mathcal{F}_y[m]}{\sqrt{E_s}\mathcal{F}_r[m]\mathcal{A}[m]}. \tag{4.20}$$

The RHS of (4.20) is equivalent to an exponential wave, our objective is to estimate the frequency and phase of this exponential wave. Therefore the timing

estimation problem becomes a frequency estimation problem, which has been studied for many years. For example, the linear regression on the phase of the RHS is proportional to τ [47].

Another estimator can be derived from (4.10). It is easy to verify that the ML estimator is equivalent to the following

$$\begin{aligned}(\tau,\phi) &= \arg\ \max_{\tau,\phi}\left\{\frac{1}{N_0}\Re(\underline{y}^H Q\underline{m}_y)\right\}\\ &= \arg\ \max_{\tau,\phi}\left\{\frac{\sqrt{E_s}}{N_0 K}\Re\left(e^{j\phi}\sum_{k=-K/2}^{K/2-1}\mathcal{F}_y[k]^*\mathcal{A}[k]e^{-j2\pi k\tau/(N+R)}\right)\right\}\\ &= \arg\ \max_{\tau,\phi}\left\{\frac{\sqrt{E_s}}{N_0 K}\Re\left(\sum_{k=-K/2}^{K/2-1}\mathcal{F}_y[k]\mathcal{A}[k]^* e^{j(2\pi k\tau/(N+R)-\phi)}\right)\right\}\end{aligned} \tag{4.21}$$

Define $\mu(\tau)$

$$\mu(\tau) = \frac{1}{K}\sum_{k=-K/2}^{K/2-1}\mathcal{F}_y[k]\mathcal{A}[k]^* e^{j2\pi k\tau/(N+R)}. \tag{4.22}$$

The two-dimensional maximization can be downsized to one-dimension search

$$(\tau,\phi) = \arg\ \max_{\tau,\phi}\left\{|\mu(\tau)|\Re\left(e^{-j(\phi-\arg(\mu(\tau)))}\right).\right\} \tag{4.23}$$

From (4.22), the variable $\mu(\tau)$ is the cross-correlation between the time-shifted $\underline{y}$ and the TS $\underline{a}$ in the frequency domain. The ML timing offset estimate is given by

$$\hat{\tau} = \arg\ \max_{\tau}|\mu(\tau)| \tag{4.24}$$

i.e., it is the τ that maximizes the magnitude of the cross-correlation between the time-shifted $\underline{y}$ and the TS, and the ML phase offset estimate is given by

$$\hat{\phi} = \arg(\mu(\hat{\tau})). \tag{4.25}$$

Parseval's relation serves as a bridge to connect the time domain processing and the frequency domain processing. Since the K-point DFT is an orthonormal

transform, we can apply Parseval's relation, and (4.22) becomes the following:

$$\mu(\tau) = \sum_{n=-N/2}^{N/2-1} y(nT + \tau T)a_n^* \tag{4.26}$$

Therefore the ML estimate of τ is the argument that maximizes the magnitude of the cross-correlation between the received samples and TS in either the frequency domain or the time domain. In fact the ML estimator (4.26) was proposed in [12], which was derived based on other techniques.

4.3.2 Simulation Results

Computer simulations were conducted to test the ML channel estimator in this chapter. The simulation result of the DA ML joint timing and phase estimator will be addressed in Chapter 5 .

An M-sequence with length 63 was used in our slow frequency-selective fading channel estimator simulation. M sequence is good for channel estimation, because its PSD (i.e. $|\mathcal{A}[m]|$) is a constant except for the DC component. For more information on the TS design, refer to [42]. The square root raised-cosine shaping pulse with rolloff factor 0.75 was adopted in both the transmitter and the receiver. In our case, $K = 63L$, and from the simulation we find that this K is large enough to apply our theorem. A carrier at 800 MHz was assumed, and we used a 6-ray typical urban (TU) channel model. Different sampling rates (L) were tested.

Computer simulation results are shown in Figure 4.2, 4.3 and 4.4, where x-axis is the spectrum with 63L equal to 2π, the y-axis is the normalized magnitude response of $H[m]\mathcal{F}_r[m]$. Figure 4.2 shows the averaged estimation result (over 500 tests) at 0dB and $L = 4$. It is shown that the estimator is unbiased. Figure

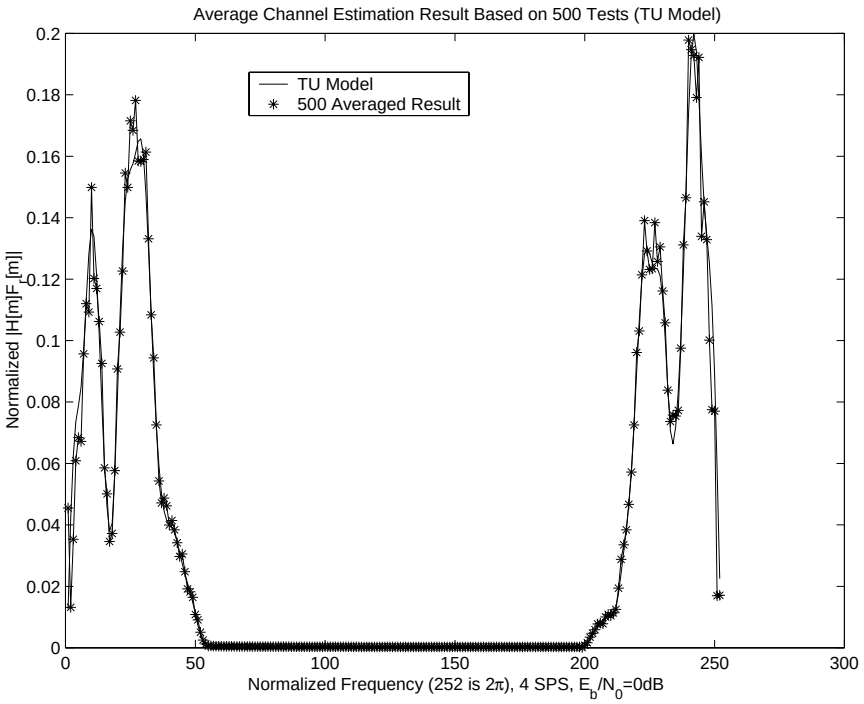

Figure 4.2: Channel Estimation Result Averaged over 500 Tests, 4 Samples Per Symbol

4.3 shows similar results with lower sampling rate ($L = 2$). We can see that higher sampling rate does not provide extra information when it is larger than the Nyquist sampling rate. Figure 4.4 shows one shot test result at 0dB.

We also ran computer simulations for the ML joint timing and phase estimator derived here. In engineering practice, a simplified algorithm that uses *curve-fitting* technique based on (4.26) was used in our simulation [36]. The detailed algorithm and its performance will be addressed in the next chapter.

4.4 Conclusions

In this chapter, the ML channel estimator with the general Gaussian noise and over-sampling assumption was derived in the frequency domain. The derivation

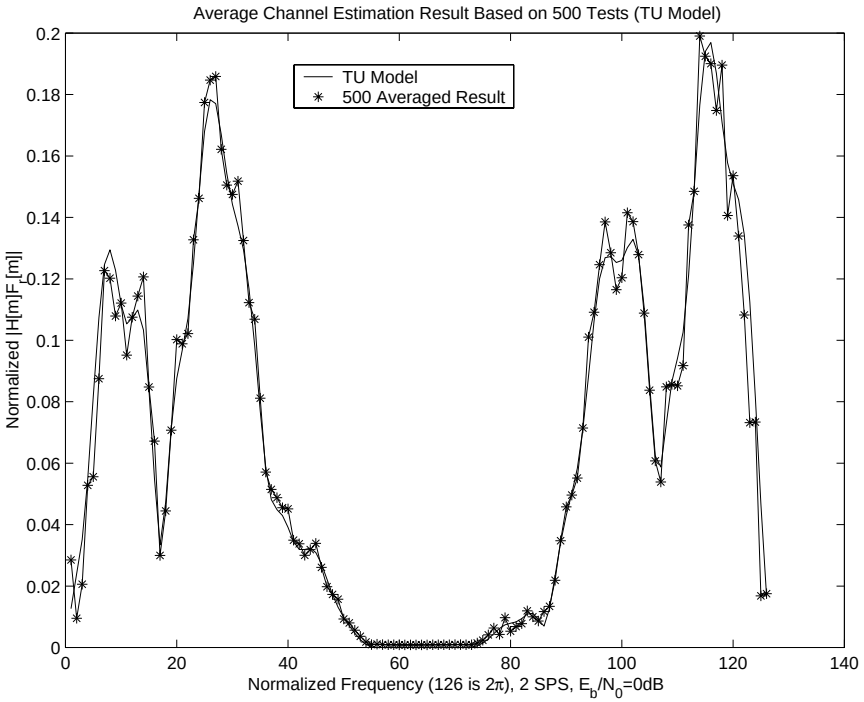

Figure 4.3: Channel Estimation Result Averaged over 500 Tests, 2 Samples Per Symbol

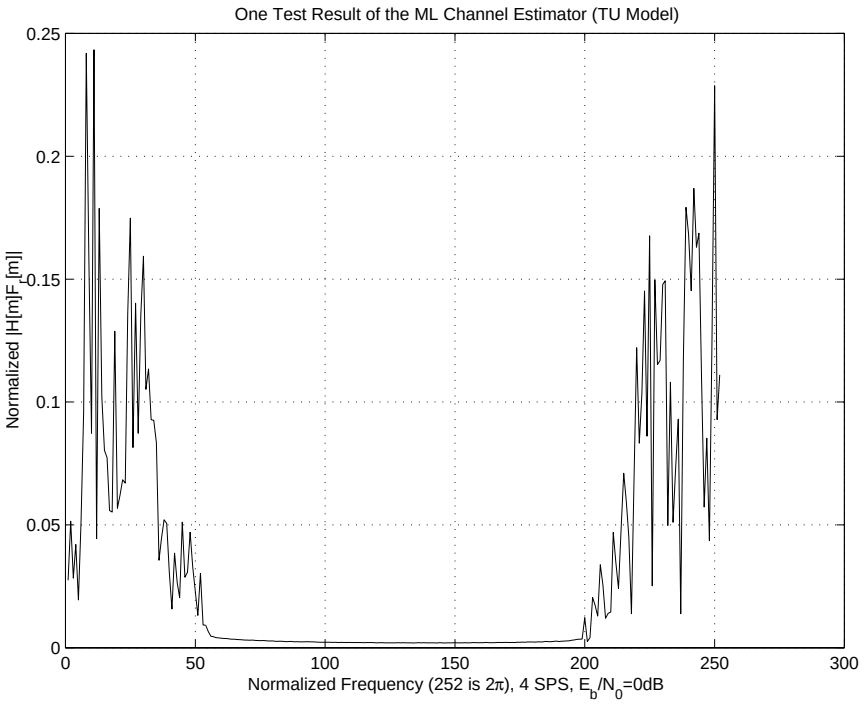

Figure 4.4: Channel Estimation Result of One Test, 4 Samples Per Symbol

was based on *the finite boundary strong sense convergence theorem* for the inverse of Toeplitz matrices. With the help of this theorem, many good algorithms that take advantage of the transform domain approach can be derived. As a special case, the ML joint carrier phase and timing offsets estimator was presented.

Chapter 5

Data-Aided ML Synchronization Parameter Estimators with Systolic VLSI Implementations

This chapter will address the design and VLSI implementations of synchronization parameter estimators in practice.

5.1 Introduction

Fast estimation of synchronization parameters such as carrier frequency, phase and timing offsets is a crucial step in the demodulation process of burst modems. Powerful and generic parameter estimators are necessary for high-performance "universal" digital receivers that can accommodate several modulation schemes (e.g., BPSK, QPSK, OQPSK, 8PSK) and modes. In this chapter, we present an approximate maximum likelihood (ML) carrier frequency offset estimator for both the MPSK data modulated (non-data-aided (NDA)) and the data-aided (DA) cases, a DA ML joint carrier phase and timing offsets estimator, and their

systolic VLSI implementations for PSK burst modems. The performance of these estimators approaches the Cramer-Rao lower bounds (CRB) at low signal to noise ratio (SNR). Compared with theoretic solutions the estimators proposed here are much simpler and easier to implement using current VLSI technology. The rest of the chapter is organized as follows. Section 5.2 presents the carrier frequency estimator for MPSK modems. The DA ML joint carrier phase and timing offsets estimator is addressed in Section 5.3. Section 5.4 concludes this chapter.

5.2 Quasi-ML Carrier Frequency Offset Estimator

Carrier frequency estimator is a very important module in digital receivers. The presence of large frequency offsets and low SNR can make frequency estimation quite difficult. Several carrier frequency offset estimation methods are discussed in [33, 48]. The optimal ML frequency estimator is well known to be given by the location of the peak of a periodogram [32]. However the computation requirements make this approach prohibitive even with an FFT implementation. Therefore simpler approximation methods are desired.

A frequency estimator based on power spectral density estimation, was first proposed by Fitz [49] for an unmodulated carrier. For a MPSK modulated signal, the non-linear method in [50] can be used to remove data modulation. A variant of this algorithm was proposed by Luise [51]. The performance of these methods, at low SNR, is close to the CRB for a carrier with unknown frequency and phase. The maximum frequency offset that can be estimated by Fitz algorithm

is $R_s/(2MW)$, where R_s is the symbol rate, W is the maximum auto-correlation lag and M is the number of phase states in MPSK. Under the assumption that the carrier phase has a constant slope equal to the angular frequency offset, Tretter [52] proposed a frequency estimator by performing linear regression or a line-fit operation on the received signal phase values. This algorithm is ML at high SNR. This algorithm can estimate a maximum frequency of $R_s/(2M)$ and performs well at high SNR values. Phase change over time is proportional to the frequency offset. Kay [53] used the same idea and proposed a frequency estimator by weighting the sum of phase differences over consecutive symbols, which is equivalent to Tretter's algorithm. Chuang [54] also presented algorithms based on differential symbol estimates.

In this section, we revisit the algorithms of Kay [53] and Chuang [54] and present our frequency estimator. An efficient VLSI implementation for the frequency estimator is also proposed.

5.2.1 The Derivation of the Frequency Estimator

In order to simplify our presentation, the following assumptions are made for the development of the algorithm:

- The symbol timing is known.
- Discrete time samples are taken from the output of a pulse shape matched filter, one sample per symbol.
- The pulse shape satisfies the Nyquist Criterion for zero inter-symbol interference.

Let us assume that we have a block of N symbols. The kth complex sample derived from the matched filter can be expressed as

$$r_k = \sqrt{E_s} a_k e^{j(2\pi \Delta f k T + \phi_0)} + n_k, \ k = 0, \cdots, N-1 \tag{5.1}$$

where a_k is the MPSK data symbol and $|a_k| = 1$, Δf is the frequency offset, T is the symbol interval, ϕ_0 is the carrier phase, and n_k represents additive white Gaussian noise (AWGN) with two-sided PSD $N_0/2$.

At first, the following method is used to remove data modulation from complex sample r_k, obtaining

$$S_k = F(r_k) e^{jG \cdot \arg(r_k)} \tag{5.2}$$

where

$$F(r_k) = \begin{cases} |r_k|^w, w \text{ even } \leq M, & \text{in the NDA case,} \\ r_k a_k^* & \text{in the DA case.} \end{cases}$$

The algorithm in [50] is adopted in the NDA case, $w = 0$ is preferred. In the DA case, the training symbol a_k correlates r_k to remove data modulation. The G in (5.2) is given by

$$G = \begin{cases} M & \text{in the NDA case} \\ 1 & \text{in the DA case} \end{cases}$$

According to the work done by Tretter [52], the noise term n_k in r_k can be represented as phase noise at high SNR's:

$$r_k = \sqrt{E_s} e^{j(2\pi \Delta f k T + \theta_k + \phi_0 + V_k)}$$

where θ_k is the data modulation, which is a multiple of $2\pi/M$, and V_k is the equivalent phase noise. Therefore, the phase γ_k of S_k can be modeled as

$$\gamma_k \triangleq \arg(S_k) = G(2\pi \Delta f k T + \phi_0 + V_k). \tag{5.3}$$

If we differentiate γ_k, we obtain

$$\delta_k \triangleq \gamma_{k+1} - \gamma_k = G(2\pi\Delta f T + V_{k+1} - V_k). \tag{5.4}$$

Furthermore, δ_k is passed through an exponential function $\exp[j(*)]$, and after applying Viterbi's feed-forward phase estimator [50], we arrive at Chuang's frequency estimator [54]:

$$\hat{\Delta} f = \frac{1}{2\pi G T_s} \tan^{-1}\left(\frac{\sum_{k=0}^{N-2} \sin\delta_k}{\sum_{k=0}^{N-2} \cos\delta_k}\right). \tag{5.5}$$

Based on the weighting sum of the phase difference δ_k, Kay's algorithm [53] is given by

$$\hat{\Delta f} = \frac{1}{2\pi G T_s} \sum_{k=0}^{N-2} \delta_k w_k, \tag{5.6}$$

where the weighting function w_k is defined as

$$w_k = \frac{1.5N}{N^2-1}\left\{1 - \left[\frac{k-(N/2-1)}{N/2}\right]^2\right\}. \tag{5.7}$$

Our frequency estimator is based on the auto-correlation of r_k (Chuang's algorithm) and Kay's algorithm. Given γ_k in (5.3), let us define the auto-correlation $R(m)$ as follows:

$$\begin{aligned} R(m) \triangleq & \frac{1}{N-m} \sum_{k=m}^{N-1} e^{j(\gamma_k - \gamma_{k-m})} \\ = & \frac{1}{(N-m)E_s^q} \sum_{k=m}^{N-1} S_k S_{k-m}^* \end{aligned} \tag{5.8}$$

and $m = 1, \cdots, L$ with L an integer less than $N-1$. The variable q is equal to 0 in the NDA case and 1 in the DA case. At high SNR, $R(m)$ represents the average phase change over m symbols with the first term averaged over $N-1$ terms. This can be modeled as

$$R(m) \approx e^{j(2\pi G \Delta f T)} + \text{noise}(m).$$

From simulation we find that for N large enough the noise(m) can be approximated by white Gaussian noise. The sequence $\{R(m)\}$ can be treated as a continuous wave (with frequency $G\Delta f$) which is passed through a noise removal process. At high SNR, many good frequency estimation methods have been derived, e.g., Kay's algorithm. Let us define the following process:

$$\theta(m) = \arg[R(m)],\ m = 1, \cdots, L \tag{5.9}$$

and

$$\Delta(m) = \begin{cases} \theta(1), & m = 0 \\ (\theta(m+1) - \theta(m)) \mod (2\pi) & 1 \le m < L \end{cases} \tag{5.10}$$

We then borrow from Kay's frequency estimator; that is the weighting sum of phase difference. Because $R(m_1)$ is calculated based on more data than $R(m_2)$ when $m_1 < m_2$, after some arithmetic we derived the following carrier frequency offset estimator:

$$\hat{\Delta} f = \frac{1}{2\pi GT} \sum_{m=0}^{L-1} w_m^* \Delta(m) \tag{5.11}$$

where

$$w_m^* = \frac{3[(2L+1)^2 - (2m+1)^2]}{[(2L+1)^2 - 1](2L+1)},\ m = 0, \cdots, L-1.$$

The maximum frequency offset that the algorithm can digest is $1/(2GT)$, i.e., in the DA case it is 0.5 symbol rate R_s (in fact much less than that), and in the NDA case it is $R_s/(2M)$.

The weighting function is shown in Figure 5.1. It is easy to see that the weight w_m^* decreases as m increases. That is because as m gets larger and larger, the number of terms required to compute $R(m)$ reduces and makes $\Delta(m)$ less and less accurate. Mengali [55] proposed a frequency estimator based on modeling

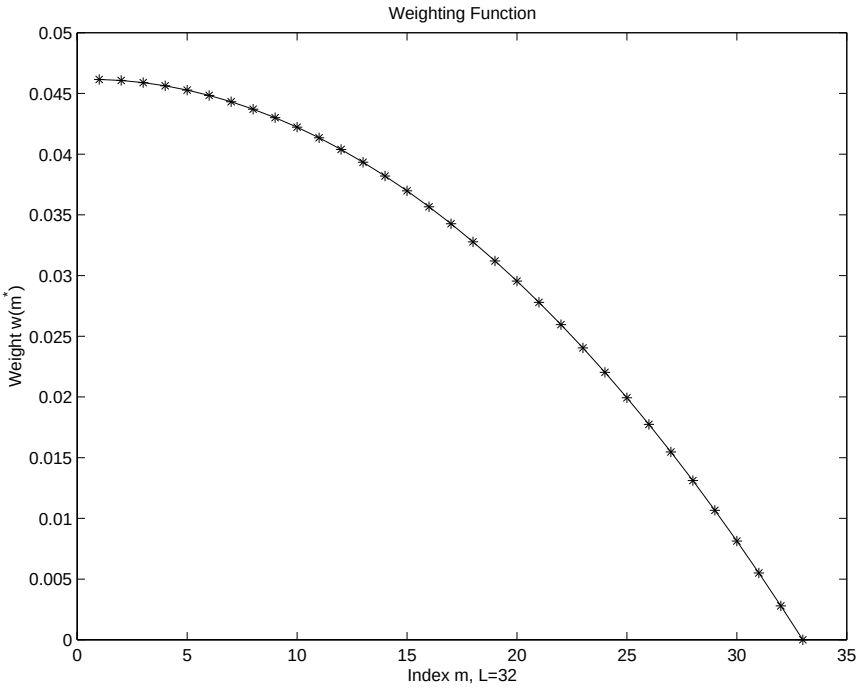

Figure 5.1: Weighting Function $\{w_m^*\}$

the noise process noise(m) and Kay's algorithm. Compared with Mengali's algorithm, our estimator adopts different weighting function, L can be less than $N/2$ (e.g., in the DA case, when $N = 96$, $L = 32$ the estimator's performance meet the CRB at SNR=0dB).

5.2.2 The Systolic VLSI Implementation of the Frequency Estimator

Because the frequency estimator derived in the last subsection utilizes correlation, a lot of concurrency in the computation can be exploited. Systolic structure [56, 57, 58, 59] has a simple and regular design, uses concurrency and communication instead of high speed component, and balances computation with I/O. Therefore it is a good candidate for VLSI implementations. There are two

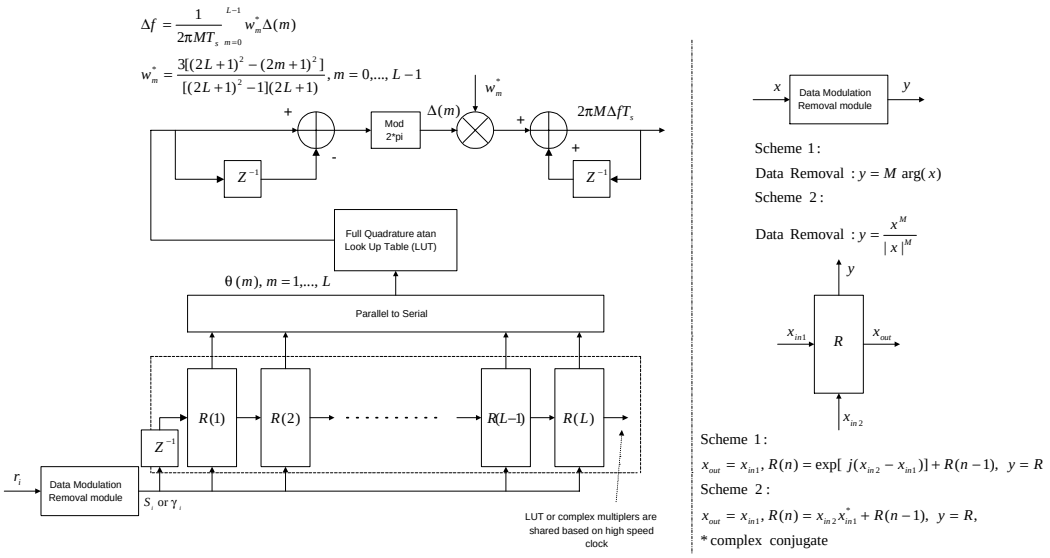

Figure 5.2: Systolic VLSI Structure of MPSK Frequency Offset Estimator (NDA Case)

criteria for the design of systolic structures:

- The design makes multiple use of each input data item.
- The design uses extensive concurrency.

We proposed the systolic VLSI implementation for carrier frequency estimator in [33, 35, 60]. The calculation of $\{R(m)\}$ (5.8) is a hardware intensive task which requires $(2N - L - 1)L/2$ complex multiplication and $(2N - L - 3)L/2$ additions. The systolic VLSI implementation for the frequency estimator in the NDA case is shown in Figure 5.2.

There are two possible schemes for calculating $\{R(m)\}$ as shown in Figure 5.2:

Scheme 1: Equation (5.3) is used to remove data modulation a_k and get γ_k, which is implemented via a lookup table (LUT), and the first equality in (5.8) is used to calculate $R(m)$. Another LUT is used to calculate the term $e^{j(\gamma_i - \gamma_{i-m})}$.

If a higher speed clock is available, these LUTs can be shared on a time division basis.

Scheme 2: Mth power method is used to remove data modulation [50], and complex multiplication and accumulations are used to get $R(m)$, i.e.,

$$S_i = \frac{r_i^M}{|r_i|^M}$$

and $R(m)$ is given by the second equality of (5.8).

It is easy to verify that *Scheme 1* and *Scheme 2* are equivalent. If a higher speed clock is available, the complex multipliers can also be shared on a time division basis. In both schemes, $\{R(m)\}$ will be available on the clock cycle following the one latching the Nth data symbol into the estimator. Frequency offset can then be calculated via (5.11). One advantage of this structure is that it is scalable. If we want to increase L to get a better performance, more elements can be added at the right hand side in Figure 5.2.

The VLSI structure for the DA frequency estimator is the same as the NDA case except a correlator (multiplier) is used to remove the data symbol to get S_i.

5.2.3 Performance and Simulation Results

At high SNR, some approximation methods can be used to analyze the variance of $\hat{\Delta}f$. This is similar to works presented in [50, 52, 53]. Unfortunately at low SNR, the analytical performance approximation is intractable. Hence we resort to computer simulation results.

Two performance indexes are of interest, one is the range over which the frequency estimator is unbiased and its performance degradation is small. The second is the variance of the unbiased estimate $\hat{\Delta}f$ compared with the CRB.

The CRB for DA frequency estimation is given by [32] as follows:

$$E[(\Delta fT - \hat{\Delta} fT)^2] \geq 6 \left\{ 4\pi^2 \frac{E_s}{N_0} N(N^2-1) \right\}^{-1}. \tag{5.12}$$

Cowley [61] derived a modified CRB for the frequency estimators based on a block of BPSK or QPSK symbols at low SNRs. The bound for QPSK is given by the following:

$$E[(\Delta fT - \hat{\Delta} fT)^2] \geq 6 \left\{ 4\pi^2 N(N^2-1) \frac{E_s}{N_0} F_Q\left(\frac{N_0}{E_s}\right) \right\}^{-1} \tag{5.13}$$

where $F_Q(\sigma^2)$ is defined as

$$F_Q(\sigma^2) \triangleq \int\int \frac{\left(\sinh^2\left(\frac{1+x}{\sigma^2}\right)\frac{y^2}{\sigma^2} + \sinh^2\left(\frac{y}{\sigma^2}\right)\frac{(1+x)^2}{\sigma^2}\right) e^{-(x^2+y^2)/(2\sigma^2)}}{\left(\cosh\left(\frac{1+x}{\sigma^2}\right) + \cosh\left(\frac{y}{\sigma^2}\right)\right)^2} - \frac{2\sinh\left(\frac{1+x}{\sigma^2}\right)\sinh\left(\frac{y}{\sigma^2}\right)(1+x)\frac{y}{\sigma^2}e^{-(x^2+y^2)/(2\sigma^2)}}{\left(\cosh\left(\frac{1+x}{\sigma^2}\right) + \cosh\left(\frac{y}{\sigma^2}\right)\right)^2} dxdy$$

Figure 5.3 shows the root mean square (RMS) frequency estimation error in the NDA case with rolloff factor 0.25 squared root raised-cosine shaping, $N = 100$, $L = 32$ and frequency offset equal to 5 percent symbol rate. The simulation result is compared with CRB (5.12) and MCRB (5.13). From the simulation we can see that the estimation performance of the NDA case is close to CRB when SNR $\geq$ 6dB. If SNR $<$ 6dB, the RMS estimation error increases dramatically as SNR decreases.

Figure 5.4 shows the performance comparison of three algorithms in the NDA case; one is the algorithm derived in this work (5.11), one is the algorithm derived by Chuang (5.5) and the other is the algorithm derived by Tretter or Kay (5.6). From simulation we can draw the following conclusion: the line-fit algorithm (derived by Tretter [52]) is biased at low SNR and numerically error prone after the Mth nonlinear processing to remove the data modulation; the algorithm

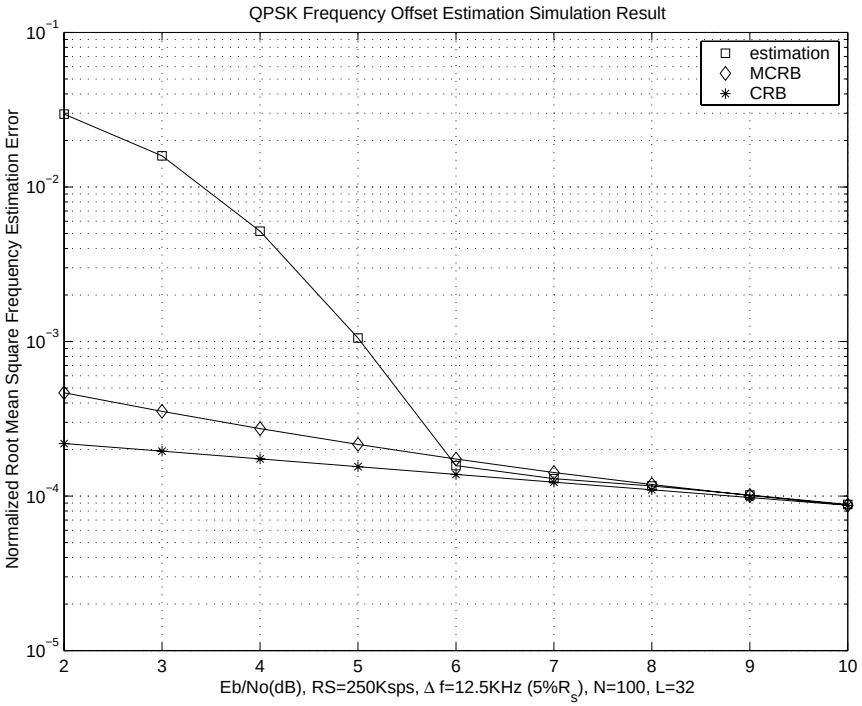

Figure 5.3: RMS Frequency Estimation Error Compared with MCRB and CRB in the NDA Case

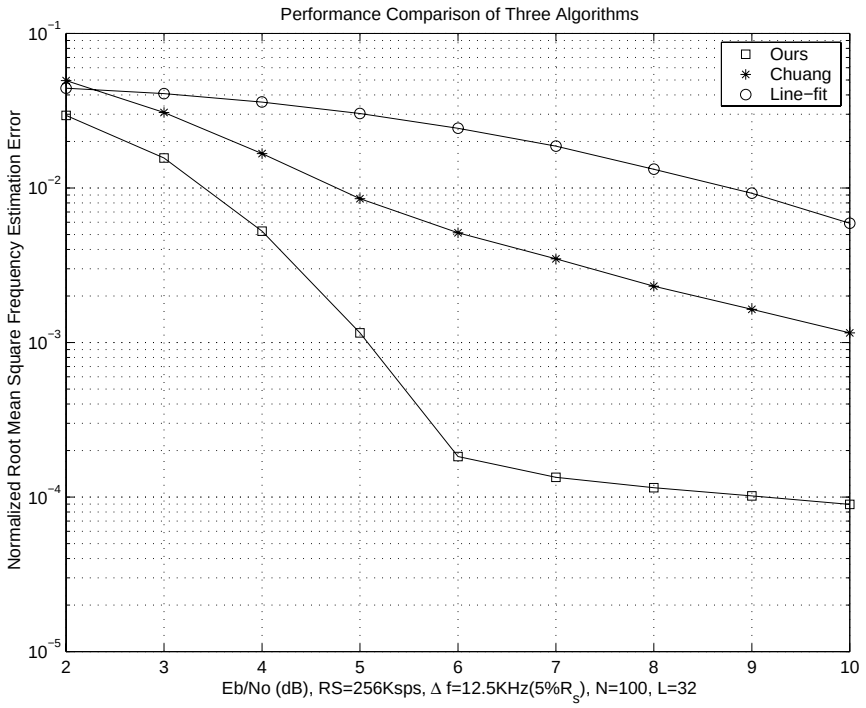

Figure 5.4: Performance Comparison of Three Algorithms in the NDA Case

based on phase difference (5.5) is unbiased at low SNR but the variance is large because it does not use linear regression method to calculate the slope of a line, which is optimal in the sense of least squares; the algorithm in our work is much better than these two when SNR is larger than some threshold.

Figure 5.5 shows the frequency estimation range of our algorithm in the NDA case. The estimation range increases as SNR increases, which is intuitive. At 6dB, the frequency offset estimation range is about 7% of symbol rate, at 8dB, it increases to 9%.

Figure 5.6 shows the RMS frequency estimation error with $\Delta f = 0.13R_s$ in the DA case, which is compared with CRB (5.12). From the simulation we can see that the estimation RSM error is very close to the CRB even at 0db, the performance degradation caused by timing error is very small. The real

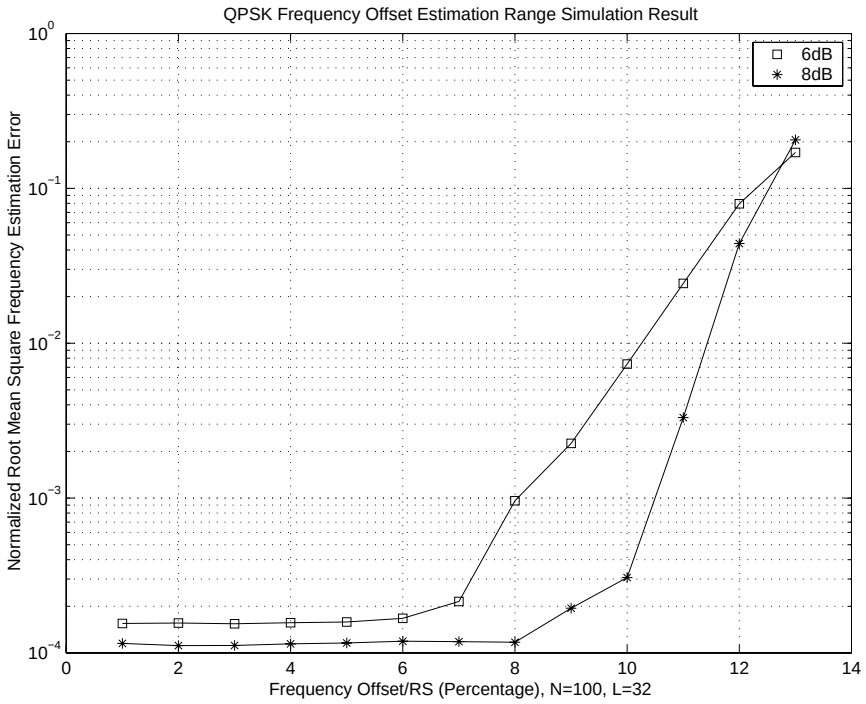

Figure 5.5: Frequency Offset Estimation Range at Different SNR in the NDA Case

frequency estimation range at 0dB is around 20% symbol rate in the DA case, which is much better than that of the NDA case due to the noise introduced by the data removal process.

5.3 Quasi-ML Joint Carrier Phase and Timing Offsets Estimator

The ML phase estimator is derived by Viterbi and Viterbi [50]. The literature [12, 62] gives good surveys on symbol timing recovery. Because of its importance in digital communications, timing recovery receives a lot of attention, e.g., [63] derived a quasi-ML non-DA timing estimator based on a cyclostationary approach; [64] proposed a near optimal timing estimator with efficient

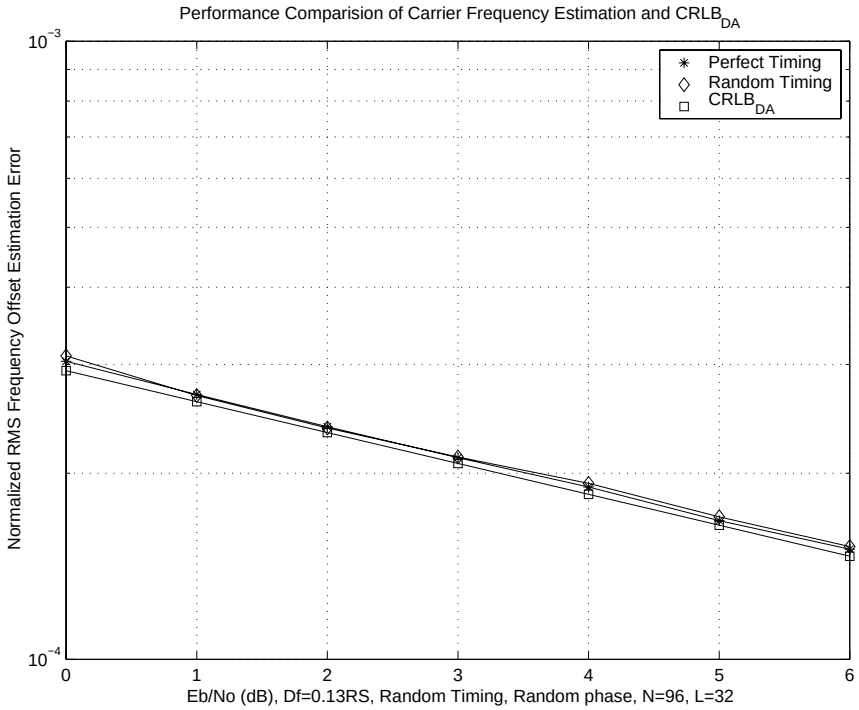

Figure 5.6: RMS Frequency Estimation Error Compared with CRB in the DA Case

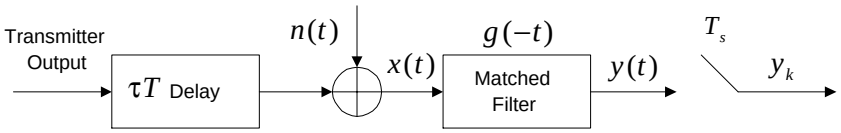

Figure 5.7: Problem Formulation

implementation.

The DA ML joint carrier phase and timing offsets estimator (4.22, 4.24, 4.25, 4.26) was derived in Chapter 4 using the frequency domain approach. The same result was also derived by Meyr in their book [12, p.296] using other method. Implementing this estimator is however hardware intensive in either the frequency domain or the time domain. Before we derive the practical joint timing and phase estimator, let us review the problem and conditions.

5.3.1 The Derivation of the Joint Timing and Phase Estimator

The baseband received signal is passed through a matched filter in the receiver front end, which is shown in Figure 5.7. The sampled signal y_k out of the matched filter is given by

$$y_k = \sqrt{E_s} \sum_{n=-N/2}^{N/2-1} a_n r(kT_s - nT - \tau T) e^{j\phi} + N_k \tag{5.14}$$

where τ and ϕ are timing and phase offsets respectively, $T_s = T/L$ with L the sampling rate in samples per symbol, all the other notations are the same as those define in Chapter 3, refer to Table 3.1 for details.

Let us define $\mu(\tau)$ as

$$\mu(\tau) = \sum_{n=-N/2}^{N/2-1} y(nT + \tau T) a_n^*. \tag{5.15}$$

The ML joint timing and phase estimator is given by

$$\hat{\tau} = \arg \max_{\tau} |\mu(\tau)| \tag{5.16}$$

and

$$\hat{\phi} = \arg[\hat{\mu}(\tau)] \tag{5.17}$$

i.e., the ML timing estimate is the argument that maximize the magnitude of the cross-correlation between the time-shifted y_k and the training sequence $\{a_k\}$.

Rempel [65] showed that the performance of the ML timing estimate would approach the CRB if the auto-correlation function of the pulse shape is quadratic. In fact the auto-correlation function of many pulse shapes are approximately quadratic near their central *peak*, i.e., the central part of $|\mu(\tau)|$ can be modeled as a quadratic function if $\hat{\tau}$ is close to the real timing offset τ enough. The *peak* of a quadratic function always exists and is easy to compute. The *curve-fitting* algorithm is based on this observation: (1) the central part of $|\mu(\tau)|$ is located through some coarse search method; (2) the quadratic function can be obtained through three adjacent samples on $|\mu(\tau)|$ around the *peak* using *Lagrange* interpolation; (3) the ML estimate can be computed through the coefficients of the quadratic function.

Let $\hat{\tau}$ be the timing offset estimate, we get

$$\begin{aligned}\mu(\hat{\tau}) =& \sqrt{E_s} \sum_{n=-N/2}^{N/2-1} \sum_{m=-N/2}^{N/2-1} a_m a_n^* r((n-m)T + (\hat{\tau}-\tau)T) e^{j\phi} + \sum_{n=-N/2}^{N/2-1} N_n \\ \approx& \sqrt{E_s} \sum_{n=-N/2}^{N/2-1} |a_n|^2 r((\hat{\tau}-\tau)T) e^{j\phi} + \sum_{n=-N/2}^{N/2-1} N_n.\end{aligned} \tag{5.18}$$

The second approximation assumes that the estimation error $\hat{\tau} - \tau$ is small enough and the inter-symbol-interference (ISI) is ignored. Without loss of gen-

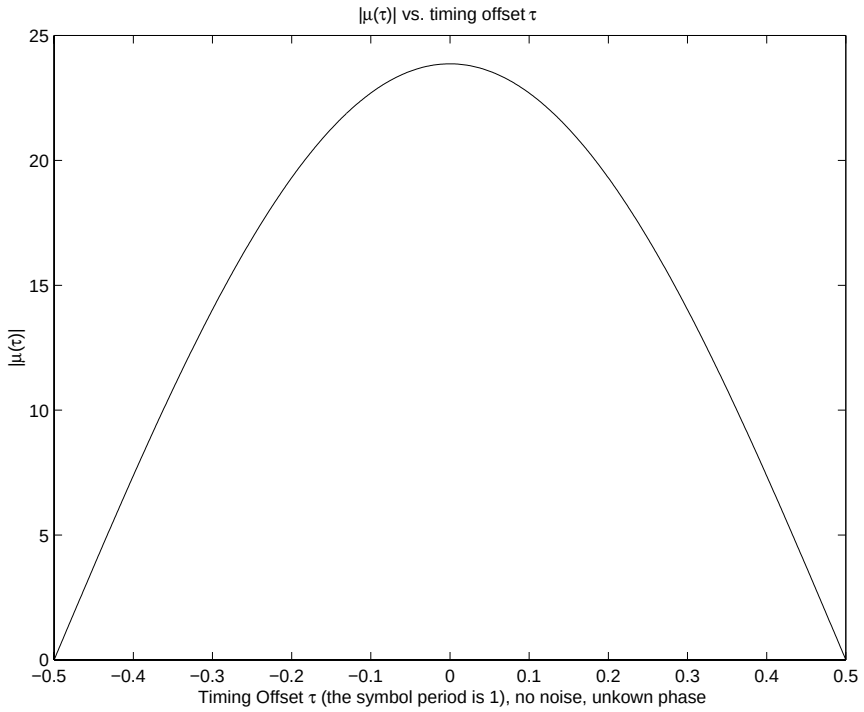

Figure 5.8: Correlation Magnitude $|\mu(\tau)|$ vs. Timing Offset Estimation Error τ

erality, assume that the real timing offset τ is 0, then the timing estimate $\hat{\tau}$ is the estimation error. We can evaluate $|\mu(\hat{\tau})|$ numerically. Let the shaping pulse $r(t)$ be a raised-cosine function with rolloff factor α, i.e.,

$$r(t) = \frac{\sin(\pi t/T)}{\pi t/T} \frac{\cos(\alpha \pi t/T)}{1 - 4\alpha^2 t^2/T^2}.$$

If $\hat{\tau}$ is close to zero enough and let us ignore the noise, we obtain

$$|\mu(\hat{\tau})| \approx \sqrt{E_s} N \left(1 - \frac{\pi^2 \hat{\tau}^2}{6}\right) \tag{5.19}$$

where PSK modulation is assumed, i.e., $|a_n| = 1$. Figure 5.8 shows the result of the numerical evaluation of $|\mu(\hat{\tau})|$ which follows a quadratic form. From (5.19) we can use a second order polynomial to approximate the magnitude of the correlation $|\mu(t)|$ as a function of the sampling time t (let $t = \tau T$) given that these sampling points are close enough to the ideal sampling point (i.e., t is close

enough to 0). Using a general form of the second order polynomial

$$|\mu(t)| = b_2 t^2 + b_1 t + b_0 \tag{5.20}$$

(5.20) suggests that a joint phase and timing estimator can be derived based on three adjacent samples of $|\mu(t)|$. These samples are the closest ones to the ideal sampling point as shown in Figure 5.9. In order to meet the condition that t is close enough to the ideal sampling point 0, two measures are adopted: (1) the sampling rate L is large enough (simulation shows that $L = 4$ can achieve good performance); (2) locating the largest available magnitude x_1 through peak search.

Let us define the sampling time of x_1 as nominal 0 on the time axis. Therefore the sampling epochs of x_0 and x_2 are $-T_s$ and T_s respectively. A *Lagrange* interpolating polynomial can be adopted based on the value of x_k $(k = 0, 1, 2)$:

$$\begin{aligned} |\mu(t)| =& \sum_{k=0}^{2} x_k \prod_{i=0, i\neq k}^{2} \frac{t - t_i}{t_k - t_i} \\ =& b_2 t^2 + b_1 t + b_0 \end{aligned} \tag{5.21}$$

where

$$\begin{aligned} b_2 =& \sum_{n=0}^{2} \frac{x_n}{\prod_{l=0, l\neq n}^{2} (t_n - t_l)} \\ b_1 =& -\sum_{n=0}^{2} \frac{x_n \sum_{l=0, l\neq n}^{2} t_l}{\prod_{l=0, l\neq n}^{2} (t_n - t_l)} \\ b_0 =& \sum_{n=0}^{2} \frac{x_n \prod_{l=0, l\neq n}^{2} t_l}{\prod_{l=0, l\neq n}^{2} (t_n - t_l)} \end{aligned} \tag{5.22}$$

Using the fact that $t_0 = -T_s,\ t_1 = 0,\ t_2 = T_s$, we can get

$$\begin{aligned} b_2 &= \frac{1}{T_s^2}\left(\frac{x_0}{2} - x_1 + \frac{x_2}{2}\right) \\ b_1 &= \frac{1}{T_s}\left(\frac{x_2}{2} - \frac{x_0}{2}\right) \\ b_0 &= x_1 \end{aligned}$$

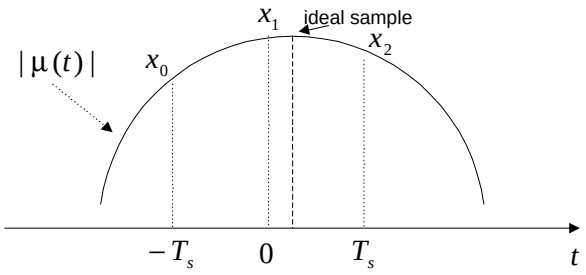

Figure 5.9: Three Sampling Points Model

The ML timing offset estimator (5.16) is the $\hat{\tau}$ which maximizes $|\mu(\tau)|$. It is easy to compute the ideal sampling time of the peak of $|\mu(t)|$ from a second order polynomial, i.e.

$$t_{peak} = -\frac{b_1}{2b_2} = \frac{(x_0 - x_2)T_s}{2x_0 - 4x_1 + 2x_2} \tag{5.23}$$

therefore, the ML estimate of τ is

$$\hat{\tau} = -\frac{t_{peak}}{T} = \frac{x_2 - x_0}{L(2x_0 - 4x_1 + 2x_2)}. \tag{5.24}$$

The phase estimator is shown in (5.17). Interpolation techniques can be applied to correct the timing offset before phase estimation. This however, introduces an additional delay in the demodulation process. Simulations show that using the time for the non-ideal sample of x_1 is sufficient for meeting the CRB (sampling time of x_1 is t_1). This leads to

$$\hat{\phi} = \arg\,[\mu(t_1)]. \tag{5.25}$$

The same algorithm can be applied to OQPSK modulation with minor modifications [36].

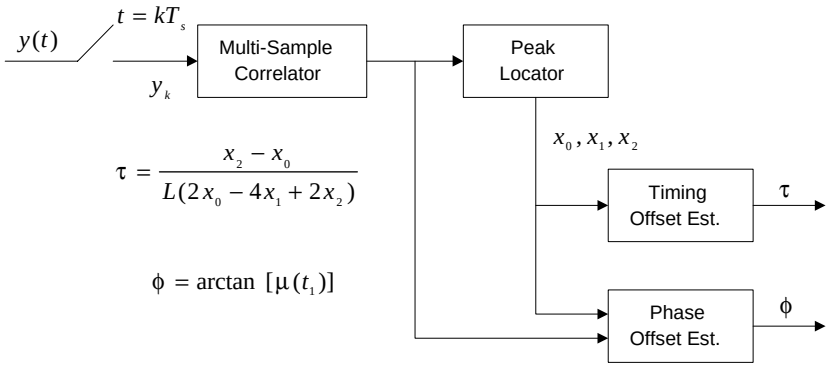

Figure 5.10: VLSI Implementation of the Joint Carrier Phase and Timing Offsets Estimator

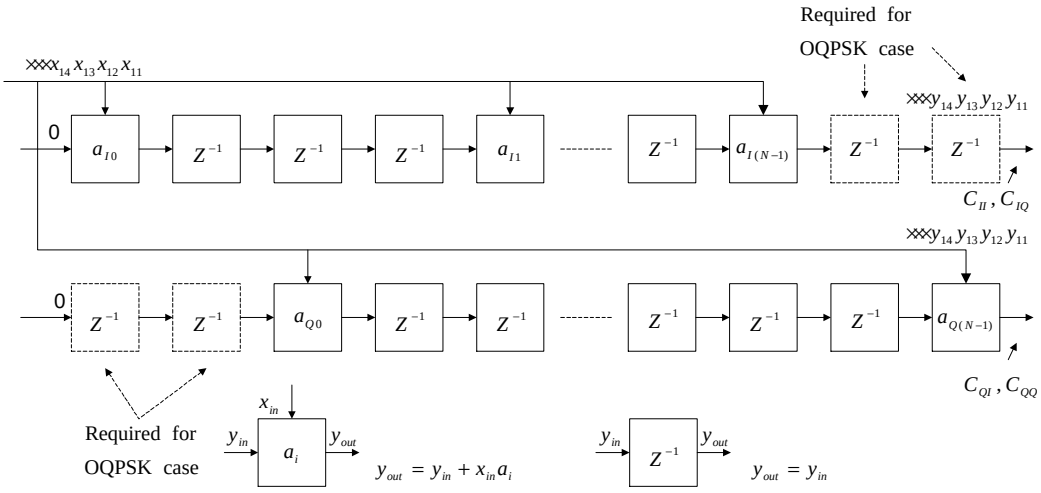

Figure 5.11: Systolic Multi-Sample Correlator for QPSK/OQPSK Modulation

5.3.2 VLSI Implementation

The VLSI structure is shown in Figure 5.10 and in [36, 34, 66]. The multi-sample correlator generates output at a higher rate than one sample per symbol. A systolic VLSI implementation of the correlator is shown in Figure 5.11 for both QPSK and OQPSK cases, where x_{ij} denotes the ith symbol ($i = -N/2, \cdots, N/2-1$), jth sample ($j = 0, 1, 2, 3$) of the output from the matched shaping filter. In QPSK/OQPSK case, $a_{Ij} = \pm 1$, $a_{Qj} = \pm 1$, only adders are necessary therefore the computational complexity is relatively small especially when using the correlator as soft-decision unique word (UW) detector. Through the *peak search* module, we can locate x_0, x_1 and x_2. An Arctan LUT is used when estimating the phase offset.

5.3.3 Performance Bounds and Simulation Results

One important contribution of this work is the CRB for DA joint timing and phase estimation. They are shown in Theorem 3 and 4. As we know the $\mathrm{CRB}_{\mathrm{DA}}(\phi)$ is independent of the training sequence pattern in the over-sampling case with the Nyquist pulse and PSK modulation. However the $\mathrm{CRB}_{\mathrm{DA}}(\tau)$ is closely related to the training sequence $\{a_k\}$.

Two data patterns have been investigated in our simulation: the alternating one-zero pattern and a unique word pattern. A 48-symbol UW was selected. The parameters for the computer simulations for QPSK and OQPSK signaling were $N = 48$ and $L = 4$ in an AWGN channel. Figure 5.12 shows the saw tooth characteristic of (5.24) under no noise conditions with random phase. From the simulations we can see that the estimator (5.24) is unbiased. Peak search (i.e., locating x_1) resolves the $m/4$ ($m = \pm 1, \pm 2$) ambiguity.

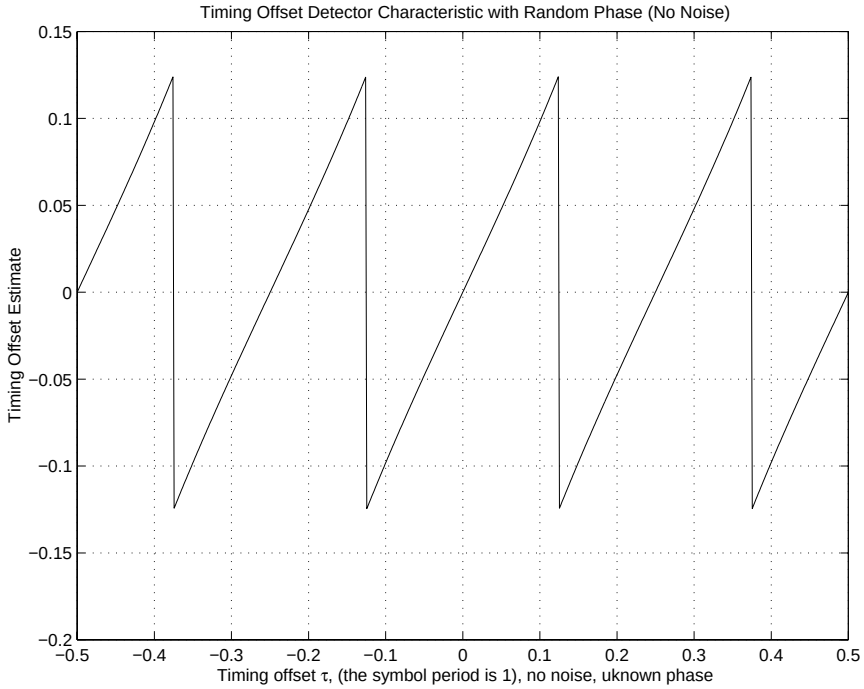

Figure 5.12: Timing Offset Estimate $\hat{\tau}$ vs. Timing Offset τ

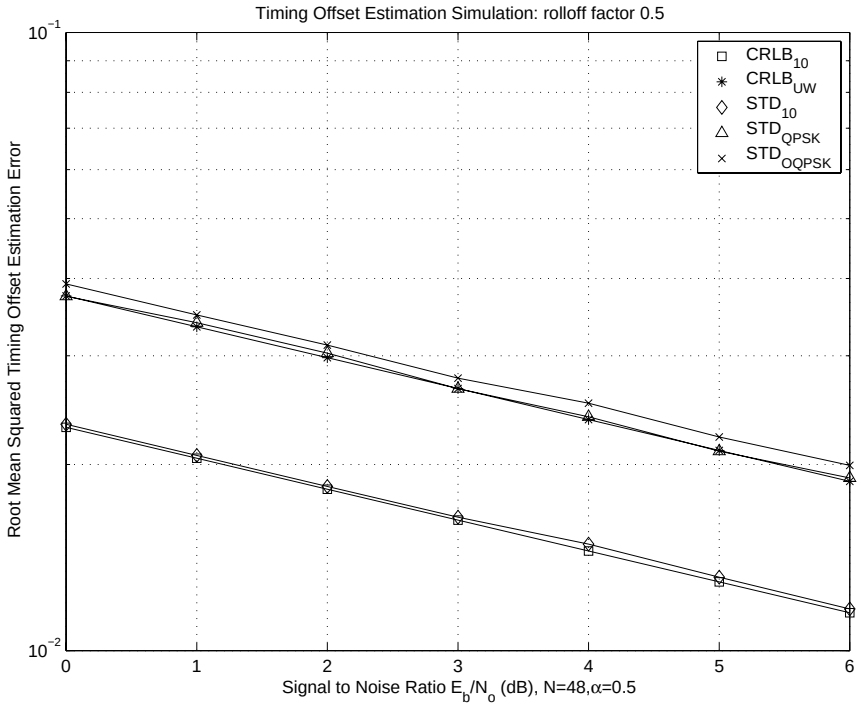

Figure 5.13: Timing Offset Estimation Performance of QPSK/OQPSK (one-zero pattern vs. UW pattern, $\alpha = 0.5$)

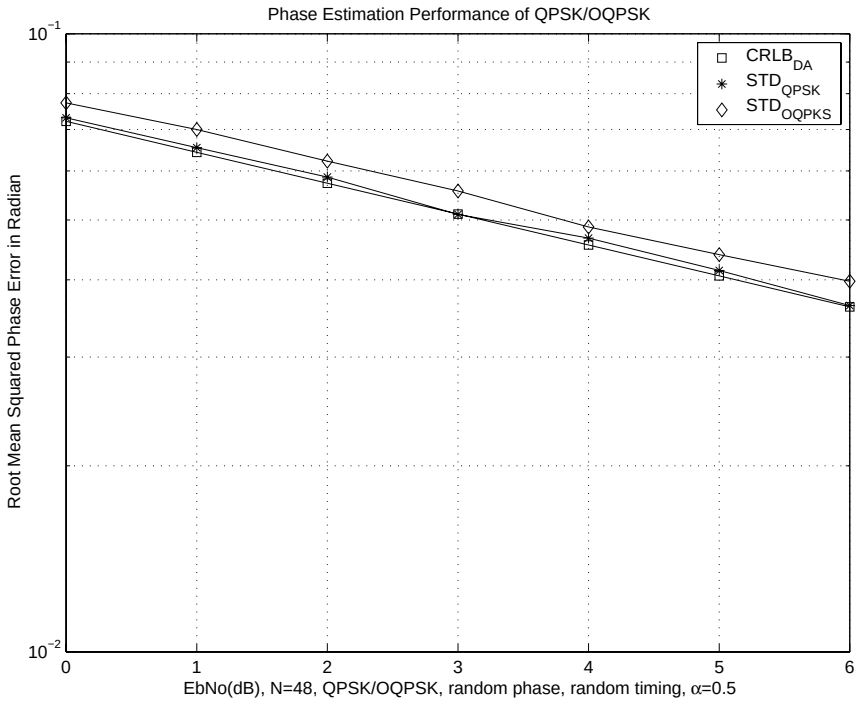

Figure 5.14: Phase Offset Estimation Performance of QPSK/OQPSK (UW Pattern, $\alpha = 0.5$)

Different rolloff factors for the raised-cosine shaping function were also tested. Simulation shows that the RMS timing estimation error of QPSK meets the $\mathrm{CRB}_{\mathrm{DA}}(\tau)$ for all the rolloff factors and data patterns. Simulation also supports that for the one-zero pattern the RMS timing error is independent of rolloff factor, while for the UW pattern it decreases as α increases. This is in agreement with the evaluation of the $\mathrm{CRB}_{\mathrm{DA}}(\tau)$. The performance of different data patterns varies significantly, sometimes the difference is as large as 4dB (shown in Figure 5.13). Therefore we found a joint timing and phase estimation algorithm that can meet the CRB for different data patterns and shaping functions, which supports the validity of our theorems.

For the OQPSK case the timing estimation performance degrades slightly compared with QPSK due to the crosstalk between the in-phase and the quadrature channels in the presence of timing and phase offsets. Figure 5.13 shows the timing offset estimation performance with $\alpha = 0.5$, where the one-zero pattern of QPSK and UW pattern of QPSK/OQPSK are illustrated. Figure 5.14 shows the phase estimation performance. The RMS phase estimation error meets the $\mathrm{CRB}_{\mathrm{DA}}(\phi)$ for phase estimation in the QPSK case while it degrades slightly in the OQPSK case.

5.4 Conclusions

In this chapter, we presented a carrier frequency estimation method for MPSK signals and its systolic VLSI implementations in both the NDA and the DA cases. The performance of this estimator is close to the CRB for frequency estimation when SNR is no less than 6dB in the NDA case and 0dB in the DA

case. The estimation range is $\pm 7\%$ symbol rate at 6dB in the NDA case, and $\pm 20\%$ symbol rate at 0dB in the DA case. The data modulation removal process introduces a significant amount of noise in the NDA case, and therefore makes several frequency estimators perform badly at low SNR.

We also presented a simplified DA ML joint carrier phase and timing offsets estimator and its systolic VLSI implementation for both QPSK and OQPSK modulations in this chapter. Intrigued by the observation that the central part around the global maximum of an optimization objective function can often be modeled by a quadratic function, if it is close enough to the true peak, a two stage searching algorithm is proposed in this work: *1)* a coarse search method is adopted to roughly locate the global maximum; *2)* a fine search method using *Lagrange* interpolation is adopted to locate the true global maximum. The proposed *curve-fitting* algorithm has superior timing and carrier phase estimation performance that approaches the CRB derived previously for the DA case at low SNR. The achievable timing estimation performance shows the validity of the theorems derived in Chapter 3.

Chapter 6

Conclusions

In this dissertation, synchronization and channel parameter estimation problems have been investigated in depth. Intrigued by the simple observation that the information is conveyed through wireless channels by uniformly spaced pulses that are some kind of "distorted" *convolution* of data symbols and a shaping pulse, we studied the estimation problems in the frequency domain and derived several useful results. Toeplitz matrices provide us a tool to connect the time domain processing and the frequency domain processing.

Toeplitz matrices play a pivotal role in digital communications and signal processing. Many issues in signal processing involve the analysis of their inverse. In Chapter 2, the convergence issue of the inverse of Toeplitz matrices was studied in depth. Through a simple example we illustrated that a widely used assertion was incorrect in general. We showed that under the condition that the z-transform of the sequence with which the Toeplitz matrices are associated has no zero on the unit circle, the inverse converges in the weak sense to a circular matrix. What is more, for the finite boundary quadratic form problem, the convergence can be strengthened into strong sense. The eigendecomposition of

a circular matrix is equivalent to DFT, which introduces the frequency domain approach that is desired in our problems.

There is a misunderstanding in the synchronization field: the synchronization parameter estimation performance has little to do with a specific training sequence (TS) in the data-aided (DA) PSK modulation since typically the correlation method is used to remove the training sequence and the magnitude of data symbols is constant. In Chapter 3 we showed that the general assertion was incorrect. The performance limits - the Cramer-Rao lower Bound and modified CRB for the DA synchronization parameter estimation were derived and discussed in depth in this chapter. Both the Gaussian channel and flat fading channel cases were addressed. The close relation between the TS and the fundamental performance limits sheds insight on the TS design for synchronization. The optimal TS's for timing acquisition in different scenarios were proposed. In this work, we proved that the alternating one-zero TS pattern could achieve minimum timing estimation variance for the band-limited low-pass Nyquist shaping pulses in the over-sampling case, which is widely encountered in modern digital receivers.

In Chapter 4, following the ML approach we derived the ML channel estimator with the general Gaussian noise and over-sampling assumption in the frequency domain. The derivation is based on *the finite boundary strong sense convergence theorem* for the inverse of Toeplitz matrices. With the help of this theorem, many good algorithms that take advantages of the transform domain approach can be derived. As a special case, the ML joint carrier phase and timing offsets estimator was presented.

Several practical synchronization parameter estimators were proposed in Chap-

ter 5 with their corresponding VLSI implementations. The carrier frequency estimation is conducted based on the auto-correlation of the input signal and linear regression of the auto-correlation phase. The DA ML joint carrier phase and timing offsets estimator is based on the *curve-fitting* technique. The two-stage global maximum searching method can be applied in general areas. The performance of these estimators approaches the CRB at low signal to noise ratios.

Currently, joint carrier frequency and timing offset estimation in fading channel is under investigation. The second order cyclostationary (CS) statistics [67, 68] can be used to design parameter estimators. The underlying common idea is to use nonlinear combinations of the data to reveal periodic components containing synchronization parameters. Another interesting topic - the synchronization and channel estimation problems for multicarrier systems is also under investigation. Multicarrier modulation [69, 70] is popular in wireless communication due to its good performance in fast fading environments. The synchronization and channel estimation for OFDM have received a lot of attention in the literature [38, 71, 72]. Our research results on these topics will be reported in future publications.

Bibliography

[1] A. J. Viterbi. *CDMA: Principles of Spread Spectrum Communications.* Addison-Wesley, Reading, Massachusetts, 1995.

[2] M. Y. Rhee. *CDMA Cellular Mobile Communications and Network Security.* Prentice Hall, New Jersey, 1998.

[3] K. Fehrer. *Wireless Digital Communications: Modulation and Spread Spectrum Applications.* Prentice-Hall, 1995, Upper Saddle River, New Jersey.

[4] J. M. Holtzman and D. J. Goodman. *Wireless and Mobile Communications.* Kluwer, Boston, 1994.

[5] I. Brodsky. *Wireless: The Revolution in Personal Communications.* Artech, Boston, 1995.

[6] V. K. Garg, K. Smolik, and J. E. Wikes. *Applications of CDMA in Wireless/Personal Communications.* Prentice-Hall, Upper Saddle River, New Jersey, 1997.

[7] T. S. Rappaport, B. E. Woerner, and J. H. Reed. *Wireless Personal Communications: The Evolution of Personal Communications Systems.* Kluwer, Boston, 1996.

[8] D. Grillo, A. Sasaki, R. A. Skoog, and B. Warfield Eds. Issue on personal communications - service, architecture and performance issues. *IEEE Journal on Selected Areas in Communications*, 15(8), October 1997.

[9] W. W. Wu, E. F. Miller, W. L. Pritchard, and R. L. Pickholtz. Mobile satellite communications. *Proceeding of IEEE*, 82:1431–1448, September 1994.

[10] H. V. Poor and G. W. Wornell. *Wireless Communications Signal Processing Perspectives.* Prentice Hall, New Jersey, 1998.

[11] T. M. Cover and J. A. Thomas. *Elements of Information Theory.* Wiley, New York, 1991.

[12] H. Meyr, M. Moeneclaey, and S. Fechtel. *Digital Communication Receivers, Synchronization, Channel Estimation, and Signal Processing.* Wiley, New York, 1998.

[13] U. Mengali and A. N. D'Andrea. *Synchronization Techniques for Digital Receivers.* Plenum, New York, 1997.

[14] W. C. Jakes Ed. *Microwave Mobile Communications.* IEEE Press, New York, 1974.

[15] J. C.-I. Chuang. The effect of time delay spread on portable radio communications channel with digital modulation. *IEEE Transaction on Selected Areas in Communications*, SAC-5:879–889, June 1987.

[16] H. L. Van Trees. *Detection, Estimation and Modulation Theory, Part I.* Wiley, New York, 1968.

[17] H. V. Poor. *An Introduction to Signal Detection and Estimation.* Springer-Verlag, New York, 2nd edition, 1994.

[18] A. N. D'Andrea, U. Mengali, and R. Reggiannini. The modified Cramer-Rao bound and its application to synchronization parameters. *IEEE Transaction on Communications*, COM-42(2):1391–1399, February/March/April 1994.

[19] S. Haykin. *Adaptive Filter Theory.* Prentice Hall, New Jersey, 3rd edition, 1996.

[20] T. Kailath, A. Vieira, and M. Morf. Inverses of Toeplitz operators, innovations, and orthogonal polynominals. *SIAM Review*, 20(1):106–119, January 1978.

[21] T. Kailath, B. Levy, L. Ljung, and M. Morf. Fast time-invariant implementations of gaussian signal detectors. *IEEE Transaction of Information Theory*, IT-24(4):469–476, July 1978.

[22] U. Grenander and G. Szego. *Toeplitz Forms and Their Applications.* University of California Press, Berkeley California, 1958.

[23] R. M. Gray. Toeplitz and circulant matrices. Technical Report 6502-1, Information Systems Laboratory, Center for Systems Research, Stanford University, 1971.

[24] H. Kobayashi. Simultaneous adaptive estimation and decision algorithms for carrier modulated data transmission systems. *IEEE Transaction on Communications*, COM-19(3):268–280, June 1971.

[25] F. W. Sun, Y. Jiang, and J. S. Baras. On the convergence of the inverse of Toeplitz matrices and its applications. *submitted to IEEE Transaction on Information Theory*, June 2000.

[26] Y. Jiang, F. W. Sun, and J. S. Baras. On the true Cramer-Rao lower bound for the DA joint estimation of carrier phase and timing offsets. In *Proc. of IEEE International Conference on Communications (ICC'00)*, pages 331–335, New Orleans, June 2000. a full version submitted to *IEEE Transaction on Communications*.

[27] Y. Jiang, F. W. Sun, and J. S. Baras. Maximum likelihood slow frequency-selective fading channel estimation using frequency domain approach. *submitted to IEEE Globecom'2000*, March 2000.

[28] M. Moeneclaey. On the true and the modified Cramer-Rao bounds for the estimation of a scalar parameter in the presence of nuisance parameters. *IEEE Transaction on Communications*, COM-46(11):1536–1544, November 1998.

[29] M. Moeneclaey. A fundamental lower bound on the performance of practical joint carrier and bit synchronizers. *IEEE Transaction on Communications*, COM-32(9):1007–1012, September 1984.

[30] M. Moeneclaey. A simple lower bound on the linearized performance of practical symbol synchronizers. *IEEE Transaction on Communications*, COM-31(9):1029–1032, September 1983.

[31] C. Georghiades and M. Moeneclaey. Sequence estimation and synchronization from nonsynchronized samples. *IEEE Transaction on Information Theory*, IT-37(6):1649–1657, November 1991.

[32] D. Rife and R. Boorstyn. Single-tone parameter estimation from discrete-time observations. *IEEE Transaction on Information Theory*, IT-20(5):591–598, September 1974.

[33] Y. Jiang, W. Ting, F. B. Verahram, R. L. Richmond, and J. S. Baras. A carrier frequency estimation method of MPSK signals and its systolic implementation. In *Proc. of the 33rd Conference on Information Science and Systems (CISS'99)*, pages 142–145, Johns Hopkins University, March 1999.

[34] Y. Jiang, F. B. Verahrami, W. Ting, R. L. Richmond, and J. S. Baras. Data-aided ML parameter estimators of PSK burst modems and their systolic VLSI implementations. In *Proc. IEEE Globecom'99*, Rio de Janeiro, Brazil, December 1999.

[35] Y. Jiang, F. B. Verahrami, W. Ting, R. L. Richmond, and J. S. Baras. VLSI implemented data-aided ML parameter estimators of PSK burst modems. In *Proc. of IEEE Vehicular Technology Conference (VTC'99)*, pages 868–873, Amsterdam, Netherlands, September 1999.

[36] Y. Jiang, F. B. Verahrami, W. Ting, R. L. Richmond, and J. S. Baras. VLSI implemented ML joint carrier phase and timing offsets estimator for QPSK/OQPSK burst modems. In *Proc. of IEEE Wireless Communications and Networking Conference (WCNC'99)*, New Orleans, September 1999.

[37] R. A. Horn and C. R. Johnson. *Matrix Analysis*. Cambridge University Press, United Kingdom, 1996.

[38] Y. Li, L. J. Cimini, and N. Sollenberger. Robust channel estimation for OFDM systems with rapid dispersive fading channels. *IEEE Transactions on Communications*, COM-46(7):902–915, July 1998.

[39] S. White and N. Beaulieu. On the application of the Cramer-Rao and detection theory bounds to mean square error of symbol timing recovery. *IEEE Transaction on Communications*, COM-40(10):1635–1643, October 1992.

[40] A. V. Oppenheim, R. W. Schafer, and J. R. Buck. *Discrete-Time Signal Processing*. Prentice Hall, New Jersey, 2nd edition, 1998.

[41] J. G. Proakis. *Digital Communications*. McGraw-Hill, Inc., New York, 1995.

[42] C. Tellambura, M. G. Parker, Y. J. Guo, S. J. Shepherd, and S. K. Barton. Optimal sequences for channel estimation using discrete Fourier transform techniques. *IEEE Transaction on Communications*, 47(2):230–238, February 1999.

[43] A. P. Clark, Z. C. Zhu, and J. K. Joshi. Fast start-up channel estimation in the presence of noise. *IEE Proceedings*, 131:375–381, July 1984.

[44] T. Felhauer. Digital signal processing for optimum wideband channel estimation. *IEE Proceedings*, 140(3):179–186, June 1993.

[45] D. K. Borah and B. D. Hart. Frequency-selective fading channel estimation with a polynomial time-varying channel model. *IEEE Transaction on Communications*, 47(6):862–873, June 1999.

[46] E. Baccarelli and R. Cusani. Combined channel estimation and data detection using soft statistics for frequency-selective fast-fading digital links. *IEEE Transaction on Communications*, 46(4):424–427, April 1998.

[47] S. Kay. *Modern Spectral Estimation Theory and Application*. Prentice Hall, New Jersey, 1988.

[48] Y. Jiang, R. L. Richmond, and J. S. Baras. Carrier frequency estimation of MPSK modulated signals. Technical report, Center for Satellite and Hybrid Communication Networks, University of Maryland, College Park, September 1998.

[49] M. P. Fitz. Planar filtered techniques for burst mode carrier synchronization. In *Proc. of IEEE Globecom'91*, pages 365–369, 1991.

[50] A. J. Viterbi and A. M. Viterbi. Nonlinear estimation of PSK-modulated carrier phase with application to burst digital transmission. *IEEE Transaction on Information Theory*, IT-29(4):543–551, July 1983.

[51] M. Luise and R. Reggiannini. Carrier frequency recovery in all-digital modems for burst mode transmission. *IEEE Transaction on Communications*, COM-43(2):1169–1178, February/March/April 1995.

[52] S. Tretter. Estimating the frequency of a noisy sinusoid by linear regression. *IEEE Transaction on Information Theory*, IT-31(6):832–835, November 1985.

[53] S. Kay. A fast and accurate single frequency estimator. *IEEE Transaction on Acoustics Speech and Signal Processing*, ASSP-37(12):1987–1990, December 1989.

[54] J. Chuang and N. Sollenberger. Burst coherent demodulation with combined symbol timing, frequency offset estimation, and diversity selection. *IEEE Transaction on Communications*, COM-39(7):1157–1164, July 1991.

[55] U. Mengali and M. Morelli. Data-aided frequency estimation for burst digital transmission. *IEEE Transaction on Communications*, COM-45(1):23–25, January 1997.

[56] H. T. Kung. Why systolic architecture. *IEEE Computer*, 15(1):37–46, January 1982.

[57] S.-Y. Kung. On supercomputing with systolic/wavefront array processors. *Proceeding of IEEE*, 72:867–884, July 1984.

[58] S. K. Rao and T. Kailath. Regular iterative algorithms and their implementation on processor arrays. *Proceeding of IEEE*, 76:259–269, March 1988.

[59] K. J. R. Liu and K. Yao Ed. *High-performance VLSI signal processing innovative architectures and algorithms*. IEEE Press, New York, 1998. Volume 1 and 2.

[60] Y. Jiang. VLSI implementation description of frequency estimator. Hughes Network Systems internal memo, May 1999.

[61] W. Cowley. Phase and frequency estimation for psk packets: Bounds and algorithms. *IEEE Transaction on Communications*, COM-44:26–28, January 1996.

[62] J. Bingham. *The Theory and Practice of Modem Design*. Wiley, New York, 1988.

[63] M. Oerder and H. Meyr. Digital filter and square timing recovery. *IEEE Transaction on Communications*, COM-36(5):605–612, May 1988.

[64] V. Tuukkanen, J. Vesma, and M. Renfors. Efficient near optimal maximum likelihood symbol timing recovery in digital modems. In *Proc. of IEEE International Symposium on Personal, Indoor and Mobile Radio Communication (PIMRC'97)*, pages 825–829, May 1997.

[65] G. Rempel. On the efficiency of maximum likelihood bit synchronizers. In *Proc. of IEEE International Conference on Communications (ICC'96)*, volume 3, pages 1286–1290, June 1996.

[66] Y. Jiang. VLSI implementation description of phase and timing estimator. Hughes Network Systems internal memo, July 1999.

[67] K. Scott and E. Olasz. Simultaneous clock phase and frequency offset estimation. *IEEE Transaction on Communications*, COM-43(7):2263–2270, July 1995.

[68] F. Gini and G. Giannakis. Frequency offset and symbol timing recovery in flat-fading channels: a cyclostationary approach. *IEEE Transaction on Communications*, COM-46(5):400–411, March 1998.

[69] J. A. C. Bingham. Multicarrier modulation for data transmission: An idea whose time has come. *IEEE Communication Magazine*, 28:5–14, May 1990.

[70] W. Y. Zou and Y. Wu. COFDM: An overview. *IEEE Transaction on Broadcasting*, 41:1–8, March 1995.

[71] T. Pollet, M. V. Bladel, and M. Moeneclaey. BER sensitivity of OFDM systems to carrier frequency offset and Wiener phase noise. *IEEE Transaction on Communications*, 43(2/3/4):191–193, February/March/April 1995.

[72] J. van de Beek, M. Sandel, and P. O. Borjesson. ML estimation of timing and frequency offsets in OFDM systems. *IEEE Transaction on Signal Processing*, 45(3):1800–1805, July 1997.